New Maps of the Dark Side: Redshift drift cosmography

Bruno André Ribeiro Rocha
Mestrado em Astronomia e Astrofísica
Departamento de Física e Astronomia
2021

Orientador
Prof. Dr. Carlos Martins, Centro de Astrofísica da Universidade do Porto, Instituto de Astrofísica e Ciências do Espaço

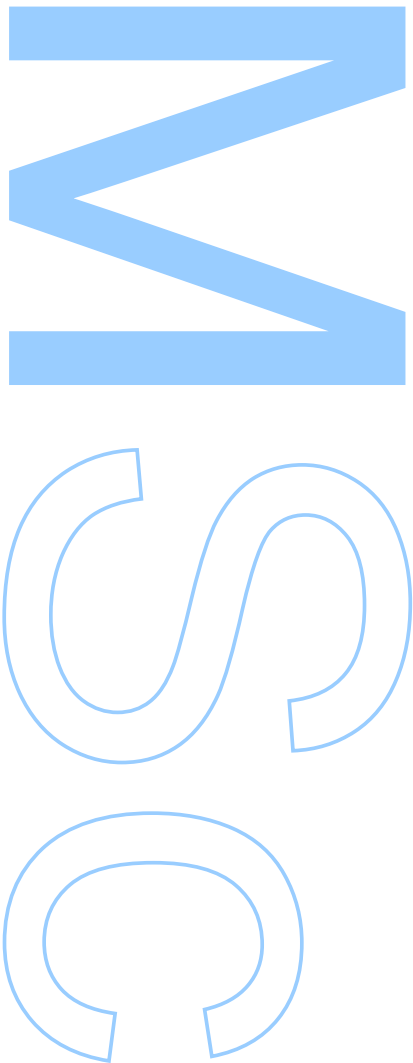

U.PORTO

FACULDADE DE CIÊNCIAS
UNIVERSIDADE DO PORTO

Todas as correções determinadas pelo júri, e só essas, foram efetuadas.

O Presidente do Júri,

Porto, _____/_____/_____

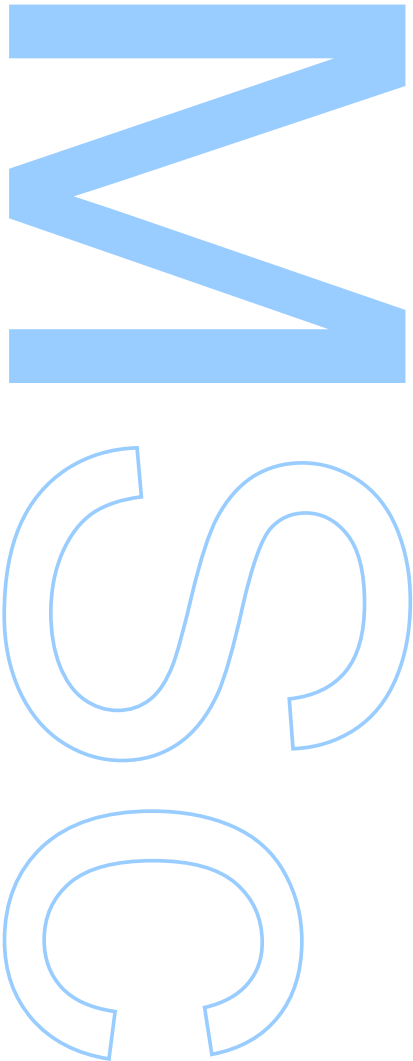

Universidade do Porto

Masters Thesis

New Maps of the Dark Side: Redshift drift cosmography

Author:
Bruno Rocha

Supervisor:
Carlos Martins

A thesis submitted in fulfilment of the requirements
for the degree of MSc. Astronomy and Astrophysics

at the

Faculdade de Ciências da Universidade do Porto
Departamento de Física e Astronomia

December 16, 2021

Acknowledgements

Firstly I would like to thank my supervisor Carlos Martins for his guidance. I don't believe that any other supervisor would make me feel so unstressed during the development of this thesis.

I also would like to say thanks to the friends I made in the Department of Physics and Astronomy. With them, the department truly felt like a second home. I would also like to express my gratitude to all the professors that have helped me.

Finally, I would like to say thanks to my parents for all the things that they have given to me. They made me who I am today. I would also like to say thanks to my brother Marcos Rocha, my cousin Mariana Ferreira and my one of a kind friend Rui Gândara for their unconditional support.

UNIVERSIDADE DO PORTO

Abstract

Faculdade de Ciências da Universidade do Porto
Departamento de Física e Astronomia

MSc. Astronomy and Astrophysics

New Maps of the Dark Side: Redshift drift cosmography

by Bruno Rocha

The growing amount of observational evidence for the recent acceleration of the universe unambiguously demonstrates that canonical theories of cosmology and particle physics are incomplete (if not incorrect) and that new physics is out there, waiting to be discovered. The most fundamental task for the next generation of astrophysical facilities is therefore to search for, identify and ultimately characterise this new physics. The acceleration is seemingly due to a dark component whose low-redshift gravitational behaviour is very similar to that of a cosmological constant. However, currently available data provides very little information about the high-redshift behaviour of this dark sector or its interactions with the rest of the degrees of freedom in the model.

It is becoming increasing clear that tackling the dark energy enigma will entail significantly extending the redshift range where its behaviour can be accurately mapped. A new generation of astrophysical facilities, including Euclid, the ELT, and the SKA have dark energy characterization as a key science driver, and in addition to significantly increasing the range and sensitivity of current observational probes will allow for entirely new tests. The goal of this thesis will be to carry out an assessment of the cosmological impact and model discriminating power of one such probe: measurements of the redshift drift of objects following the Hubble flow. We will also make a comparison between different cosmographic expansions and the impact that they cause in the analysis of redshift drift measurements. In addition, the synergies of the combination of SKA and ELT data will be studied as well as which cosmographic expansion is best suited for each redshift region.

Keywords: Cosmography, Redshift Drift, SKA, ELT

UNIVERSIDADE DO PORTO

Resumo

Faculdade de Ciências da Universidade do Porto
Departamento de Física e Astronomia

Mestrado em Astronomia e Astrofísica

Titulo da Tese em Portugês

por Bruno Rocha

A crescente quantidade de evidência observacional para a recente aceleração do universo demonstra sem ambiguidade que as teorias canónicas de cosmologia e física de partículas estão incompletas (se não incorrectas) e que nova física anda por aí, à espera de ser descoberta. A tarefa mais fundamental para a próxima geração de instalações astrofísicas é, portanto, procurar, identificar e, em última análise, caracterizar esta nova física. A aceleração é aparentemente devida a uma componente escura onde o comportamento gravitacional para baixos *redshifts* é muito semelhante ao de uma constante cosmológica. No entanto, os dados actualmente disponíveis fornecem muito pouca informação sobre o comportamento a *redshifts* altos desta energia escura e as suas interacções com o resto dos graus de liberdade do modelo.

Está a tornar-se cada vez mais claro que enfrentar o enigma da energia escura implicará um alargamento significativo da gama de *redshifts* onde o seu comportamento pode ser mapeado com precisão. Uma nova geração de infraestruturas astrofísicas, incluindo o Euclid, o ELT, e o SKA têm a caracterização da energia escura como um dos seus focos, e além de aumentarem significativamente o alcance e a sensibilidade das sondas observacionais actuais, permitirão testes inteiramente novos. O objectivo desta tese será a realização de uma avaliação do impacto cosmológico e do poder discriminador de modelos de uma dessas sondas: a medição do *redshift drift* de objectos que seguem o fluxo Hubble. Também será feita uma comparação entre as diferentes expansões cosmográficas e o impacto que estas causam na análise das medições do *redshift drift*. Além disso, serão também estudadas as sinergias da combinação de dados SKA e ELT e qual a expansão cosmográfica mais adequada para cada região de *redshift*.

Palavras-Chave: Cosmografia, *Redshift Drift*, SKA, ELT

Contents

List of Figures

List of Tables

Chapter 1

Introduction

Current day Cosmology is at an exciting stage by progressing into a so called precision Cosmology [1]. There is a standard model, much like the analogous of the standard model of Particle Physics, and the main scientific focus is to try to refine the essential parameters. That model is the ΛCDM model, often called concordance model. It is one of the most simple yet successful ways to describe the Universe. It follows Einstein's General Relativity and considers the existence of a cosmological constant Λ, which corresponds to the energy density of space and is assumed to be the dark energy preferred by observations, and a vanishing spatial curvature. Additionally, the matter present in the Universe is pressure-less and composed by baryonic matter plus cold dark matter (i.e. non-relativistic dark matter). With the previously mentioned assumptions, the ΛCDM model proved to be able to describe the formation of the Universe and its evolution. However, like any model, there are problems that remain unanswered/can't be answered in its current state. Two of the more concerning problems are the fine-tuning problem and the coincidence problem [2]. The first one arises from the fact that the energy density of the cosmological constant Λ from quantum field theory predictions and observations differ in approximately 120 orders of magnitude. To do Cosmology it is necessary to fine-tune 120 decimal places, a massive concern. The second problem results from the inability to explain why today the cosmological constant density and the matter density have the same order of magnitude, something that dark energy models tend to agree that has a very low probability to occur.

With such problems in mind, it is safe to say that the Universe's expansion acceleration rate is far from being explained. Furthermore, many other models are compatible with the same observations or degenerate into the ΛCDM model. At this point in time it is impossible to distinguish dark energy models from Modified Gravity Models. Even models

with different approaches to the description of dark matter can be indistinguishable from each other. So, it is crucial to have a clearer way to discern which model is better. New facilities like Euclid [3], the ELT [4], and the SKA [5] [6] will start to operate within the next 10 years and will provide observations with higher quality than ever. This upcoming data will give more insight about the characterization of the Universe's expansion acceleration. The new instruments will also, in theory, allow real-time measurements of the Universe's expansion [6] [7] [8]. One of the physical parameters that can be studied in real-time is the redshift drift, the main focus of this thesis.

Chapter 2

Redshift Drift

The way that the Universe expands is one of the most compelling topics of study in Cosmology. Currently, it is known that the Universe is expanding at an accelerating pace. Most, if not all, of the data from the measurements of this accelerated expansion are evaluated in relation to our current light cone. Those measurements are made as a function of the redshift that the objects in study display. Redshift is the name given to the decrease in frequency that photons can obtain through various ways, one off them being the expansion of the Universe. This decrease in frequency happens because in an expanding Universe the wavelengths of photons will increase. As consequence, the relation $c = \lambda\nu$ imposes that the frequency must decrease. An object with a higher redshift corresponds to a more distant body and the emission event will be also older.

Furthermore, since the Universe is expanding, most models predict that the distance from a light source that only follows the expansion of the Universe to an observer will vary with time, causing also a redshift variation. This phenomenon is called redshift drift and was firstly described by Sandage [9] and McVittie [10] in 1962. Redshift drift measurements are model independent and can measure directly the expansion rate. They can also in theory be used to mitigate degeneracies between cosmological models as well as test the Copernican principle [11].

With the advancement in the technology of observational facilities, it will be possible to examine our Universe's evolution in real-time. This new branch of Cosmology is referred as real-time cosmology. Some of the possible study observables are the redshift drift, cosmic parallax, drift of the polarization of inverse-Compton scattered CMB photons and flux drift [11] [12]. From these observables, the redshift drift is the one that is most promising and has most research on it. As such, it will be the only one studied in this work.

To get the standard expression for the redshift drift, it is only necessary to consider a homogeneous and isotropic Universe with a Friedmann-Lemaitre-Robertson-Walker (FLRW) space-time (equation 2.1).

$$ds^2 = -dt^2 + a(t)^2 \left(\frac{dr^2}{1 - kr^2} + r^2 \left(d\theta^2 + sin^2\theta d\phi^2 \right) \right) \tag{2.1}$$

With this in mind, it is possible to obtain the equalities presented in 2.2.

$$1 + z = \frac{\lambda_0}{\lambda} = \frac{a_0}{a} = \frac{dt_0}{dt} \tag{2.2}$$

Where a and a_0 are, respectively, the scale factors from the moment when the emission happened and present time, z is the cosmological redshift. From here on the absence of subscript represents the event's emission time and the subscript 0 the current epoch, which represents the moment in time that said event is observed. Differentiating the left side of the expression 2.2 (the usual definition of redshift) in order to t_0 one can obtain

$$\frac{dz}{dt_0} = \frac{1}{a}\frac{da_0}{dt_0} - \frac{a_0}{a^2}\frac{da_0}{dt}\frac{dt}{dt_0} \tag{2.3}$$

From the definition of Hubble parameter (equation 2.4) and recalling equation 2.2 it follows that the redshift drift will depend on the Hubble parameter of the chosen cosmological model (equation 2.5).

$$H \equiv \frac{1}{a}\frac{da}{dt} \tag{2.4}$$

$$\frac{\Delta z}{\Delta t} = (1 + z)H_0 - H(z) \tag{2.5}$$

Figure 2.1 illustrates the redshift drift as a function of z for different different models and cosmological parameters. As it can be seen, the expected signal to be observed is extremely small, just a variation of 10^{-10} in redshift in a time span of 10 years. For comparison, this variation is comparable in orders of magnitude to the redshift drift expected from other sources beyond the cosmic expansion like plate tectonics and the Sun's motion within the galaxy [12].

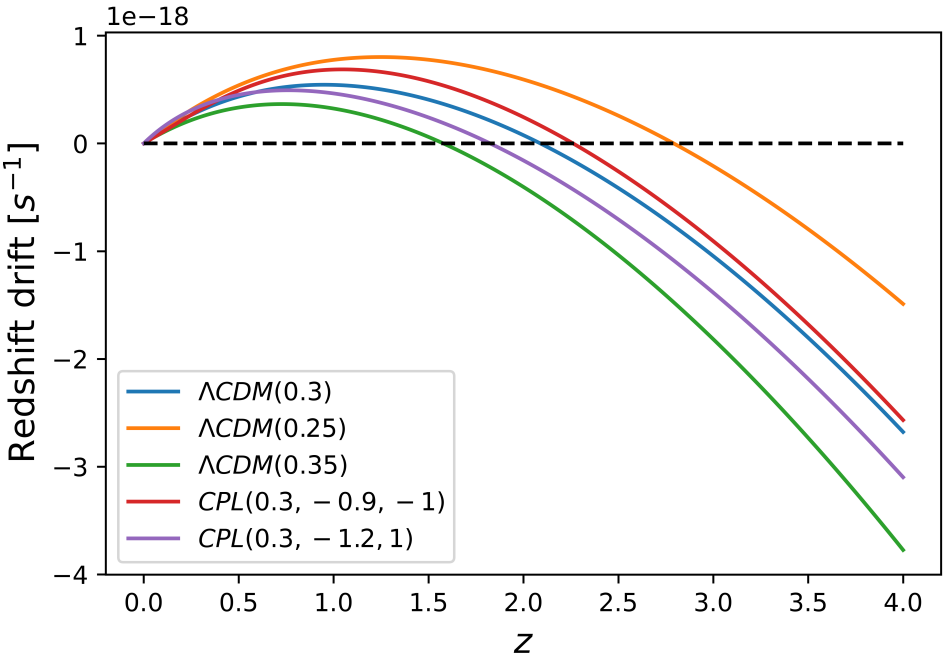

Figure 2.1: Redshift drift as a function of z for different cosmological parameters of flat ΛCDM and CPL models (these models will be explained with more detail in sections 4.1 and 4.2 respectively).The scale of $1x10^{-18}s^{-1}$ is approximately equal to $3x10^{-11}year^{-1}$

2.1 How to measure the Redshift Drift?

Redshift drift measurements are obtained from the measurement of the spectroscopic velocity drift, Δv. These quantities are related as shown in equation 2.6 ($E(z)$ is the re-scaled Hubble parameter and is equal to $H(z)/H_0$, c is the speed of light).

$$\Delta v = \frac{c\Delta z}{1+z} = cH_0\Delta t\left(1 - \frac{E(z)}{1+z}\right) \tag{2.6}$$

When inputting a Hubble parameter correspondent to a ΛCDM model with $\Omega_{m0} = 0.3$ in the previous relation we obtain a spectroscopic change of a few cm/s in a decade. With this in mind, it is crucial to choose a good cosmic accelerometer, i.e., a type of object that from which it is possible to retrieve satisfactory redshift drift data. Liske et al. [4] made a list of useful traits that potential accelerometers should have:

- be capable to precisely capture motion of galaxies due to the expansion of the Universe (Hubble Flow);
- a sharp spectrum in order to alleviate the error on redshift measurements;

- extensive useful spectral features, because observations on redshift drift will be very time consuming and it is crucial to maximize the amount of information obtained;
- be bright;
- be able to be observed in a wide range of redshifts.

The authors also call attention for the fact that some features seem to clash with each other, showing once more the difficulty in choosing the right object to study. From the possible cosmic accelerometers that present a favorable amount of the previous requirements, the Lyman-α absorption lines and Neutral Hydrogen (HI) are the ones that spark most interest.

2.1.1 Lyman-α absorption lines

The Lyman-α (Ly-α) forest is the name given to the phenomenon that occurs when radiation from quasi-stellar objects (QSOs) is intercepted by intergalactic neutral hydrogen (HI). Those mediums with HI absorb radiation from the Ly-α region of the QSOs continuum. Since this continuum arrives redshifted to the gas concentrations, the absorption lines produced will be blueshifted multiple times into lower wavelengths creating a ”forest” in the spectrum. The further the QSO is from the observer (and by extension with a higher redshift) the bigger is the forest in the observed spectrum. The Ly-α absorption lines appear in the Ultraviolet and visible wavelengths and can be observed from ground telescopes in objects with redshifts between $1.7 \lesssim z \lesssim 5$, a region where most of cosmological models say that the redshift drift is negative and will be strictly decreasing in value [4] [13]. This way of measuring the redshift drift was first proposed by Loeb [14] and, for that reason, it is sometimes called the Sandage-Loeb test [15]. High resolution spectrographs operating in the visible region of the electromagnetic spectrum, like the ELT (see section 5.2), will be capable to detect this phenomenon [4].

In figure 2.2 [16] we have an example of this phenomenon. The top side spectrum corresponds to quasar 3C 273 with a redshift equal to 0.158, obtained from Hubble’s Space Telescope Faint-Object Spectrograph (which explains the fact that the redshift is inferior from what was stipulated for ground telescopes), and the bottom side to quasar Q1422+2309 that has a redshift of 3.62 from Keck I HIRES. As it can be seen, quasars from more distant regions in space, like Q1422+2309, have a high density of Ly-α absorption lines while closer QSOs just as 3C 273 present only a couple.

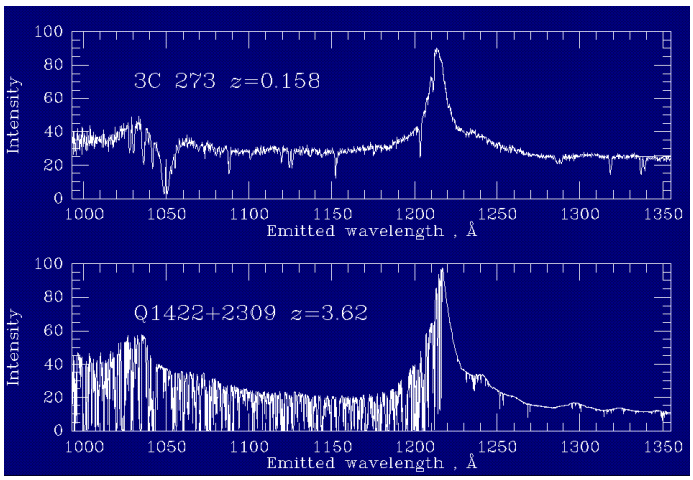

Figure 2.2: Example of a Lyman-α forest. The quasar 3C 273 with $z = 0.158$ has only a few Ly-α absorption lines. Meanwhile the quasar Q1422+2309 with $z = 3.62$ has a high density of Ly-α absorption lines. The density of absorption lines is proportional to the distance of the observed QSO, the more distant is the object the higher is the density. [16]

2.1.2 Neutral Hydrogen (HI)

Another method to measure redshift drift is through the change of frequency of the neutral hydrogen signal of galaxies measured at different epochs. Neutral hydrogen emits very rarely a photon with a frequency of 1420 MHz, commonly referred in Astronomy as the 21 cm line. This emission happens when a HI atom with an aligned proton spin and electron spin, a state with more energy than when the spins are anti-aligned, has its electron spin inverted making the system lose energy by radiation [17]. The HI signals can be observed by ground telescopes in redshift ranges of $0 < z < 1$, a region different from the Ly-α forest where the redshift drift is expected to be positive and strictly increasing, being a good complement to the data obtained from Lyman-α absorption lines [8]. Darling [18] tried to measure the redshift drift using indirectly this method. The results showed instrumental systematic uncertainties with the measurements obtained being three orders of magnitude larger than the expected. He also concluded that it would take about 125 years for current technology to measure directly the cosmic acceleration. In the future, powerful radio telescopes like the SKA (see section 5.1) will be able to measure HI frequency shifts with enough precision to do real-time cosmology [6].

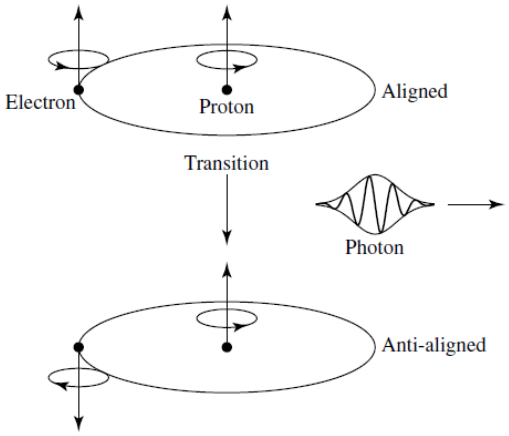

Figure 2.3: Emission of the 21 cm wavelength photon occurs when a neutral hydrogen atom has its aligned proton and electron spins flipped to anti-aligned [17]

Chapter 3

Cosmography

In the same way that redshift drift measurements are independent of the cosmological model chosen, it is possible to characterize the Universe's evolution without postulating *a priori* a model through cosmography (also called cosmokinetics). This form of Cosmology emerges from the symmetries and geometry of a FLRW space-time, without using directly Einstein's field equations. This way, the number of assumptions made is kept to a minimum. From these assumptions, it is possible to write the scale factor using current date observations as a cosmographic series obtained from a Taylor expansion around the present time, t_0. Until the fifth order we obtain equation 3.1. For notation simplicity $t_H = H_0(t - t_0)$.

$$a(t_H) = a_0 \left[1 + t_H - \frac{q_0}{2}(t_H)^2 + \frac{j_0}{3!}(t_H)^3 + \frac{s_0}{4!}(t_H)^4 + \frac{c_0}{5!}(t_H)^5 + \frac{p_0}{6!}(t_H)^6 + O((t_H)^7)\right] \tag{3.1}$$

The cosmographic coefficients are respectively the Hubble parameter (H), the deceleration parameter (q), the jerk (j), the snap (s), the crackle (c) and the pop (p).*

$$H \equiv \frac{1}{a}\frac{da}{dt} \qquad q \equiv -\frac{1}{aH^2}\frac{d^2a}{dt^2} \qquad j \equiv \frac{1}{aH^3}\frac{d^3a}{dt^3} \tag{3.2}$$

$$s \equiv \frac{1}{aH^4}\frac{d^4a}{dt^4} \qquad c \equiv \frac{1}{aH^5}\frac{d^5a}{dt^5} \qquad p \equiv \frac{1}{aH^6}\frac{d^6a}{dt^6} \tag{3.3}$$

*The crackle and pop parameters can also be referred as lerk (l) and the max-out (m) parameters respectively.

Each of these parameters holds information about the way that the Universe expands. For example, the signal of q tells if our Universe's expansion is accelerating or decelerating. A positive sign means that we are in a Universe that is decelerating and a negative sign the opposite. The j holds information on the changes from positive acceleration to negative acceleration and vice-versa, much like a second order derivative of a function. The snap quantifies the way that dark energy evolves [19]. The others are less clear in what information they give and the s parameter is usually considered the minimum order in which it is possible to distinguish cosmological models from the concordance model (see section 4.1) [20] [21].

Lets then describe the Hubble parameter in terms of a cosmographic series. From the definition of redshift (equation 2.2), it is obtained the following expression

$$\frac{1}{1+z} = 1 + t_H - \frac{q_0}{2}(t_H)^2 + \frac{j_0}{3!}(t_H)^3 + \frac{s_0}{4!}(t_H)^4 + \frac{c_0}{5!}(t_H)^5 + \frac{p_0}{6!}(t_H)^6 + O((t_H)^7) \tag{3.4}$$

Now, it will be introduced the variable α.

$$\alpha = \frac{1}{1+z} - 1 = \frac{a - a_0}{a_0} \tag{3.5}$$

This variable will be useful to shorten some calculations and facilitate an easier transition between different redshift parameterizations, something that will be addressed in future sub-chapters. Computing α in equation 3.4 results in an equation where α is described by a power series.

$$\alpha = t_H - \frac{q_0}{2}(t_H)^2 + \frac{j_0}{3!}(t_H)^3 + \frac{s_0}{4!}(t_H)^4 + \frac{c_0}{5!}(t_H)^5 + \frac{p_0}{6!}(t_H)^6 + O((t_H)^7) \tag{3.6}$$

This power series can be inverted so that now t_H is the one described by a power series as a function of α. [22]

$$\begin{aligned} t_H = {} & \alpha + \frac{q_0}{2}\alpha^2 + \frac{1}{3!}(-j_0 + 3q_0^2)\alpha^3 + \frac{1}{4!}(-10j_0q_0 + 15q_0^3 - s_0)\alpha^4 \\ & + \frac{1}{5!}(-c_0 + 10j_0^2 - 105j_0q_0^2 + 105q_0^4 - 15q_0s_0)\alpha^5 \\ & + \frac{1}{6!}(-21c_0q_0 + 280j_0^2q_0 - 1260j_0q_0^3 + 35j_0s_0 - p_0 + 945q_0^5 - 210q_0^2s_0)\alpha^6 + O(\alpha^7) \end{aligned} \tag{3.7}$$

Now, to obtain an expression for the redshift drift it is needed to compute the cosmographic expansion for the Hubble parameter. From the definition of Hubble parameter in equation 2.4 and writing it in respect for the variable t_H we will have

$$dt_H = H_0 dt \quad \text{then} \quad H = \frac{1}{a}\frac{da}{dt} = \frac{H_0}{a}\frac{da}{dt_H} \tag{3.8}$$

And so, the Hubble parameter as a function of t_H will be equal to

$$\begin{aligned} H(t_H) = H_0 \Bigg[& 1 + (-q_0 - 1)t_H + \frac{1}{2}(j_0 + 3q_0 + 2)t_H^2 + \frac{1}{3!}(-4j_0 - 3q_0^2 - 12q_0 + s_0 - 6)t_H^3 \\ & + \frac{1}{4!}(c_0 + 10j_0q_0 + 20j_0 + 30q_0^2 + 60q_0 - 5s_0 + 24)t_H^4 + \frac{1}{5!}(-6c_0 - 10j_0^2 - 120j_0q_0 \\ & - 120j_0 + p_0 - 30q_0^3 - 270q_0^2 + 15q_0s_0 - 360q_0 + 30s_0 - 120)t_H^5 + O(t_H^6) \Bigg] \end{aligned} \tag{3.9}$$

When combining equations 3.7 and 3.9 we obtain the cosmographic expansion until the fifth order of our chosen α.

$$\begin{aligned} H(\alpha) = H_0 \Bigg[& 1 + (-q_0 - 1)\alpha + \frac{1}{2}(j_0 - q_0^2 + 2q_0 + 2)\alpha^2 + \frac{1}{3!}(4j_0q_0 - 3j_0 - 3q_0^3 + 3q_0^2 + s_0 \\ & - 6q_0 - 6)\alpha^3 + \frac{1}{4!}(c_0 - 4j_0^2 + 25j_0q_0^2 - 16j_0q_0 + 12j_0 - 15q_0^4 + 12q_0^3 - 12q_0^2 + 7q_0s_0 \\ & - 4s_0 + 24q_0 + 24)\alpha^4 + \frac{1}{5!}(11c_0q_0 - 5c_0 - 70j_0^2q_0 + 20j_0^2 + 210j_0q_0^3 - 125j_0q_0^2 \\ & + 80j_0q_0 - 15j_0s_0 - 60j_0 + p_0 - 105q_0^5 + 75q_0^4 - 60q_0^3 + 60q_0^2s_0 + 60q_0^2 - 35q_0s_0 \\ & + 20s_0 - 120q_0 - 120)\alpha^5 + O(\alpha^6) \Bigg] \end{aligned} \tag{3.10}$$

Substituting α and expanding it for low redshifts

$$\alpha = \frac{1}{1+z} - 1 = -z + z^2 - z^3 + z^4 - z^5 + ... \tag{3.11}$$

We obtain the cosmographic expansion of the Hubble parameter as a function of z.

$$H(z) = H_0\Bigg[1 + (q_0+1)z + \frac{1}{2}\left(j_0 - q_0^2\right)z^2 + \frac{1}{3!}\left(-3j_0 - 4j_0q_0 + 3q_0^3 + 3q_0^2 - s_0\right)z^3 + \frac{1}{4!}\left(c_0 - 4j_0^2 + 25j_0q_0^2 + 32j_0q_0 + 12j_0 - 15q_0^4 - 24q_0^3 - 12q_0^2 + 7q_0s_0 + 8s_0\right)z^4 + \frac{1}{5!}\left(-11c_0q_0 - 15c_0 + 70j_0^2q_0 + 60j_0^2 - 210j_0q_0^3 - 375j_0q_0^2 - 240j_0q_0 + 15j_0s_0 - 60j_0 - p_0 + 105q_0^5 + 225q_0^4 + 180q_0^3 - 60q_0^2s_0 - 105q_0s_0 + 60q_0^2 - 60s_0\right)z^5 + O(z^6)\Bigg] \tag{3.12}$$

This expression is consistent to what is obtained from the literature [23]. Finally, we can get an expression for the redshift drift in terms of cosmographic coefficients when using equation 3.12 in equation 2.5. The cosmographic expansion for the redshift drift will be

$$\frac{\Delta z}{\Delta t} = -H_0\Bigg[q_0z + \frac{1}{2}\left(j_0 - q_0^2\right)z^2 + \frac{1}{3!}\left(-3j_0 - 4j_0q_0 + 3q_0^3 + 3q_0^2 - s_0\right)z^3 + \frac{1}{4!}\left(c_0 - 4j_0^2 + 25j_0q_0^2 + 32j_0q_0 + 12j_0 - 15q_0^4 - 24q_0^3 - 12q_0^2 + 7q_0s_0 + 8s_0\right)z^4 + \frac{1}{5!}\left(-11c_0q_0 - 15c_0 + 70j_0^2q_0 + 60j_0^2 - 210j_0q_0^3 - 375j_0q_0^2 - 240j_0q_0 + 15j_0s_0 - 60j_0 - p_0 + 105q_0^5 + 225q_0^4 + 180q_0^3 - 60q_0^2s_0 - 105q_0s_0 + 60q_0^2 - 60s_0\right)z^5 + O(z^6)\Bigg] \tag{3.13}$$

The same can be done as well for the spectroscopic velocity drift when inputting equation 3.12 in equation 2.6, obtaining

$$\Delta v = -\frac{cH_0\Delta t}{1+z}\Bigg[q_0z + \frac{1}{2}\left(j_0 - q_0^2\right)z^2 + \frac{1}{3!}\left(-3j_0 - 4j_0q_0 + 3q_0^3 + 3q_0^2 - s_0\right)z^3 + \frac{1}{4!}\left(c_0 - 4j_0^2 + 25j_0q_0^2 + 32j_0q_0 + 12j_0 - 15q_0^4 - 24q_0^3 - 12q_0^2 + 7q_0s_0 + 8s_0\right)z^4 + \frac{1}{5!}\left(-11c_0q_0 - 15c_0 + 70j_0^2q_0 + 60j_0^2 - 210j_0q_0^3 - 375j_0q_0^2 - 240j_0q_0 + 15j_0s_0 - 60j_0 - p_0 + 105q_0^5 + 225q_0^4 + 180q_0^3 - 60q_0^2s_0 - 105q_0s_0 + 60q_0^2 - 60s_0\right)z^5 + O(z^6)\Bigg] \tag{3.14}$$

3.1 Cosmography's shortcomings

As to be expected from such a simple way to describe the Universe, cosmography faces a lot of problems. There is a good reason why the most studied cosmographic coefficients are the deceleration parameter and the jerk. The Taylor series starts to diverge for redshifts bigger than 1, so coefficients that are well defined for low redshifts, like q and j, are more reliable and easy to study. Also, in equation 3.4 the fraction $1/(1+z)$ has a pole at $z=-1$ (a time in the future) which implies that the radius of convergence of the cosmographic series is at most equal to 1 [24] [25], i.e., the series will start to diverge for redshifts larger than 1. One way to mathematically tackle this problem is to create different parameterizations for the redshift instead of z (see sections 3.2 and 3.3). A new parameterization will not change any underlying physics and it will improve the convergence radius. It is also possible to use models based on rational approximations (see section 3.4) instead of polynomial approximations constructed when using a Taylor series. Furthermore, in parallel with the convergence issue, the cosmographic method is built around truncations of a Taylor series so deviations from the true values will most certainly occur when increasing the redshifts, worsening the predictability of this method at this domain.

The entanglement of cosmographic parameters is another problem that will always be present in cosmography. In the same way that it is possible to find a cosmographic series for $H(z)$, it is also possible to determine a cosmographic series for every other parameter. When doing that, we can verify that every parameter is expressed by combinations of the remaining parameters. This means that is impossible to measure those quantities directly since they can not be disentangled from each other. Although, there is an exception, the Hubble constant. It only appears in the description of the Hubble parameter (equation 3.12) as a multiplicative term and is never seen in any other cosmographic variable. The Hubble constant serves as an initial condition for cosmographic models[19].

By the definition of cosmography, the cosmographic coefficients are not know *a priori* but, during an analysis, it is necessary to establish a range of values in which the data will be constrained. The priors are usually built to constraint values for perturbations around the ΛCDM model. This implies that cosmography is very dependent of imposed cosmological priors. If the true values were from a range beyond the ΛCDM priors the analysis could still suggest that the data follows ΛCDM not because it is being predictive but because there wouldn't be a better solution.

3.2 Improved Redshift: y

One way to try to solve the convergence issues that cosmography suffers is to define another redshift parameterization. The improved redshift - y - was created with that purpose. This parametrization is commonly found in the literature [24]. In equation 2.2 we can see that redshift is defined as $(\lambda_0 - \lambda)/\lambda$. Why not define it as $(\lambda_0 - \lambda)/\lambda_0$? The y parameterization is defined by the previous relation. In terms of z, y is expressed as

$$y = \frac{z}{1+z} \tag{3.15}$$

This way past values for redshift are constrained between 0 and 1. The α for this parameterization is

$$\alpha = \frac{1}{1+z} - 1 = (1-y) - 1 = -y \tag{3.16}$$

Recalling equation 3.10 and inputting α accordingly we obtain the cosmographic expansion for the Hubble parameter as a function of y.

$$\begin{aligned} H(y) = H_0 \Bigg[& 1 - (-q_0 - 1)y + \frac{1}{2}(j_0 - q_0^2 + 2q_0 + 2)y^2 - \frac{1}{3!}(4j_0q_0 - 3j_0 - 3q_0^3 + 3q_0^2 + s_0 \\ & - 6q_0 - 6)y^3 + \frac{1}{4!}(c_0 - 4j_0^2 + 25j_0q_0^2 - 16j_0q_0 + 12j_0 - 15q_0^4 + 12q_0^3 - 12q_0^2 + 7q_0s_0 \\ & - 4s_0 + 24q_0 + 24)y^4 - \frac{1}{5!}(11c_0q_0 - 5c_0 - 70j_0^2q_0 + 20j_0^2 + 210j_0q_0^3 - 125j_0q_0^2 \\ & + 80j_0q_0 - 15j_0s_0 - 60j_0 + p_0 - 105q_0^5 + 75q_0^4 - 60q_0^3 + 60q_0^2s_0 + 60q_0^2 - 35q_0s_0 \\ & + 20s_0 - 120q_0 - 120)y^5 + O(y^6) \Bigg] \end{aligned} \tag{3.17}$$

Once more, the value obtained is in agreement with the literature [23] [26].

To obtain the redshift drift expressed in terms of y, and subsequently also the spectroscopic velocity drift, it is necessary to write Δz as a function of Δy.

$$\Delta z = \frac{\Delta y}{(1-y)^2} \tag{3.18}$$

Using this relation and recalling 2.5, we obtain the redshift drift (equation 3.19) and Δv (equation 3.20) for y.

$$\frac{\Delta y}{\Delta t} = (1-y)H_0 - (1-y)^2 H(y) \tag{3.19}$$

$$\Delta v = \frac{c\Delta y}{1-y} = cH_0\Delta t(1-(1-y)E(y)) \tag{3.20}$$

3.3 Exponential parameterization: x

Although in theory the improved redshift drift variable y should help with the convergence issues, studies keep suggesting that it fails to be predictive [19] [27]. So, one can test another parameterization for the redshift drift. The new variable x is equal to 3.21 as a function of z.

$$x = ln(1+z) \tag{3.21}$$

The new α will be

$$\alpha = \frac{1}{1+z} - 1 = e^{-x} - 1 \tag{3.22}$$

When expanding it for low redshifts we obtain

$$\alpha = -x + \frac{x^2}{2} - \frac{x^3}{3!} + \frac{x^4}{4!} - \frac{x^5}{5!} + ... \tag{3.23}$$

And just like what was previously made, the Hubble parameter will be equal to

$$\begin{aligned} H(x) = H_0 \Bigg[& 1 + (q_0+1)x + \frac{1}{2}\left(j_0 - q_0^2 + q_0 + 1\right)x^2 + \frac{1}{3!}\left(-4j_0q_0 + 3q_0^3 + q_0 - s_0 + 1\right)x^3 \\ & + \frac{1}{4!}\left(c_0 - 4j_0^2 + 25j_0q_0^2 + 8j_0q_0 + j_0 - 15q_0^4 - 6q_0^3 - q_0^2 + 7q_0s_0 + q_0 + 2s_0 + 1\right)x^4 \\ & + \frac{1}{5!}\Big(-11c_0q_0 - 5c_0 + 70j_0^2q_0 + 20j_0^2 - 210j_0q_0^3 - 125j_0q_0^2 - 20j_0q_0 + 15j_0s_0 - p_0 \\ & + 105q_0^5 + 75q_0^4 + 15q_0^3 - 60q_0^2s_0 - 35q_0s_0 + q_0 - 5s_0 + 1\Big)x^5 + O(x^6)\Bigg] \end{aligned} \tag{3.24}$$

Again, after determining the relation between Δx and Δz, it is possible to get the redshift drift and Δv expressed as a function of x.

$$\Delta z = e^{x}\Delta x \tag{3.25}$$

$$\frac{\Delta x}{\Delta t} = H_0 - e^{-x}H(x) \tag{3.26}$$

$$\Delta v = c\Delta x = cH_0\Delta t(1 - e^{-x}E(x)) \tag{3.27}$$

3.4 Rational model - Padé approximants

Another way to improve cosmography's issues is by utilizing Padé approximants. A Padé approximant is a rational function that best fits a given power series A(x) [28]. The numerator $p(x)$ will be a polynomial with degree m and the denominator $q(x)$ will have degree n.

$$A(x) = \sum a_i x^i = \frac{p(x)}{q(x)} = \frac{p_0 + p_1 x + p_2 x^2 + ... + p_m x^m}{1 + q_1 x + q_2 x^2 + ... + q_n x^n} \tag{3.28}$$

The values of m and n added together must be equal to the value of the power series last order, i. In this work i will always be equal to 5 since in all the previously constructed functions we have redshift truncations after the fifth order. The Padé approximants are usually referred as $[m/n]$. Below we have an example of the approximants $P[1/4]$ and $P[3/2]$.

$$P[1/4] = \frac{p_0 + p_1 x}{1 + q_1 x + q_2 x^2 + q_3 x^3 + q_4 x^4} \qquad P[3/2] = \frac{p_0 + p_1 x + p_2 x^2 + p_3 x^3}{1 + q_1 x + q_2 x^2} \tag{3.29}$$

Because a Padé approximant is a rational function, it has some advantages when comparing it with a polynomial model. Rational functions are less oscillatory than polynomial functions, can fit a wider range of curves and have outstanding asymptotic properties [29]. A Padé approximation has also another great property that differs from other rational approximations like rational Chebyshev. When most techniques only compact information already known, Padé approximants can provide new information about the power series [28]. Unfortunately, Padé approximants have the same drawbacks as rational functions as well. There is still no clear way to determine what is the best value to choose for the

degrees of the numerator and denominator and sometimes vertical nuisance asymptotes can appear in an unpredictable way [29].

More information about the determination of Padé approximants will be given in appendix A.

Chapter 4

Fiducial Models

Now it is time to test the cosmographic series developed in the last section. For that to happen, it is necessary to know the hyper-parameters of the cosmographic model, namely the set of values (H_0, q_0, j_0, s_0, c_0, p_0), for each fiducial model. It is worth noticing again that the value of H_0 only acts as a multiplicative factor in the description of the redshift drift. For that reason, H_0 will have a fixed value of 70 $km\ s^{-1}Mpc^{-1}$ throughout the rest of the work.

4.1 Flat ΛCDM model

The ΛCDM is the standard cosmological model. It is simple and can explain the large-scale structures of galaxies and the Universe's expansion for late and early epochs of its evolution. The model assumes that the Universe is dominated by non-relativistic matter and a dark energy component. To simplify even more this model, it will be considered that the Universe also has a flat geometry. This will help greatly in the calculation of cosmographic parameters as we will see. Furthermore, the dark energy is considered as described by a barotropic factor $w(a)$, a factor that represents the ratio between the pressure of the fluid p and its energy-density ρ.

To test the ΛCDM with a cosmographic approach, it is needed to know the respective Hubble parameter to get to the end goal of studying the redshift drift. Much like in section 3, we will take a general approach to determine the Hubble parameter since it can be useful for the next section where a perturbation of this model will be studied, the CPL parameterization.

Solving Einstein's Field Equations with in account all the previous assumptions, the normalized Hubble parameter will have the form [30]

$$E(a)^2 = \Omega_{m0} a^{-3} + (1 - \Omega_{m0}) F(a) \tag{4.1}$$

Where Ω_{m0} is the present day matter density parameter and the function $F(a)$ for a generic barotropic factor, $w(a)$, is equal to

$$F(a) = exp\left(-3 \int_1^a \frac{w(a) + 1}{a}\, da\right) \tag{4.2}$$

This function describes the dark energy component of the Universe and its expression is what distinguishes different dark energy models. The ΛCDM model has a barotropic factor equal to -1 which means that dark energy in this model exerts negative pressure and does not evolve with time. Its F(a) will be equal to 1 so equation 4.1 takes the form

$$E(a)^2 = \Omega_{m0} a^{-3} + (1 - \Omega_{m0}) \tag{4.3}$$

Rewriting it in function of z, we obtain the Hubble parameter as a function of redshift for the ΛCDM model.

$$H(z) = H_0 \sqrt{1 - \Omega_{m0} + \Omega_{m0}(1 + z)^3} \tag{4.4}$$

Expanding this expression in order of z and matching it with equation 3.12 it is possible to determine the present day cosmographic coefficients for the ΛCDM model.

$$q_0 = -1 + \frac{3}{2}\Omega_{m0} \qquad j_0 = 1 \qquad s_0 = 1 - \frac{9}{2}\Omega_{m0} \tag{4.5}$$

$$c_0 = 1 + 3\Omega_{m0} + \frac{27}{2}\Omega_{m0}^2 \qquad p_0 = 1 - \frac{27}{2}\Omega_{m0} - 81\Omega_{m0}^2 - \frac{81}{4}\Omega_{m0}^3 \tag{4.6}$$

As it can be verified in equation 4.5, the non obtainment of a j_0 equal to 1 with great precision is a great indicator that the Universe can not be described by a flat ΛCDM model. It is also possible to determine the present day matter density parameter from a sufficiently good determination of q_0. Again from 4.5, we obtain the value of $\Omega_{m0} = (2q_0 + 2)/3$.

We then tested the fitness of the cosmographic expansions for the parameterizations z, y, x and the best performing Padé approximants for z (z-P[3/2]), y (y-P[1,4]) and x (x-P[4,1]). The model studied has a Ω_{m0} equal to 0.3 so the hyper-parameters for it are

(70,-0.55,1,-0.35,3.115,-10.88675). Since the redshift drift is inherently dependent of the Hubble parameter, the relative error obtained from cosmographic approximations for that parameter can be used to understand the bias present in those expansions. In figure 4.1 we have the plot of the relative errors for the Hubble parameter in the range $0 < z < 6$ and the table 4.1 displays some relative errors for selected redshifts in percentage. As expected, all the studied functions are well suited to describe the Hubble parameter for redshifts below 1. The z parameterization of the redshift possesses the largest amount of relative error for high redshifts. The other two parameterizations without the use of Padé approximants perform better comparatively to z for higher redshifts with x being an all around better approximation. The use of Padé approximants reduces the relative error of the parameterizations indicating a better chance to predict true values, except for x-Padé[4/1] that is almost identical to the x parameterization for this ΛCDM model. For that reason, the values of the aforementioned cosmographic function are omitted in table 4.1.

The graphic for the spectroscopic velocity drift as a function of the redshift for the different cosmographic functions is shown in figure 4.2. In table 4.2 are presented the relative errors for Δv in the same way as table 4.1. There is a significant propagation of the errors from the Hubble parameter, demonstrating the necessity to find an extremely good approximation for the Hubble parameters so that redshift drift cosmography can be reliable at high redshifts.

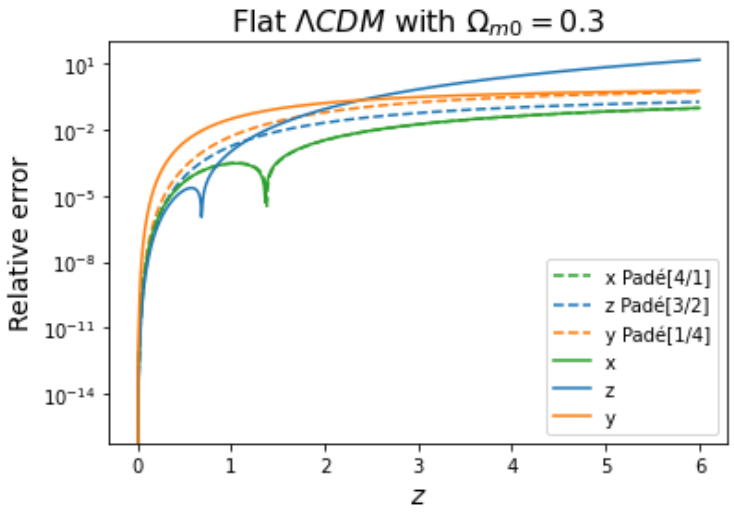

Figure 4.1: Relative error for the cosmographic expansion of the Hubble parameter for a flat ΛCDM model with $\Omega_{m0} = 0.3$. The solid lines represent traditional parameterizations and the dashed lines the Padé ones.

Hubble parameter relative error in %						
Cosmographic function	$z=1$	$z=2$	$z=3$	$z=4$	$z=5$	$z=6$
z	0.1%	9%	69%	260%	687%	1479%
y	3%	16%	31%	42%	52%	59%
x	0.03%	0.3%	2%	4%	7%	10%
z Padé[3/2]	0.2%	2%	6%	10%	14%	18%
y Padé[1/4]	0.5%	6%	18%	30%	41%	51%

Table 4.1: Relative error in percentage for the Hubble parameter cosmographic expansions of a ΛCDM model with $\Omega_{m0} = 0.3$ for some selected values of z. The values for z-Padé[4,1] were omitted for this model since they are indistinguishable from the regular x parameterization.

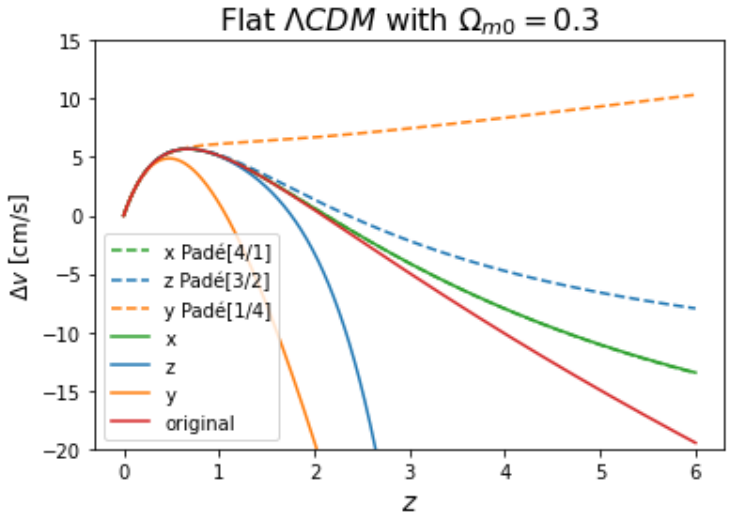

Figure 4.2: Plot of the spectroscopic velocity drift as a function of redshift for the the studied cosmographic expansions. The solid red line represents the original Δv curve, the other lines have the same color labels as figure 4.1.

Δv relative error in %						
Cosmographic function	$z=1$	$z=2$	$z=3$	$z=4$	$z=5$	$z=6$
z	0.8%	770%	665%	1359%	2658%	4735%
y	79%	4139%	870%	694%	668%	674%
x	0.2%	30%	17%	21%	26%	31%
z Padé[3/2]	1%	184%	56%	53%	56%	59%
y Padé[1/4]	19%	1296%	251%	183%	162%	153%

Table 4.2: Relative error in percentage for the spectroscopic velocity drift cosmographic expansions of a ΛCDM model with $\Omega_{m0} = 0.3$ for some selected values of z. Once again, the values for z-Padé[4,1] were omitted.

4.2 Flat CPL model

Although the ΛCDM model explains most of the Universe's properties it is not infallible, possessing some big unanswered problems, some of them cited in section 1. Alternative theories are constantly being proposed, but not every new theory will be compatible with cosmography. Modified gravity theories incompatible with a FLRW space-time framework are not suitable to be utilized in standard cosmography by definition. By contrast, models that will only differ in the form that characterize dark energy evolution can be evaluated using cosmography. One such example is the Chevallier-Polarski-Linder parameterization, CPL for short [31][32]. The model surges from the idea to describe the barotropic factor as a Taylor expansion with the form

$$w(a) = \sum w_i (1-a)^i \tag{4.7}$$

It is used the scale factor instead of the redshift directly because this way no divergences occur for small z, making it more physical [19]. When the barotropic factor is truncated at the first order we obtain the CPL model. The barotropic factor will then be

$$w(a) = w_0 + w_1(1-a) \tag{4.8}$$

The new $F(a)$ will be

$$F(a) = a^{-3(1+w_0+w_1)} exp(-3w_1(1-a)) \tag{4.9}$$

And finally we obtain $H(z)$ for the CPL model.

$$H(z) = H_0 \sqrt{\Omega_{m0}(1+z)^3 + (1-\Omega_{m0})(1+z)^{3(1+w_0+w_1)} exp\left(-\frac{3w_1 z}{1+z}\right)} \tag{4.10}$$

Doing the same procedure as section 4.1, once again we obtain the present day cosmographic parameters values.

$$q_0 = \frac{1}{2}(w_0(3-3\Omega_{m0}) + 1) \tag{4.11}$$

$$j_0 = \frac{1}{2}(w_1(3-3\Omega_{m0}) + w_0^2(9-9\Omega_{m0}) + w_0(9-9\Omega_{m0}) + 2) \tag{4.12}$$

$$s_0 = \frac{1}{4}(w_1(33\Omega_{m0} - 33) + w_0^3(-27\Omega_{m0}^2 + 108\Omega_{m0} - 81) + w_0^2(-27\Omega_{m0}^2 + 171\Omega_{m0} - 144) + w_0(81\Omega_{m0} + w_1(-9\Omega_{m0}^2 + 72\Omega_{m0} - 63) - 81) - 14) \tag{4.13}$$

$$c_0 = \frac{1}{4}(w_1^2(9\Omega_{m0}^2 - 72\Omega_{m0} + 63) + w_1(213 - 213\Omega_{m0}) + w_0^4(324\Omega_{m0}^2 - 810\Omega_{m0} + 486) + w_0^3(648\Omega_{m0}^2 - 1917\Omega_{m0} + 1269) + w_0^2(378\Omega_{m0}^2 - 1584\Omega_{m0} + w_1(297\Omega_{m0}^2 - 918\Omega_{m0} + 621) + 1206) + w_0(-489\Omega_{m0} + w_1(189\Omega_{m0}^2 - 927\Omega_{m0} + 738) + 489) + 70) \tag{4.14}$$

$$p_0 = \frac{1}{8}(w_1^2(-459\Omega_{m0}^2 + 2502\Omega_{m0} - 2043) + w_1(3321\Omega_{m0} - 3321) + w_0^5(972\Omega_{m0}^3 - 8262\Omega_{m0}^2 + 14580\Omega_{m0} - 7290) + w_0^4(1944\Omega_{m0}^3 - 23409\Omega_{m0}^2 + 46818\Omega_{m0} - 25353) + w_0^3(1134\Omega_{m0}^3 - 23814\Omega_{m0}^2 + 57267\Omega_{m0} + w_1(891\Omega_{m0}^3 - 11745\Omega_{m0}^2 + 24057\Omega_{m0} - 13203) - 34587) + w_0^2(-9315\Omega_{m0}^2 + 32328\Omega_{m0} + w_1(567\Omega_{m0}^3 - 16065\Omega_{m0}^2 + 41013\Omega_{m0} - 25515) - 23013) + w_0(7407\Omega_{m0} + w_1^2(27\Omega_{m0}^3 - 1863\Omega_{m0}^2 + 5265\Omega_{m0} - 3429) + w_1(-5508\Omega_{m0}^2 + 21645\Omega_{m0} - 16137) - 7407) - 910) \tag{4.15}$$

Since the ΛCDM model is equal to a CPL model with $w_0 = -1$ and $w_1 = 0$, it is easy to confirm that the above equations for the present day cosmographic parameters are consistent with the ones obtained in the previous section. It is also consistent with lower order expansions found in the literature [26].

With a little algebra, one can obtain the CPL parameters from those present day parameters. For the model be fully described it is only needed to know the cosmographic parameters q_0, j_0 and s_0.

$$w_0 = \frac{1 - 2q_0}{3(\Omega_{m0} - 1)} \tag{4.16}$$

$$w_1 = \frac{(-2j_0 + 6q_0 - 1)\Omega_{m0} + 2j_0 - 4q_0^2 - 2q_0}{3(\Omega_{m0} - 1)^2} \tag{4.17}$$

$$\Omega_{m0} = \frac{8j_0q_0 + 7j_0 - 16q_0^2 + 2q_0 + 2s_0 - 1 + (1 - 2q_0)\sqrt{f(q_0, j_0, s_0)}}{2j_0q_0 + 10j_0 - 8q_0 + 2s_0} \tag{4.18}$$

$$f(q_0, j_0, s_0) = 9j_0^2 + 8j_0q_0^2 - 12j_0q_0 - 14j_0 + 32q_0^2 + 8q_0s_0 - 4s_0 + 1 \tag{4.19}$$

To test the fitness of the cosmographic series studied, we calculated the mean relative error for the Hubble parameter curve in the interval $0 < z < 6$ as a function of the CPL model hyper-parameters (the set (Ω_{m0}, w_0, w_1)). The results are plotted from figures 4.3 - 4.5. The best performing parameterizations are x, z-Padé[3/2] and x-Padé[4/1], although x-Padé[4/1] is very similar to x for CPL parameters values close to ΛCDM. The usual z parameterization presents higher mean relative errors when compered with other options, meaning that is less likely to reflect the true cosmographic values upon an analysis. It is also relevant to notice that Padé approximants have generally lower mean relative errors. It also seems that cosmographic series that use Padé approximants have lower mean relative errors, sometimes two orders of magnitude lower. Curiously, the mean relative error of the y parameterization is independent of every CPL parameters chosen, at least around ΛCDM values.

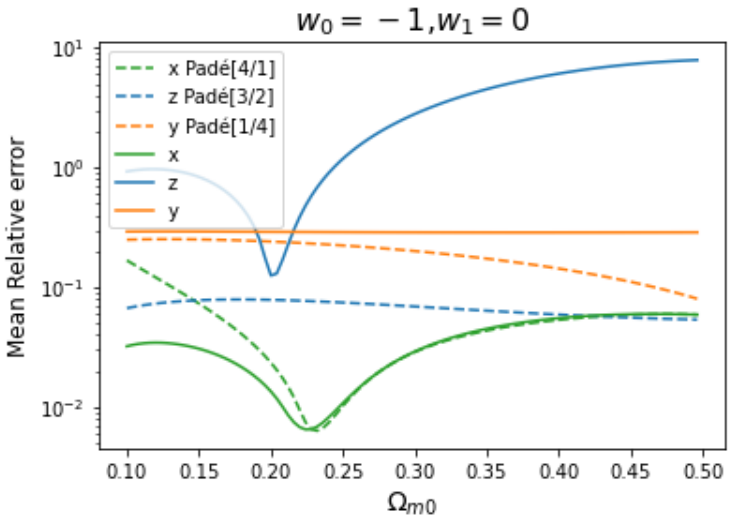

Figure 4.3: Mean relative error of the Hubble parameter in the redshift range $0 < z < 6$ as a function of Ω_{m0} for each cosmographic series.

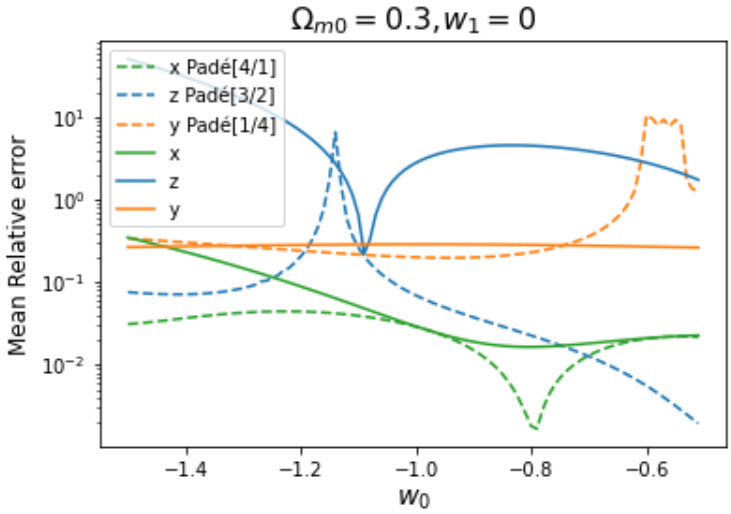

Figure 4.4: Mean relative error of the Hubble parameter in the redshift range $0 < z < 6$ as a function of w_0 for each cosmographic series.

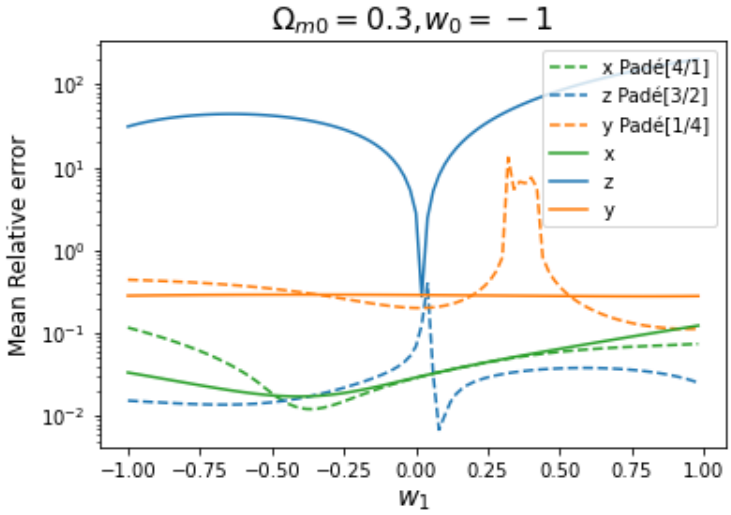

Figure 4.5: Mean relative error of the Hubble parameter in the redshift range $0 < z < 6$ as a function of w_1 for each cosmographic series.

Chapter 5

Forecasts

As seen in the previous sections, it will be crucial to determine if a cosmographic approach will be useful to retrieve information from the future redshift drift measurements for low and high redshift regimes. For the estimation of the future data measurements, we used a Markov Chain Monte Carlo (MCMC) code named *emcee* for *Python* [33]. For the visualization of the MCMC results the *Python*'s module *corner* was utilized [34]. Next, one needs to define cosmological priors for the cosmographic parameters. Some typical values found in the literature, for example the one found in Dunsby and Luongo [19], consist of uninformative uniform priors with: $q_0 \in [-0.95, -0.3]$, $j_0 \in [0, 2]$, $s_0 \in [-2, 7]$, $c_0 \in [-5, 10]$, $p_0 \in [-10, 50]$. These values will be slightly increased because the models studied will have parameters beyond the previously presented ranges (for example the p_0 for the ΛCDM model is equal to -10.88675), and are shown in table 5.1. For the present day Hubble constant we assumed two scenarios, the first one being an uniform prior with values between $[60, 80]$. Since other types of data that set smaller bounds for the values of H_0 can be used to constrain better the cosmographic parameters [35], the second case will be a prior where H_0 is described by a normal distribution with a standard deviation equal to 3 $km\ s^{-1}Mpc^{-1}$. The value for the standard deviation was chosen to closely resemble the ones from the literature for observations of H_0 [36].

Cosmological priors used		
Parameter	Uniform H_0 (U)	Normal distribution H_0 (N)
H_0	$[60, 80]$	$\mathcal{N}(70, 3^2)$
q_0	$[-1, 1]$	$[-1, 1]$
j_0	$[-10, 10]$	$[-10, 10]$
s_0	$[-30, 30]$	$[-30, 30]$
c_0	$[-50, 50]$	$[-50, 50]$
p_0	$[-100, 100]$	$[-100, 100]$

Table 5.1: Cosmological priors used

5.1 SKA

The Square Kilometer Array or SKA when completed will be the world's largest radio telescope. As it is planned, its construction will be divided in two phases. Phase 1 will represent about 10% - 20% of the final array with telescopes in Australia and South Africa. Phase 2 will correspond to the phase where construction will be fully completed with the addition of more telescopes in the previous countries plus some in other African nations [37]. It was conceptualized to explore the evolution of the Universe from the observation of hydrogen and will study areas like planetary formation, gravitational waves, cosmology and dark energy. It will also in theory be capable to study real-time cosmology from the observation of the shift in frequency of natural hydrogen, as seen in section 2.1.2. In the book "Advancing Astrophysics with the Square Kilometre Array" published by the SKA Organisation there is an article written by Klöckner et al. [6] detailing the experiment. It will consist of measurements of the 21 cm line frequency shifts for billions of Milky Way-type galaxies for any given redshift bin during two distinct epochs in time. The high number of measurements will compensate its uncertainties leading to a precision in the determination of the frequency shift of about 0.001 Hz. This value will translate to a precision of a few cm/s per year for the spectral velocity drift making possible the distinction between different cosmological models. These observations will have to take in account systematic errors by peculiar velocities from the galaxies, obtained when these are under influence of a local gravitational well which makes them stray away from the Hubble flow. Other sources of uncertainties come from changes in the position of the array of telescopes caused by, for example, plate tectonics and tides (as mentioned in section 2), and technical limitations of the hardware.

We follow the recipe for the uncertainties for the spectral velocity drift for SKA phase 2 presented in Martins et al. [7]. For this phase, the observations will take 125 days with the

possibility to repeat the experiment several times during the period that SKA will function, which will be about 50 years. In total there will be 10 bins equally spaced between the redshift values 0.1 to 1. The uncertainties will range from 1% of the Δv for the redshift bin at $z = 0.1$ and 10% for $z = 1$. We generated a mock data set for a flat ΛCDM model with $\Omega_{m0} = 0.3$. (figure 5.1) with these expected uncertainties and conducted an MCMC analysis for the cosmographic series of z, z-Padé[3/2] and x. This mock data, as well as future ones, were created without the expected dispersion from the measurements, since the main objective is to test the different cosmographic expansions and the dispersion would only introduce extra variance. Nonetheless, a case with the presence of dispersion in the data was studied in appendix B.

Firstly we studied the case with a uniform prior for the value of H_0 (U prior) and then the normal distribution prior (N prior). The results for the first are shown in figures 5.2-5.4 and in table 5.2 while for the second in figures 5.5-5.7 and in table 5.3. It was observed that all the tested cosmographic expansions present similar constraints for all the parameters that are not H_0. While there is no significant reduction in the uncertainties obtained for the cosmographic parameters, the N prior proved to be able to capture the true values more accurately than the use of the U prior. For that reason, for the future data estimations only the N prior will be used. The z expansion presents lower uncertainties for the c_0 and p_0 values. The expansion for z-Padé[3/2] appears to be worse than the others at predicting true values in the low redshift regime.

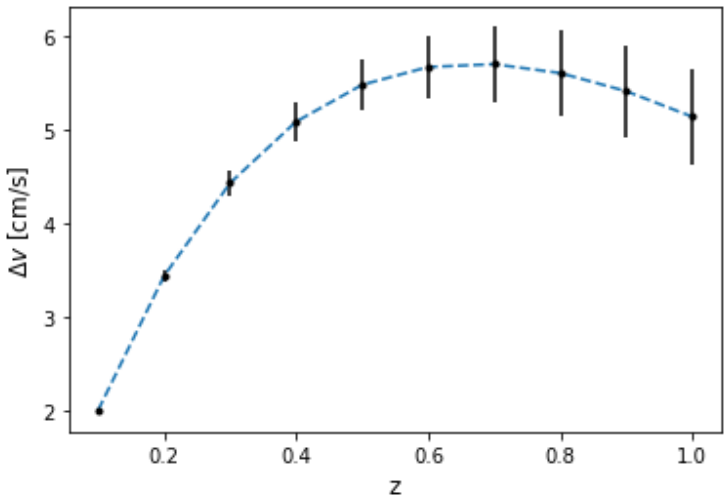

Figure 5.1: Spectroscopic velocity drift mock data for SKA observations from a flat ΛCDM model with $\Omega_{m0} = 0.3$. The blue dashed line represents the true curve for this fiducial model.

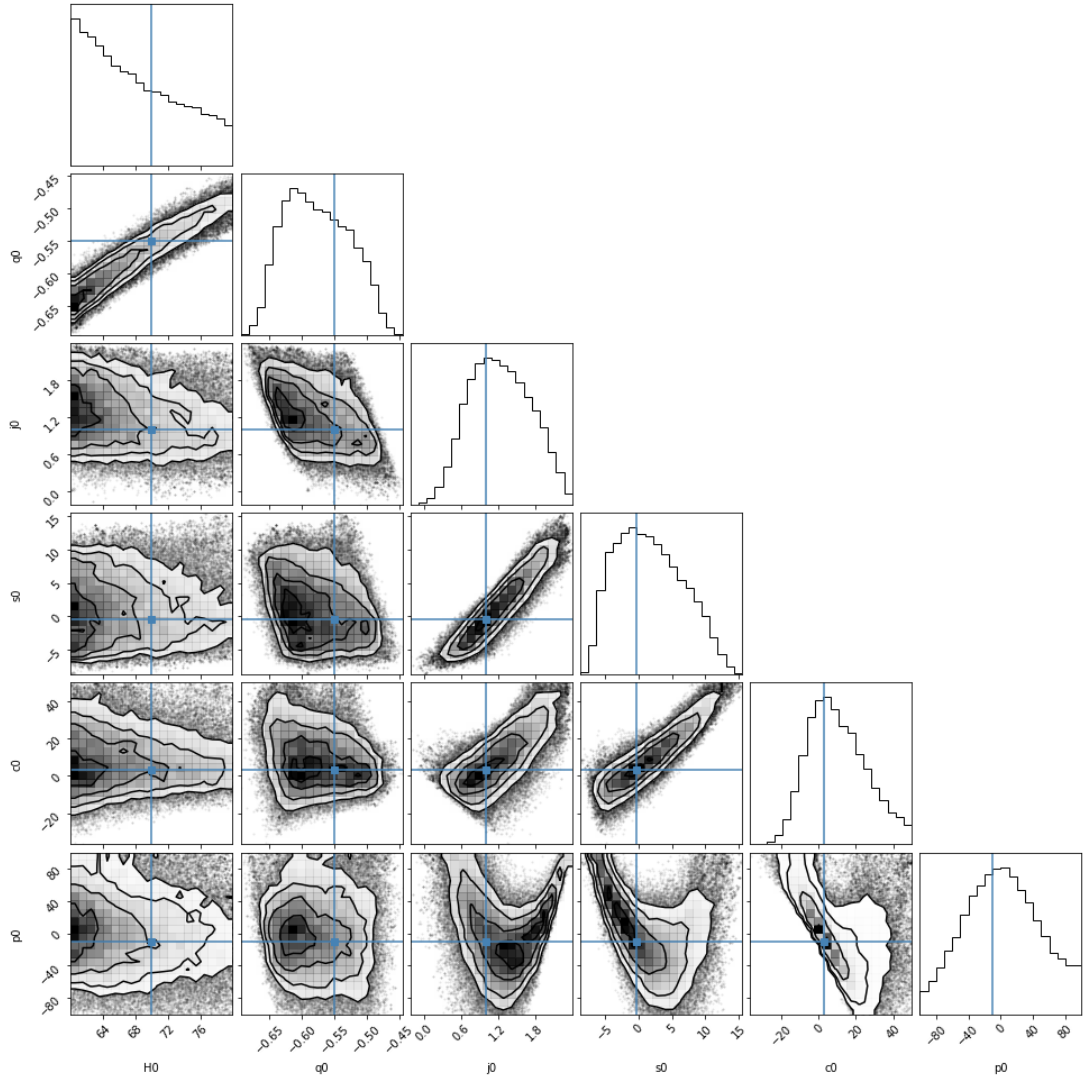

Figure 5.2: Corner plot for the cosmographic parameters obtained from SKA data when using only the z redshift parameterization and U prior. In blue we have the true values for each parameter.

SKA Results for the U prior				
Parameters	Expected	z	z-P[3/2]	x
H_0	70	$66.96^{+7.71}_{-5.07}$	$68.46^{+7.53}_{-6.05}$	$68.09^{+7.47}_{-5.78}$
q_0	-0.55	$-0.58^{+0.06}_{-0.05}$	$-0.55^{+0.06}_{-0.05}$	$-0.56^{+0.06}_{-0.05}$
j_0	1	$1.21^{+0.56}_{-0.50}$	$0.66^{+0.38}_{-0.32}$	$0.96^{+0.58}_{-0.57}$
s_0	-0.35	$1.32^{+5.93}_{-4.89}$	$-4.95^{+3.49}_{-2.96}$	$-0.88^{+5.41}_{-6.09}$
c_0	3.115	$8.37^{+18.08}_{-13.69}$	$-20.71^{+24.08}_{-20.17}$	$1.65^{+19.13}_{-26.27}$
p_0	-10.88675	$1.03^{+49.81}_{-46.58}$	$7.91^{+63.43}_{-69.58}$	$4.65^{+63.85}_{-69.05}$

Table 5.2: MCMC results for SKA observations with uninformative priors

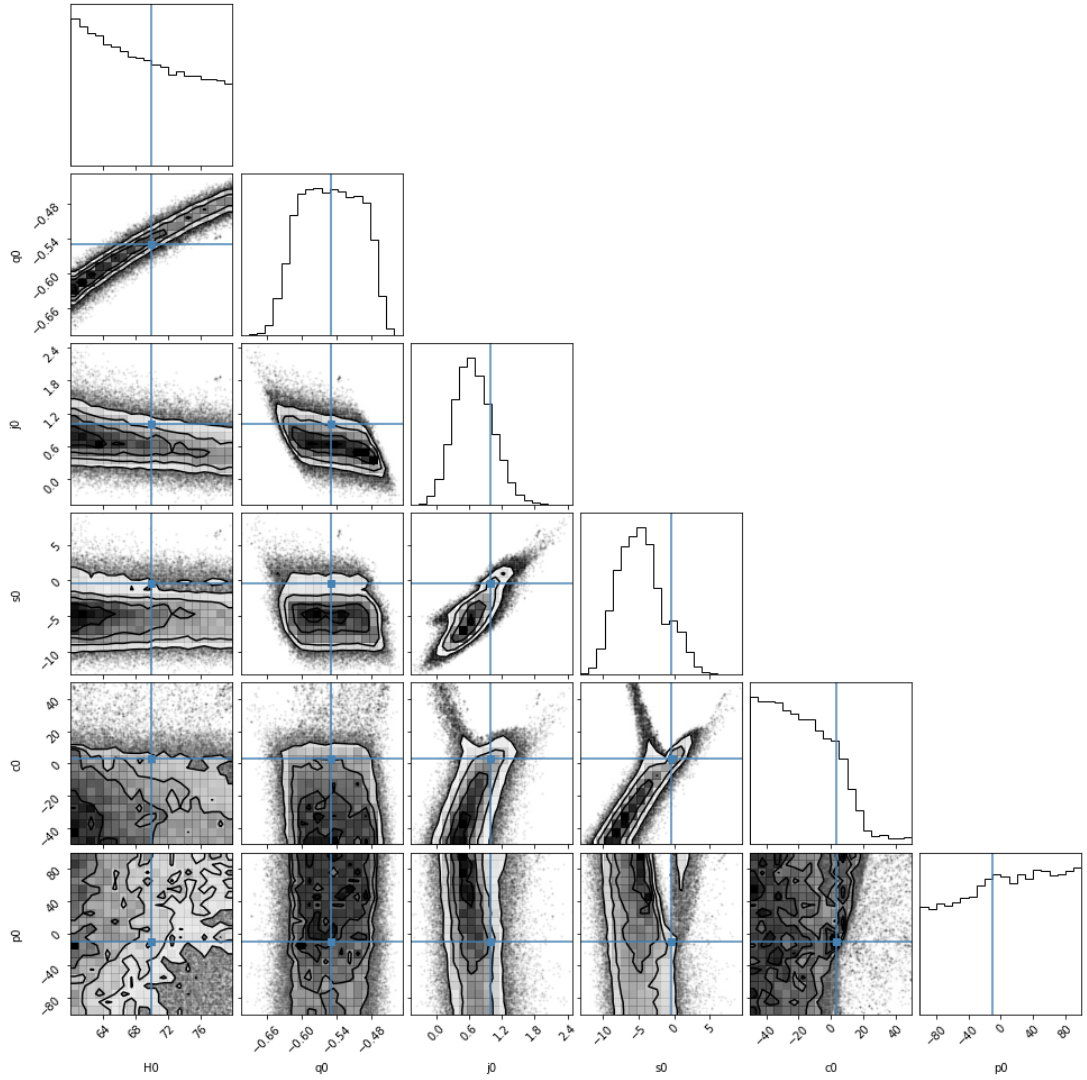

Figure 5.3: Corner plot for the cosmographic parameters obtained from SKA data when using the z redshift parameterization with Padé approximant [3/2] and U prior. In blue we have the true values for each parameter.

SKA Results for the N prior				
Parameters	Expected	z	z-P[3/2]	x
H_0	70	$69.49^{+3.06}_{-3.04}$	$69.74^{+2.96}_{-3.03}$	$69.642^{+3.02}_{-3.00}$
q_0	-0.55	$-0.56^{+0.03}_{-0.03}$	$-0.54^{+0.03}_{-0.03}$	$-0.55^{+0.03}_{-0.03}$
j_0	1	$1.17^{+0.56}_{-0.50}$	$0.63^{+0.36}_{-0.31}$	$0.93^{+0.57}_{-0.55}$
s_0	-0.35	$1.18^{+6.18}_{-4.83}$	$-5.03^{+3.18}_{-2.88}$	$-1.03^{+5.46}_{-5.95}$
c_0	3.115	$8.21^{+18.13}_{-13.14}$	$-20.79^{+23.45}_{-20.26}$	$1.48^{+19.09}_{-26.79}$
p_0	-10.88675	$-0.36^{+53.03}_{-46.11}$	$6.27^{+64.14}_{-70.07}$	$3.66^{+64.92}_{-68.47}$

Table 5.3: MCMC results for SKA observations with a normal distribution prior for H_0

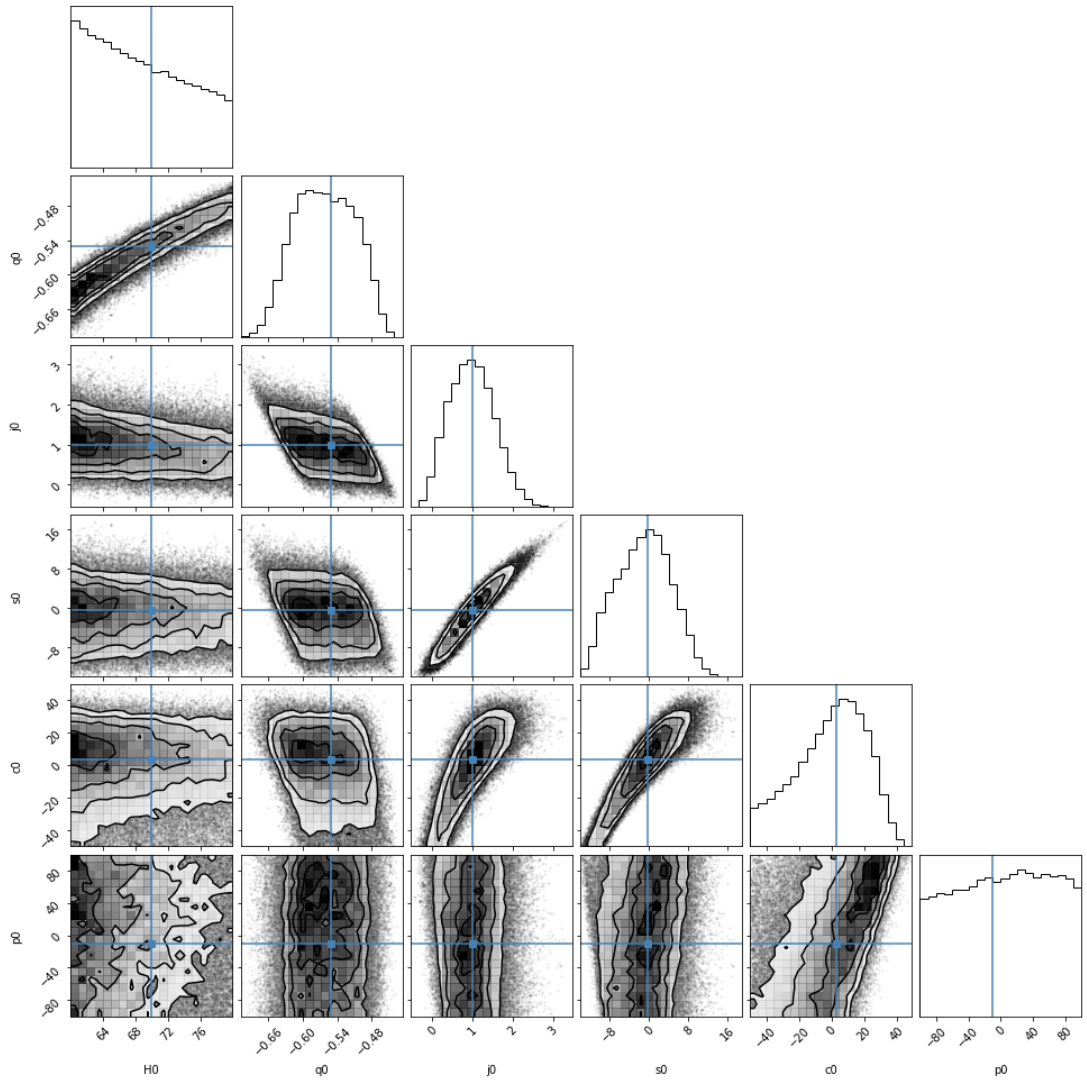

Figure 5.4: Corner plot for the cosmographic parameters obtained from SKA data when using only the x redshift parameterization and U prior. In blue we have the true values for each parameter.

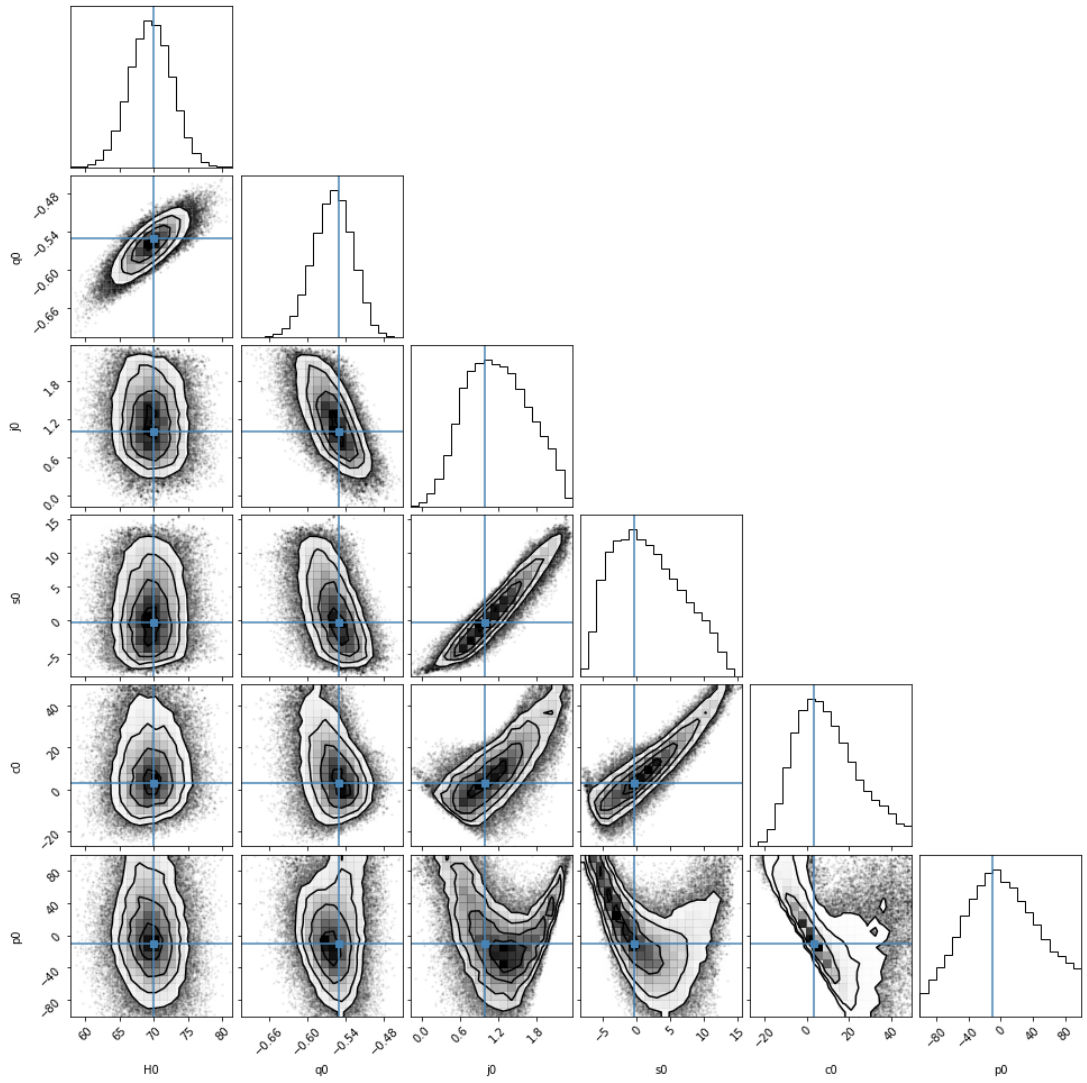

Figure 5.5: Corner plot for the cosmographic parameters obtained from SKA data when using only the z redshift parameterization and N prior. In blue we have the true values for each parameter.

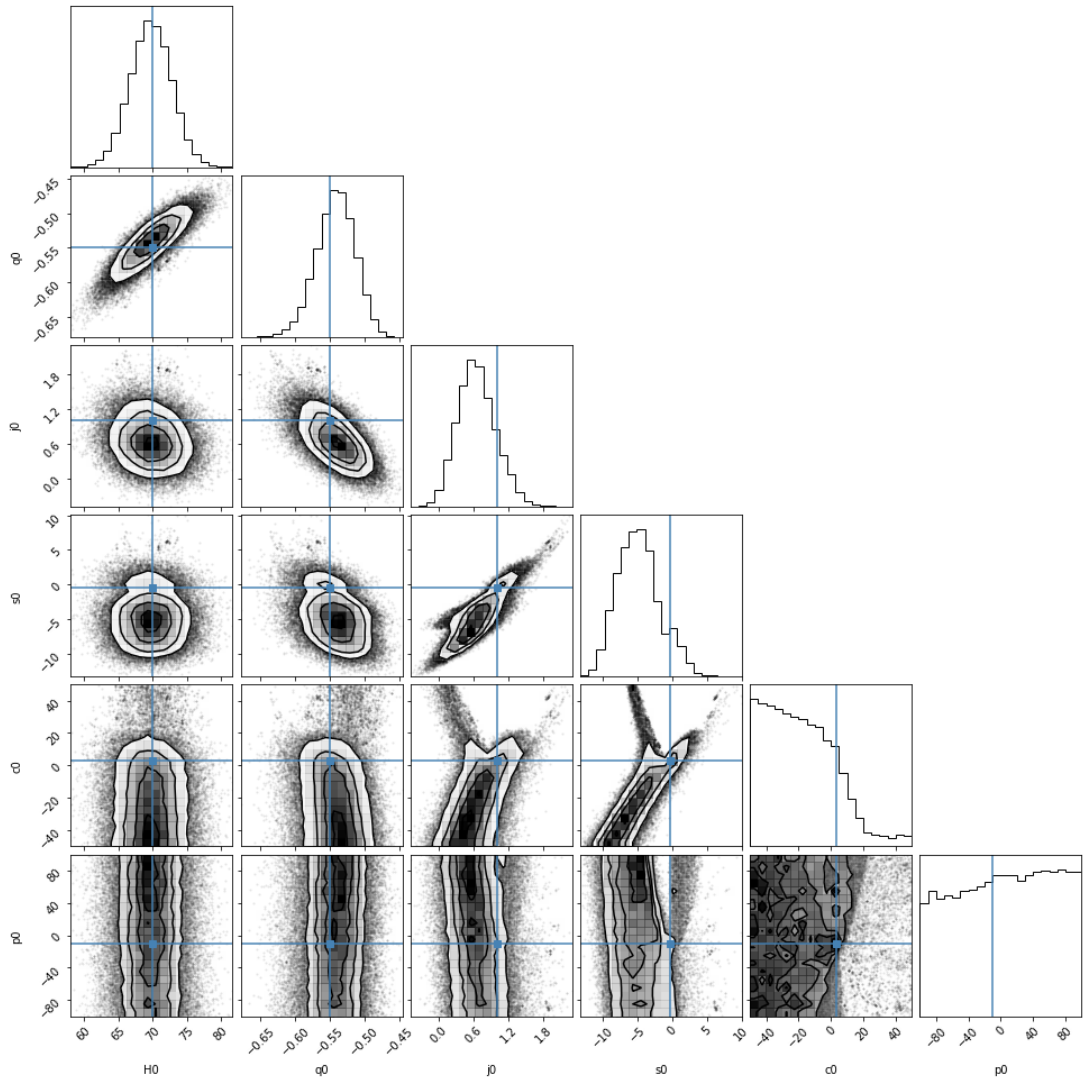

Figure 5.6: Corner plot for the cosmographic parameters obtained from SKA data when using the z redshift parameterization with Padé approximant [3/2] and N prior. In blue we have the true values for each parameter.

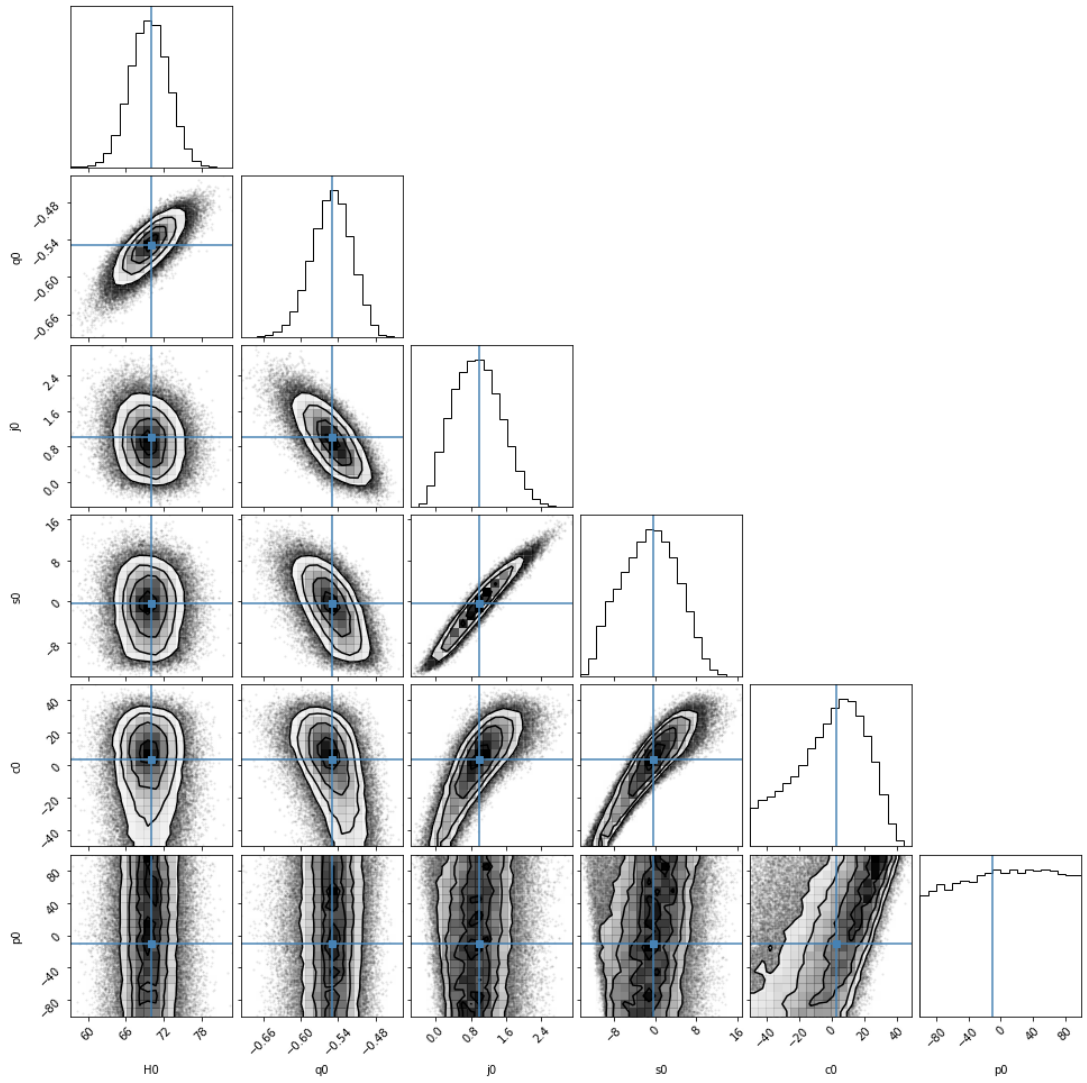

Figure 5.7: Corner plot for the cosmographic parameters obtained from SKA data when using only the x redshift parameterization and N prior. In blue we have the true values for each parameter.

5.2 ELT

Another facility that will be capable to measure the expansion of the Universe in real-time is the European Extremely Large Telescope or simply ELT. Upon its completion this telescope situated in the Atacama desert will have a main mirror with a diameter of 39 meters and will be biggest visible and infrared spectrum telescope in the world [38]. These specifications will enable redshift drift measurements from the Lyman-α absorption lines, previously discussed in section 2.1.1, by the HIgh REsolution Spectrograph (HIRES) that will be integrated on the ELT. Just as the measurements that will be obtained from SKA, ELT measurements will have to take in account other phenomena capable of interfering with the absorption lines. A study on the uncertainties obtained when measuring Lyman-α was made in the article of Liske et al. [4]. This article had an influence in the development of the COsmic Dynamics and EXo-earth experiment (CODEX), a proposed spectrograph to be added to the ELT and predecessor of the HIRES [39]. Some of the phenomena studied were the presence of peculiar motions, just like for SKA, galactic feedback and optical depth variations. It was concluded that none of them will have a significant impact on the observations, something very cited in the literature [40] [41]. Technological limitations were also taken in account being concluded that the redshift drift measurements demand a long telescope time (at least 4000 h of observing time).

In the same article the authors obtained one expression for the spectroscopic velocity drift uncertainties. That expression can be seen in equation 5.1 and it is dependent on the signal to noise ratio (S/N) of the spectra, the number of background QSO's observed for each bin (N_{QSO}) and respective redshift (z_{QSO}).

$$\sigma_{\Delta v} = 1.35 \frac{2370}{S/N} \sqrt{\frac{30}{N_{QSO}}} \left(\frac{5}{1+z_{QSO}} \right)^{x} \quad \text{, with } x = \begin{cases} 1.7, & \text{if } z \leq 4. \\ 0.9, & \text{otherwise.} \end{cases} \tag{5.1}$$

The signal to noise ratio will be assumed to being approximately equal to 3000 and the number of quasi-stellar objects (N_{QSO}) observed for each bin 10. The redshift bins will be 10 and equally spaced from redshifts 2 to 5. The time span of the observations will be chosen to be 20 years. Doing a similar procedure as in the previous section, we generated a mock data set (figure 5.8) and made an MCMC analysis. The results obtained are shown in figures 5.9-5.11 and in table 5.4. All cosmographic expansions have trouble when predicting values for q_0 since this parameter is preponderant only for lower redshift

regimes as said before. The z parameterization shows to be capable to predict parameters dependent on the high redshift regimes with good constraints (s_0, c_0 and p_0). Once again, z-Padé[3/2] appears to be worse than the other expansion at predicting cosmographic parameters.

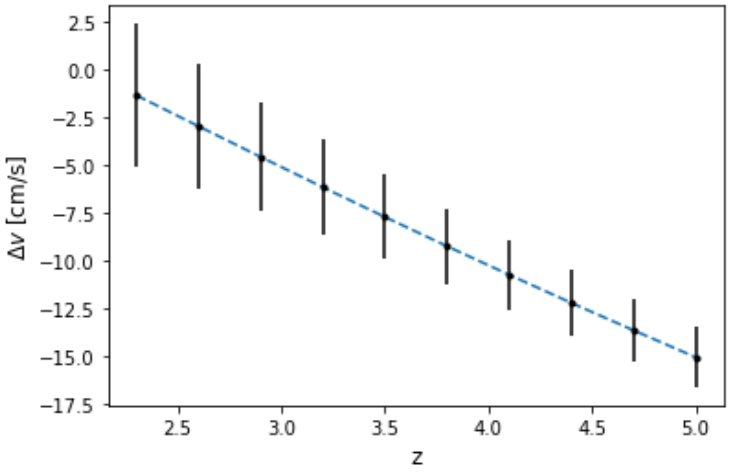

Figure 5.8: Spectroscopic velocity drift mock data for ELT observations from a flat ΛCDM model with $\Omega_{m0} = 0.3$. The blue dashed line represents the true curve for this fiducial model.

ELT results for the N prior				
Parameters	Expected	z	z-P[3/2]	x
H_0	70	$69.49^{+3.06}_{-3.18}$	$70.16^{+3.00}_{-3.05}$	$69.71^{+3.03}_{-3.04}$
q_0	-0.55	$-0.83^{+0.19}_{-0.12}$	$-0.54^{+0.40}_{-0.32}$	$-0.22^{+0.40}_{-0.38}$
j_0	1	$1.23^{+0.31}_{-0.38}$	$-0.08^{+1.48}_{-1.35}$	$0.34^{+1.17}_{-1.32}$
s_0	-0.35	$-0.15^{+0.65}_{-0.59}$	$-7.29^{+6.28}_{-4.72}$	$-0.06^{+5.54}_{-4.82}$
c_0	3.115	$3.46^{+0.87}_{-0.84}$	$-18.68^{+28.51}_{-22.30}$	$1.69^{+24.15}_{-21.07}$
p_0	-10.88675	$-12.50^{+3.37}_{-4.16}$	$5.20^{+65.83}_{-68.61}$	$5.38^{+59.38}_{-63.82}$

Table 5.4: MCMC results for ELT observations with a normal distribution prior for H_0

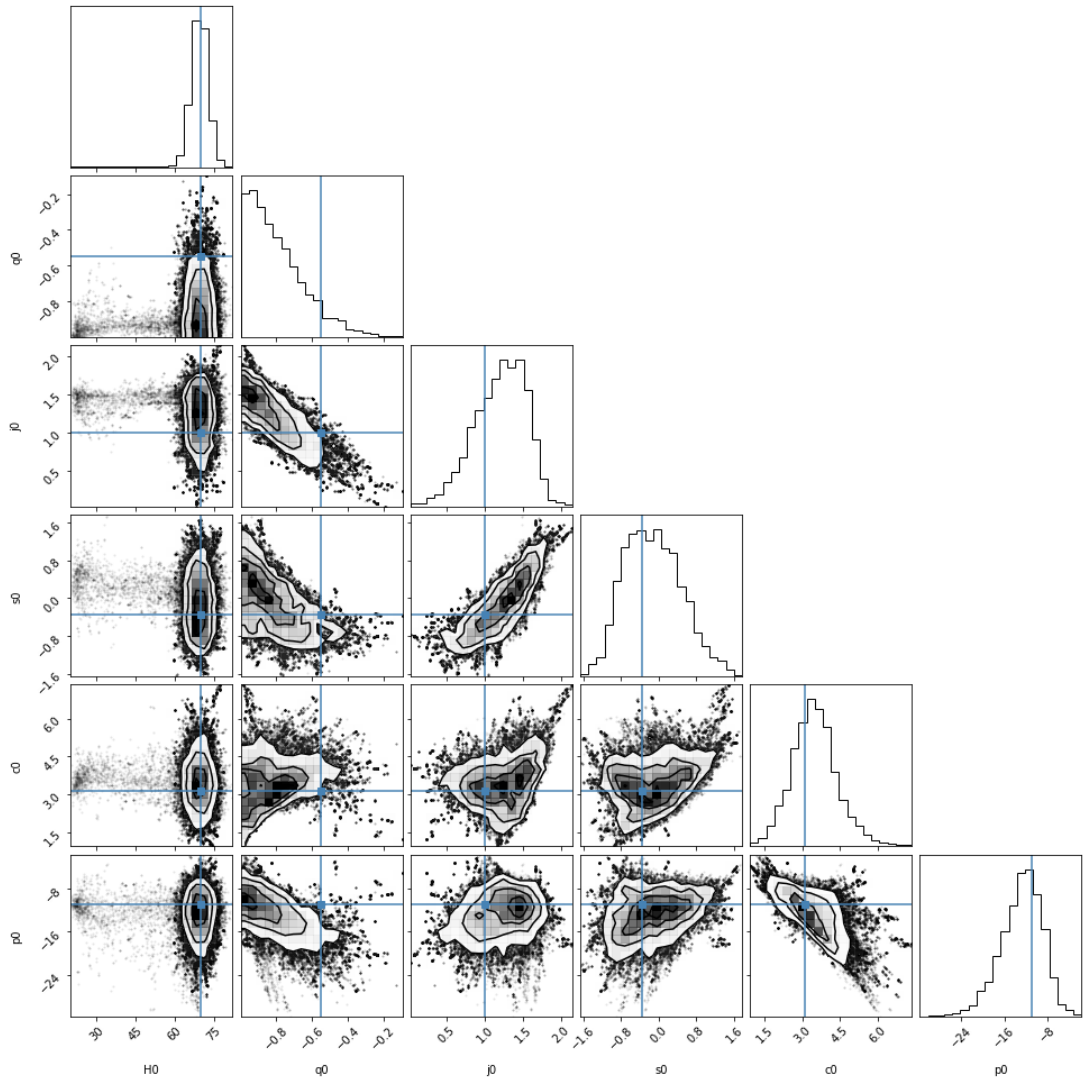

Figure 5.9: Corner plot for the cosmographic parameters obtained from ELT data when using only the z redshift parameterization and N prior. In blue we have the true values for each parameter.

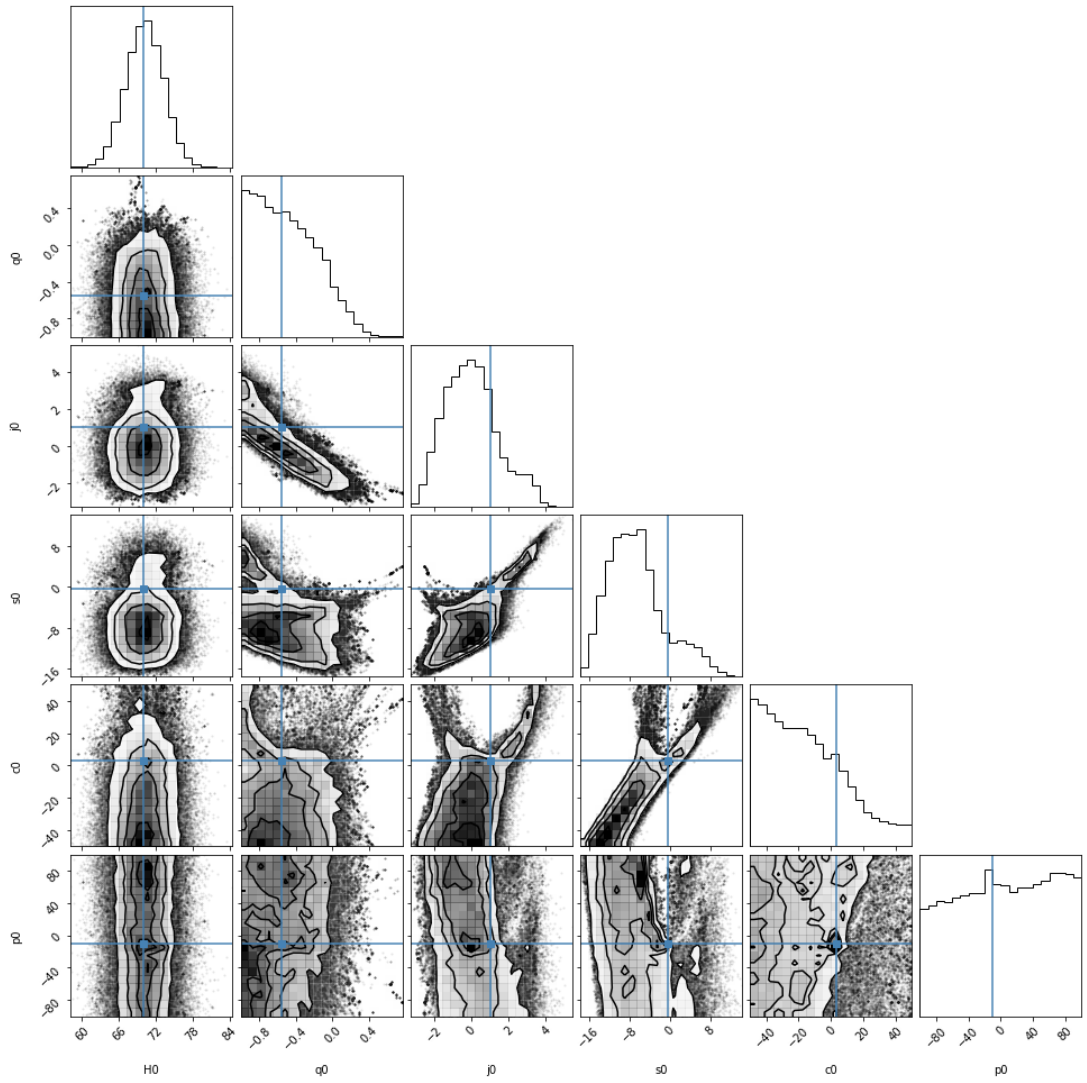

Figure 5.10: Corner plot for the cosmographic parameters obtained from ELT data when using the z redshift parameterization with Padé approximant [3/2] and N prior. In blue we have the true values for each parameter.

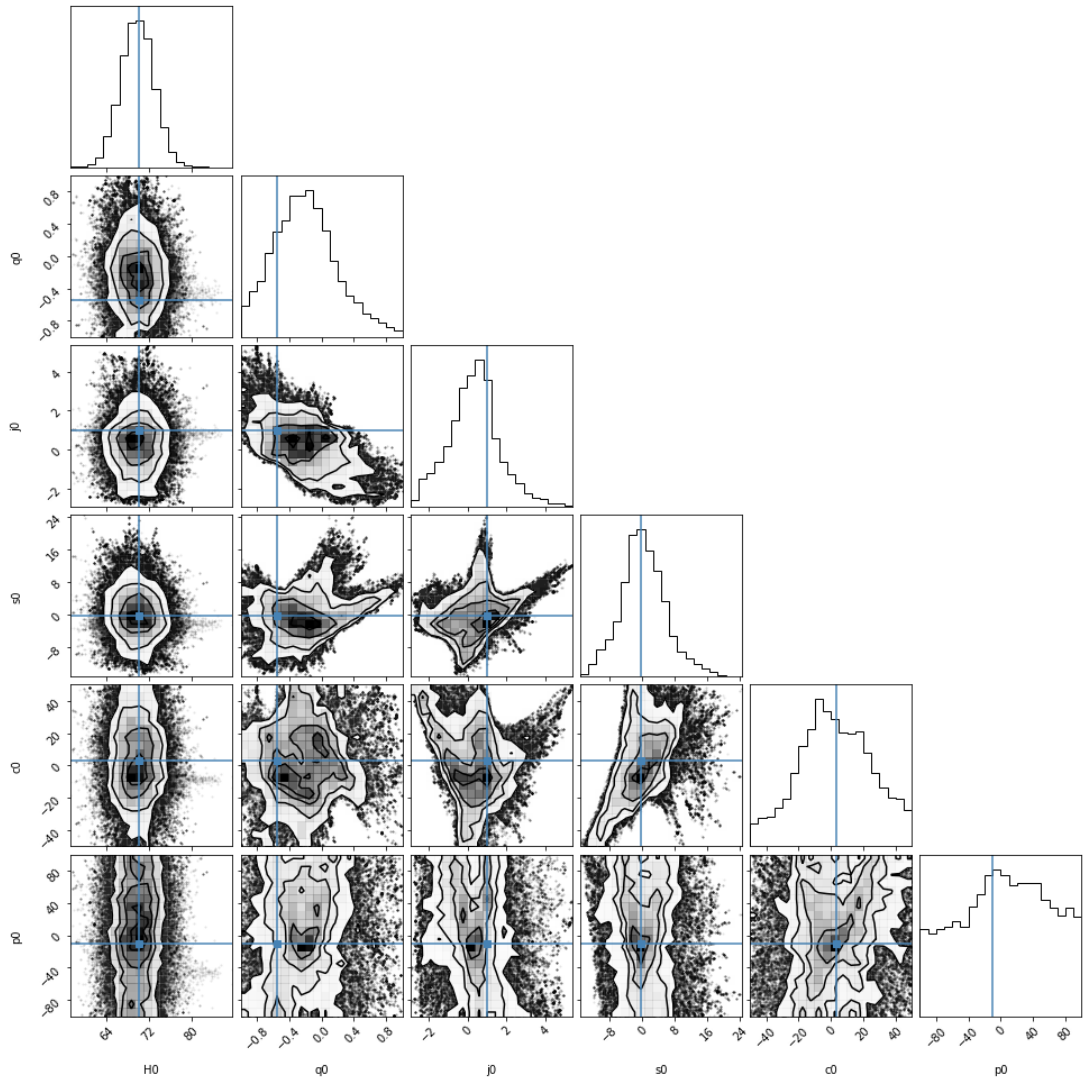

Figure 5.11: Corner plot for the cosmographic parameters obtained from ELT data when using only the x redshift parameterization and N prior. In blue we have the true values for each parameter.

5.3 SKA and ELT

It is expected that a model independent mapping of the Universe for lower and higher regimes to cause a significant impact Cosmology's future [42]. In this section a combination of the previous mock data (figure 5.12) will be used to test the accuracy of cosmography. The results are shown in figures 5.13-5.15 and in table 5.5. With the junction of the data sets z showed more difficulty in recovering values true when compared with the others, but still showed less uncertainties in its determinations. Contrary to previous results, upon the use of data from low and high redshift regimes the z-Padé[3/2] expansion is shown capable to obtain good constrains for all parameters except for s_0. That result may be caused by some kind of nuisance asymptote expected to happen sometimes for rational approximations, as discussed in 3.4.

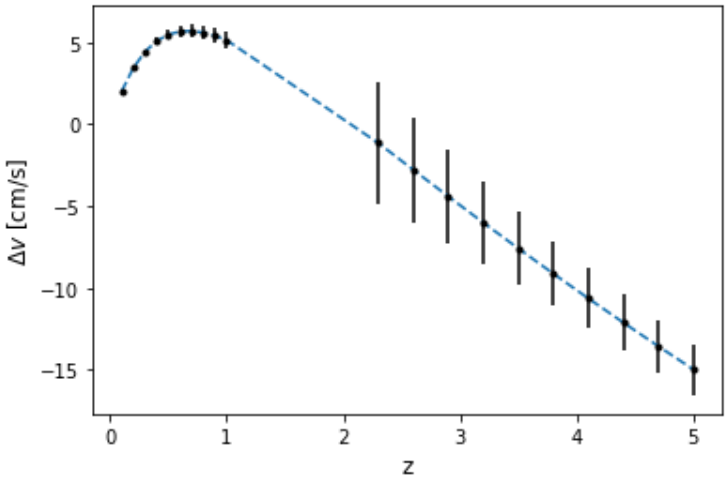

Figure 5.12: Combination of the previously mentioned mock data sets.

SKA + ELT results for the N prior				
Parameters	Expected	z	z-P[3/2]	x
H_0	70	$70.51^{+3.28}_{-3.18}$	$69.59^{+3.00}_{-2.98}$	$69.66^{+2.98}_{-2.93}$
q_0	-0.55	$-0.54^{+0.02}_{-0.03}$	$-0.55^{+0.03}_{-0.03}$	$-0.55^{+0.03}_{-0.03}$
j_0	1	$0.91^{+0.10}_{-0.11}$	$0.94^{+0.20}_{-0.41}$	$0.93^{+0.34}_{-0.41}$
s_0	-0.35	$-0.48^{+0.32}_{-0.30}$	$-0.87^{+1.39}_{-3.25}$	$-1.39^{+3.28}_{-3.78}$
c_0	3.115	$3.96^{+0.40}_{-0.42}$	$-0.92^{+9.36}_{-11.11}$	$-5.01^{+18.33}_{-17.26}$
p_0	-10.88675	$-16.90^{+3.51}_{-2.99}$	$-33.90^{+93.82}_{-47.32}$	$-38.29^{+64.91}_{-37.68}$

Table 5.5: MCMC results for SKA + ELT observations with a normal distribution prior for H_0

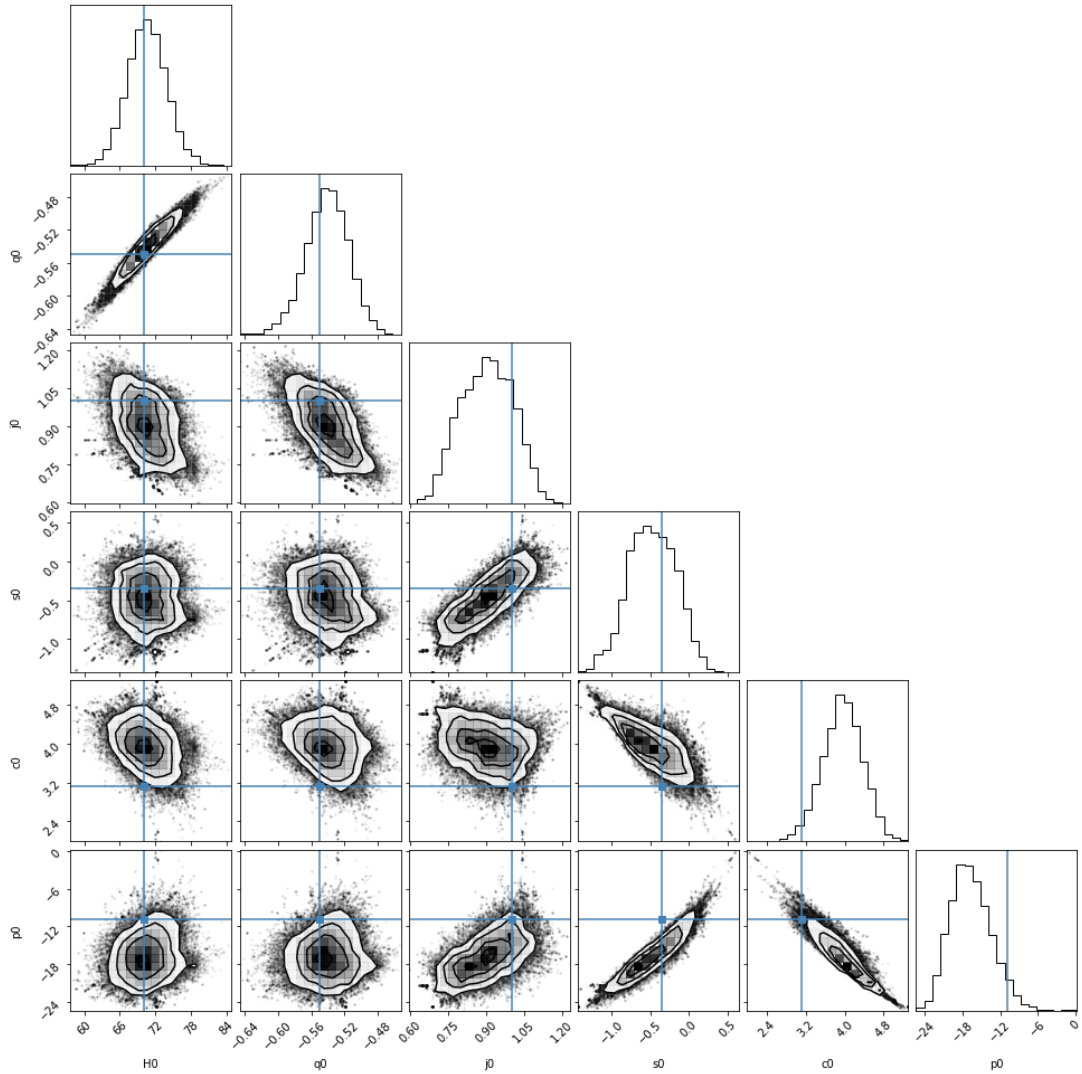

Figure 5.13: Corner plot for the cosmographic parameters obtained from SKA + ELT data when using only the z redshift parameterization and N prior. In blue we have the true values for each parameter.

5.3.1 ”Pessimistic” case

Even with new technological advanced facilities, the measurement of the redshift drift will be challenging. The observation time required is large and the number of QSO's catalogued that can be used for Lyman-α measurements is still relatively small. This new mock data will be evaluated for the values of redshift [0.1, 0.2, 0.3] with uncertainties of [3%, 5%, 10%] respectively for the SKA, and redshifts of [2.5, 3.5, 5.0] for ELT, as described in Martins et al. [7]. The new data set can be seen in figure 5.16. The results are shown in figures 5.17-5.19 and in table 5.6. We observed that the uncertainties increased for high order cosmographic parameters but lower order parameters can still be constrained well.

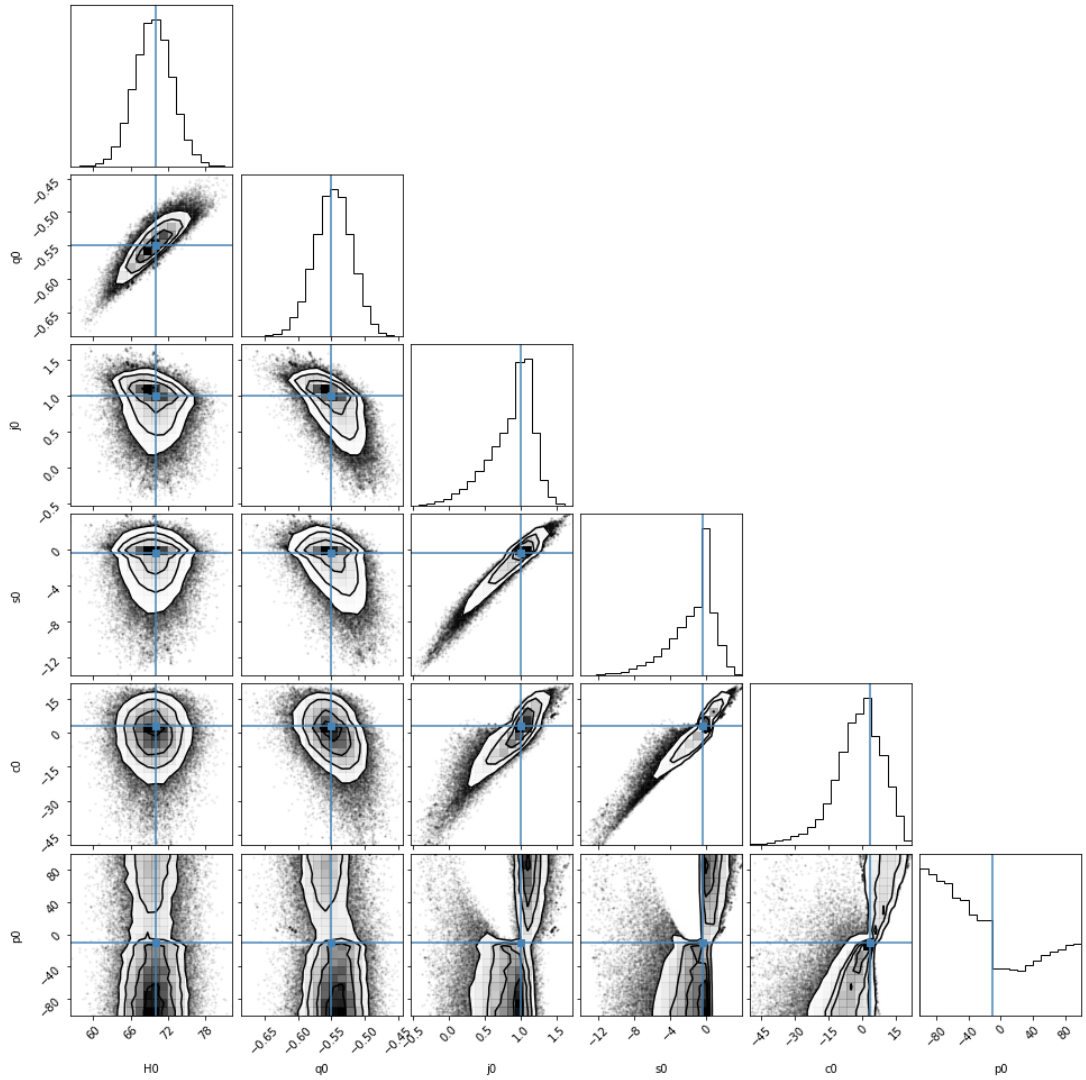

Figure 5.14: Corner plot for the cosmographic parameters obtained from SKA + ELT data when using the z redshift parameterization with Padé approximant [3/2] and N prior. In blue we have the true values for each parameter.

SKA + ELT results for the N prior ("Pessimistic" case)				
Parameters	Expected	z	z-P[3/2]	x
H_0	70	$69.29^{+3.28}_{-3.31}$	$69.78^{+3.00}_{-3.02}$	$69.71^{+3.00}_{-2.99}$
q_0	-0.55	$-0.55^{+0.03}_{-0.03}$	$-0.53^{+0.04}_{-0.04}$	$-0.54^{+0.04}_{-0.05}$
j_0	1	$0.99^{+0.18}_{-0.21}$	$0.34^{+0.70}_{-0.60}$	$0.70^{+0.74}_{-0.69}$
s_0	-0.35	$-0.15^{+0.62}_{-0.52}$	$-7.16^{+4.56}_{-3.75}$	$-1.27^{+4.23}_{-6.21}$
c_0	3.115	$3.63^{+1.67}_{-1.67}$	$-19.43^{+20.37}_{-20.27}$	$-1.13^{+20.95}_{-24.78}$
p_0	-10.88675	$-13.48^{+9.25}_{-8.84}$	$-3.43^{+69.15}_{-63.43}$	$-2.38^{+62.36}_{-62.56}$

Table 5.6: MCMC results for 3 SKA + 3 ELT observations from flat ΛCDM with $\Omega_{m0} = 0.3$ observations with a normal distribution prior for H_0

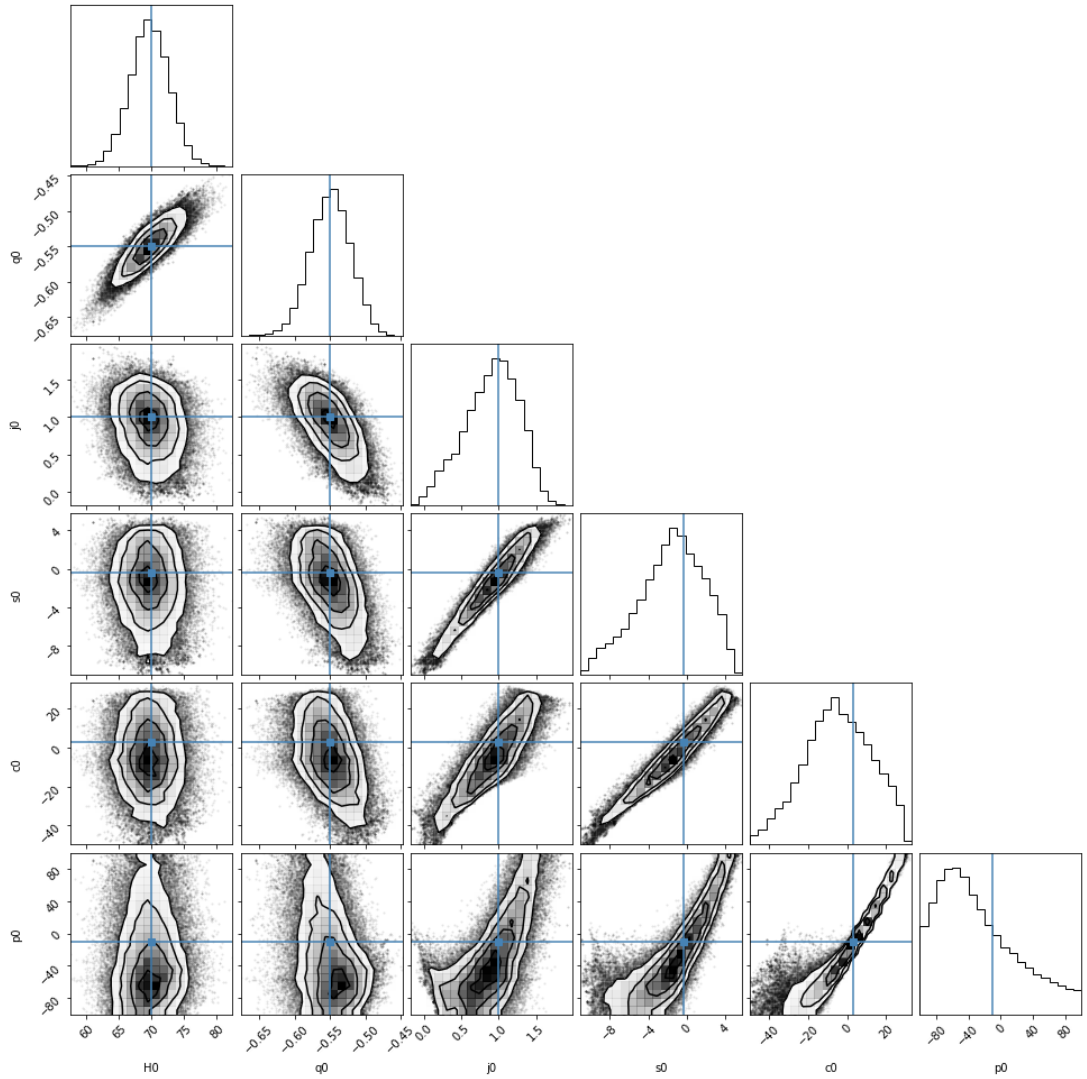

Figure 5.15: Corner plot for the cosmographic parameters obtained from SKA + ELT data when using only the x redshift parameterization and N prior. In blue we have the true values for each parameter.

5.3.2 ”Optimistic” case

We then studied a hypothetical scenario where we would have 100 SKA measurements and 100 ELT measurements with the same cosmological model tested before (figure 5.20). An increase in the number of measurements will constraint more tightly the parameters and indicate possible deviations from the true values. The redshift domain was slightly changed because some expansions presented a few numerical bugs in that range. The results are presented in figures 5.21-5.23 and in table 5.7. In this test the cosmographic expansion in x appears to be more stable, deviating less from the true values. The z expansion showed an aggravation in its capability to predict correctly high redshift dependent cosmographic parameters.

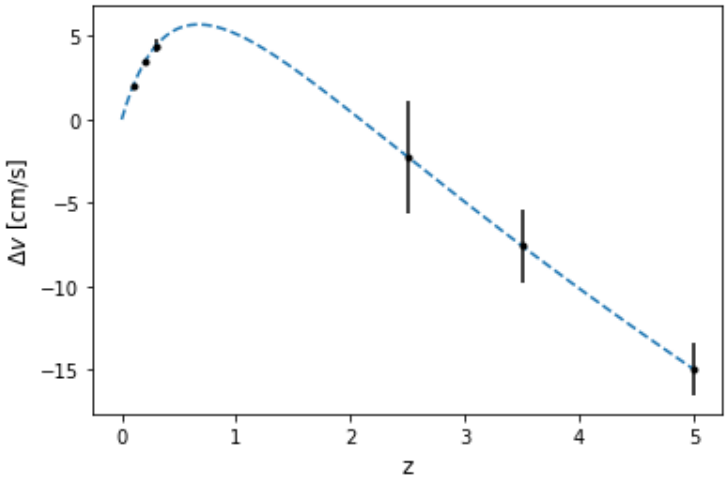

Figure 5.16: Spectroscopic velocity drift mock data for 3 SKA + 3 ELT observations from a flat ΛCDM model with $\Omega_{m0} = 0.3$. The blue dashed line represents the true curve for this fiducial model.

SKA + ELT results for the N prior ("Optimistic" case)				
Parameters	Expected	z	z-P[3/2]	x
H_0	70	$70.90^{+4.36}_{-3.47}$	$69.29^{+3.11}_{-3.21}$	$69.35^{+2.91}_{-2.98}$
q_0	-0.55	$-0.54^{+0.03}_{-0.03}$	$-0.56^{+0.02}_{-0.03}$	$-0.56^{+0.02}_{-0.03}$
j_0	1	$0.99^{+0.07}_{-0.09}$	$1.03^{+0.08}_{-0.07}$	$1.001^{+0.08}_{-0.08}$
s_0	-0.35	$-0.19^{+0.17}_{-0.21}$	$-0.14^{+0.33}_{-0.67}$	$-0.66^{+0.91}_{-0.92}$
c_0	3.115	$3.69^{+0.20}_{-0.23}$	$1.58^{+4.67}_{-4.02}$	$-0.52^{+6.85}_{-6.79}$
p_0	-10.88675	$-13.62^{+1.53}_{-1.46}$	$-44.38^{+106.30}_{-39.54}$	$-27.85^{+26.38}_{-25.32}$

Table 5.7: MCMC results for 100 SKA + 100 ELT observations from flat ΛCDM with $\Omega_{m0} = 0.3$ observations with a normal distribution prior for H_0

5.3.3 Model distinction

Finally, we studied the model distinction capabilities by making a comparison between a flat ΛCDM model with $\Omega_{m0} = 0.3$ and flat CPL model with parameters (0.3,-1,0.1). The difference between the models is lower than the expected observations uncertainties making them difficult to discern from each other, as seen in figure 5.24. By contrast, the difference between the cosmographic parameters will be more noticeable. As shown in equation 4.12, a small difference in the w_1 value will greatly change the value of j_0. In this case, it changes the j_0 from 1 for the ΛCDM model to 1.105 for this new CPL model. The results are shown in the figures 5.25-5.27 and in the table 5.8. All the cosmographic series studied favoured the CPL model demonstrating the capacity to distinguish models with similar

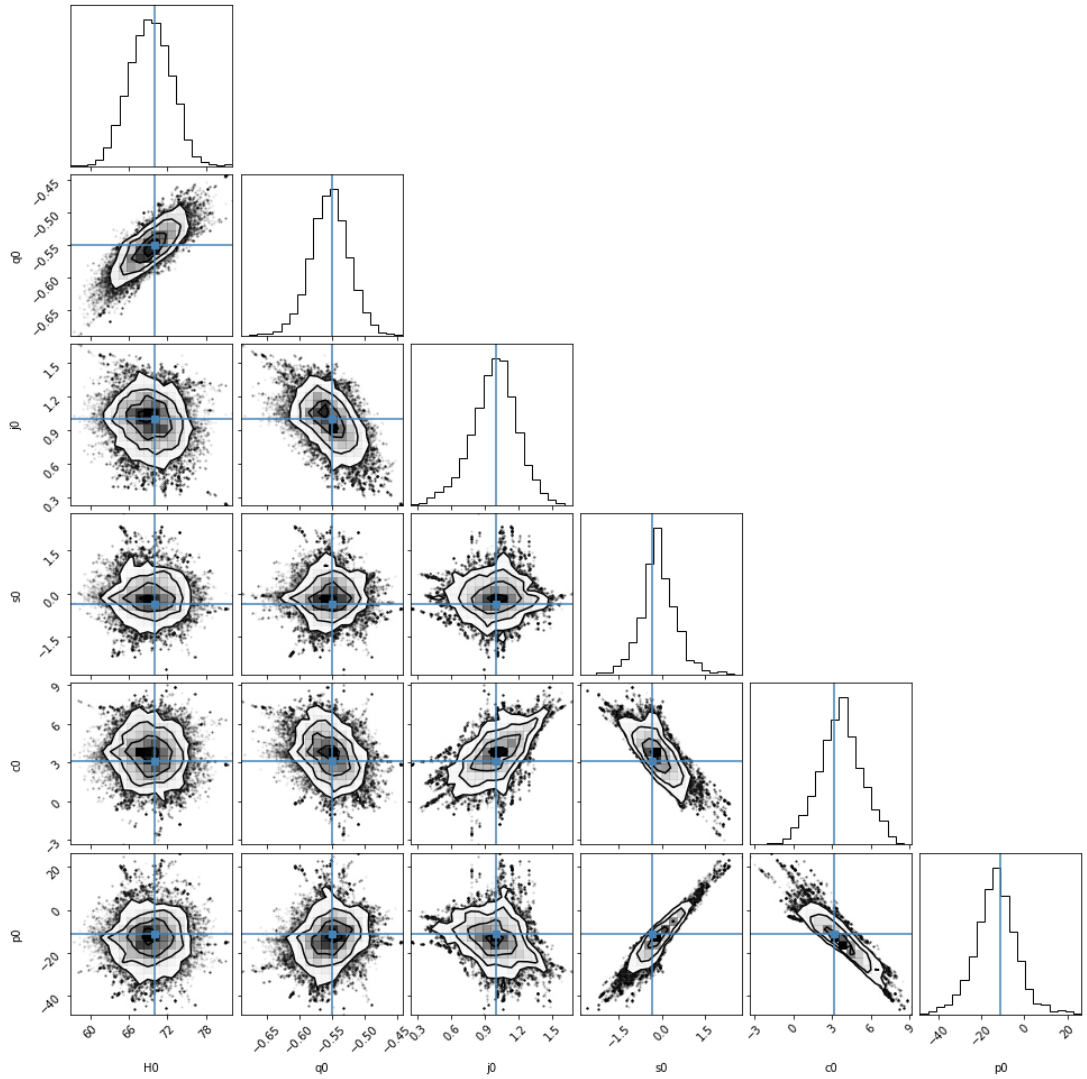

Figure 5.17: Corner plot for the cosmographic parameters obtained from 3 SKA + 3 ELT observations when using only the z redshift parameterization and N prior. The data followed a flat ΛCDM model with $\Omega_{m0} = 0.3$. In blue we have the true values for each parameter.

spectroscopic velocity drifts but with different cosmographic parameters.

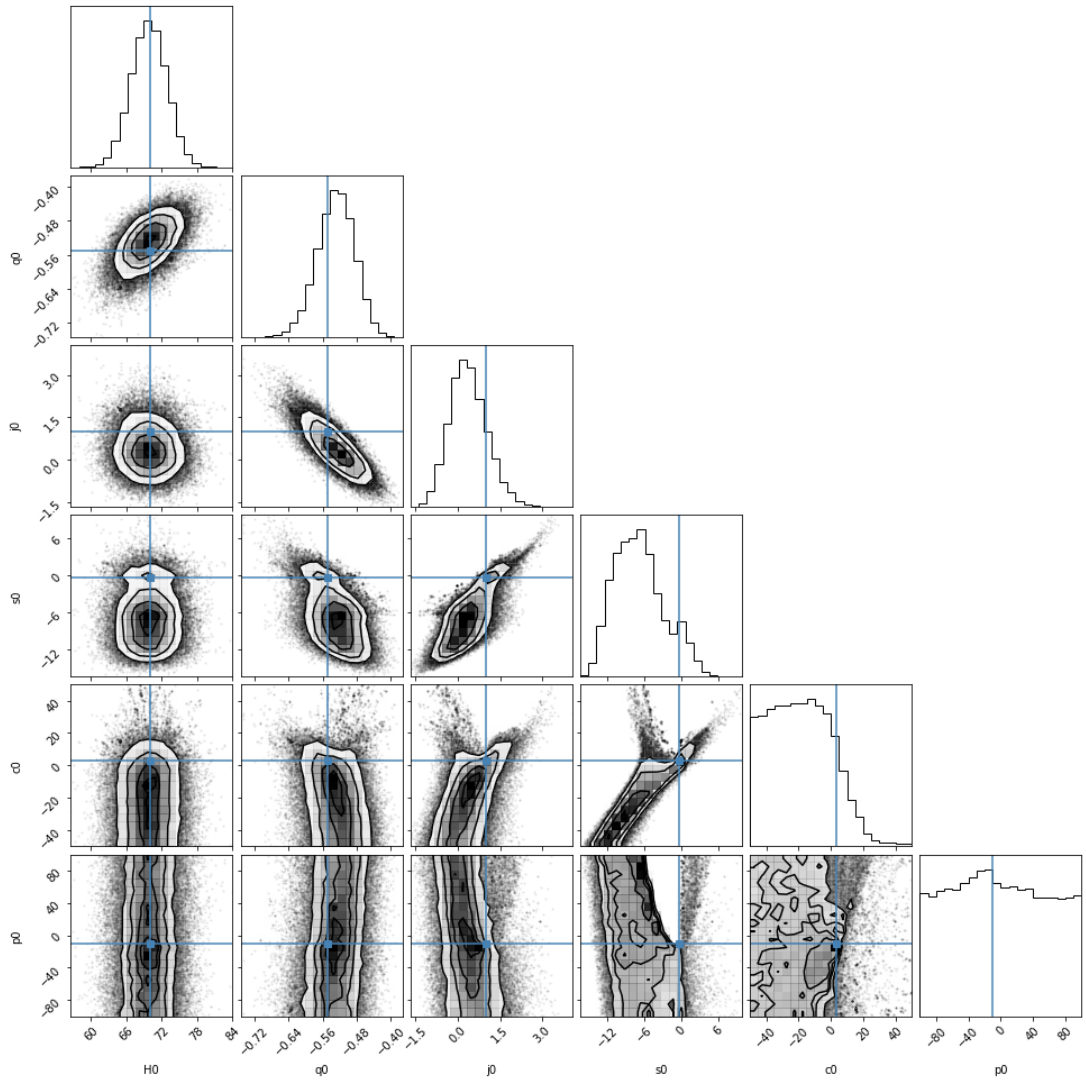

Figure 5.18: Corner plot for the cosmographic parameters obtained from 3 SKA + 3 ELT observations when using the z redshift parameterization with Padé approximant [3/2] and N prior. The data followed a flat ΛCDM model with $\Omega_{m0} = 0.3$. In blue we have the true values for each parameter.

SKA + ELT results for the N prior (Model distinction)				
Parameters	Expected	z	z-P[3/2]	x
H_0	70	$68.97^{+2.78}_{-2.76}$	$69.19^{+3.21}_{-2.99}$	$69.17^{+3.09}_{-3.03}$
q_0	-0.55	$-0.56^{+0.02}_{-0.02}$	$-0.56^{+0.03}_{-0.03}$	$-0.56^{+0.02}_{-0.03}$
j_0	1.105	$1.12^{+0.06}_{-0.05}$	$1.13^{+0.08}_{-0.07}$	$1.11^{+0.08}_{-0.08}$
s_0	0.12775	$0.11^{+0.13}_{-0.12}$	$0.39^{+0.46}_{-0.39}$	$-0.27^{+0.74}_{-0.74}$
c_0	4.333525	$3.84^{+0.24}_{-0.24}$	$6.26^{+4.29}_{-2.93}$	$-0.06^{+5.01}_{-5.01}$
p_0	-7.63618625	$-11.32^{+1.33}_{-1.31}$	$25.04^{+54.12}_{-60.15}$	$-29.06^{+19.74}_{-19.39}$

Table 5.8: MCMC results for 100 SKA + 100 ELT observations from flat CPL with parameters (0.3,-1,0.1) observations with a normal distribution prior for H_0

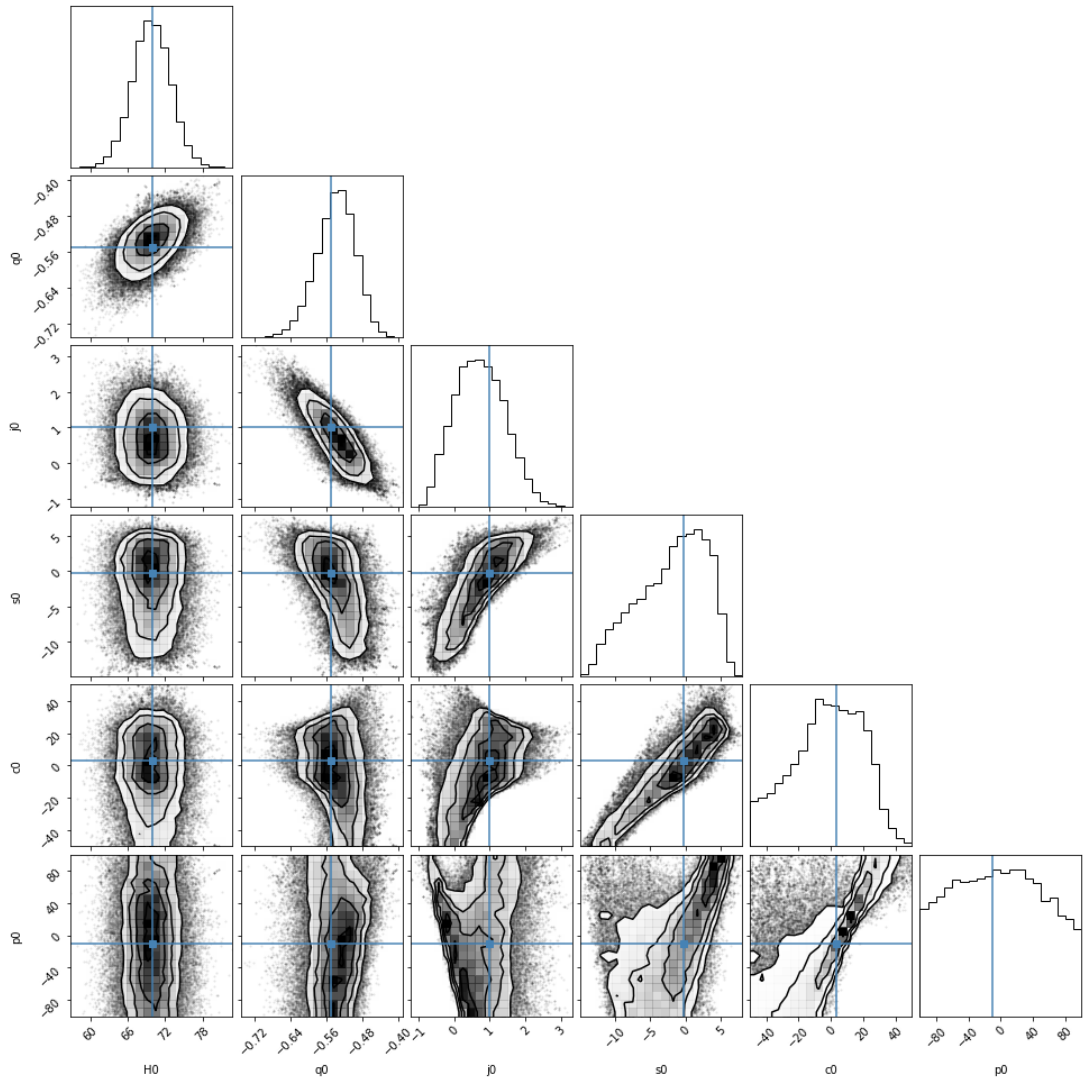

Figure 5.19: Corner plot for the cosmographic parameters obtained from 3 SKA + 3 ELT observations when using only the x redshift parameterization and N prior. The data followed a flat ΛCDM model with $\Omega_{m0} = 0.3$. In blue we have the true values for each parameter.

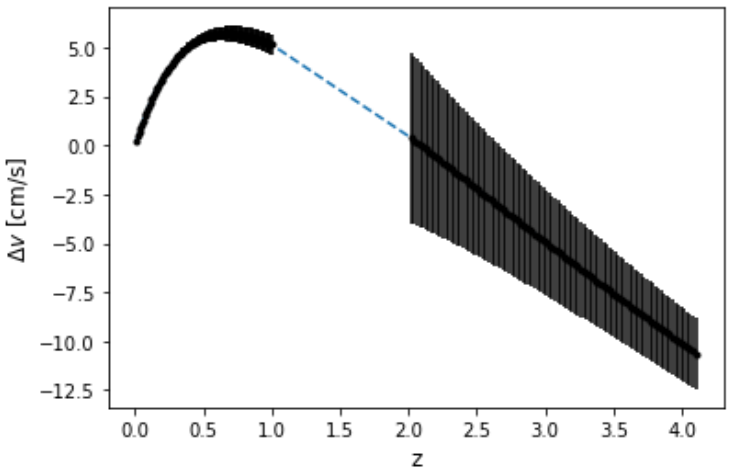

Figure 5.20: Spectroscopic velocity drift mock data for 100 SKA + 100 ELT observations from a flat ΛCDM model with $\Omega_{m0} = 0.3$. The blue dashed line represents the true curve for this fiducial model.

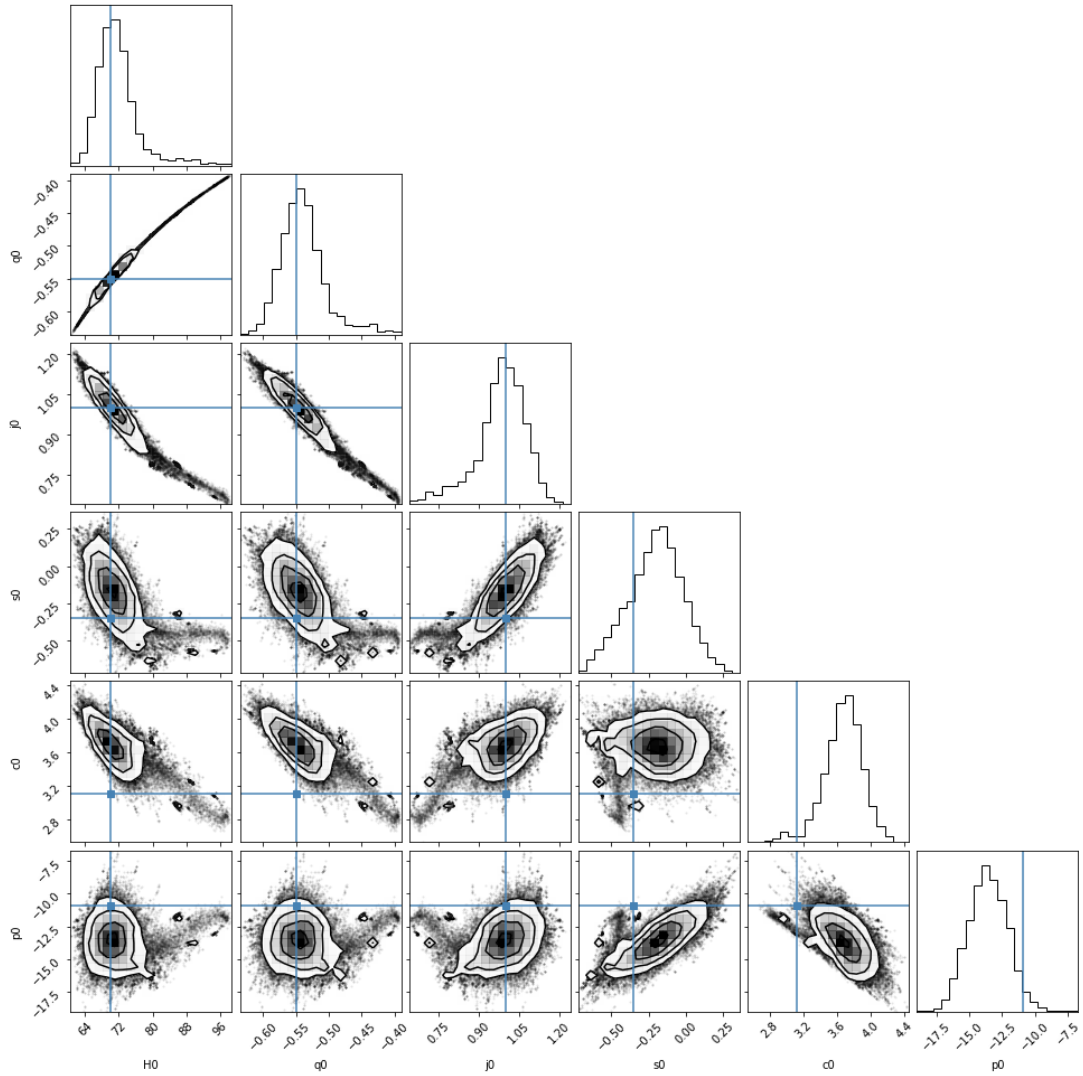

Figure 5.21: Corner plot for the cosmographic parameters obtained from 100 SKA + 100 ELT observations when using only the z redshift parameterization and N prior. The data followed a flat ΛCDM model with $\Omega_{m0} = 0.3$. In blue we have the true values for each parameter.

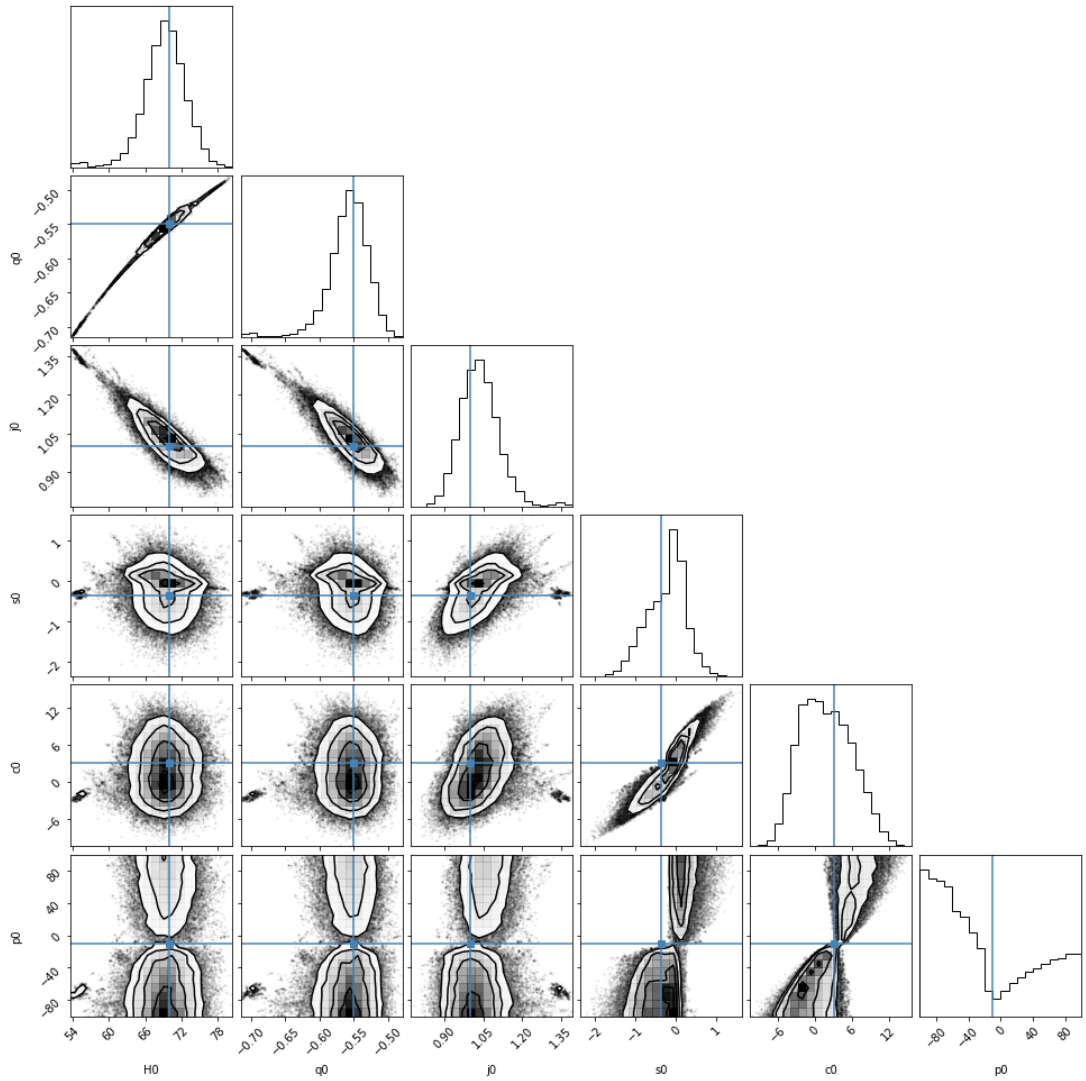

Figure 5.22: Corner plot for the cosmographic parameters obtained from 100 SKA + 100 ELT observations when using the z redshift parameterization with Padé approximant [3/2] and N prior. The data followed a flat ΛCDM model with $\Omega_{m0} = 0.3$. In blue we have the true values for each parameter.

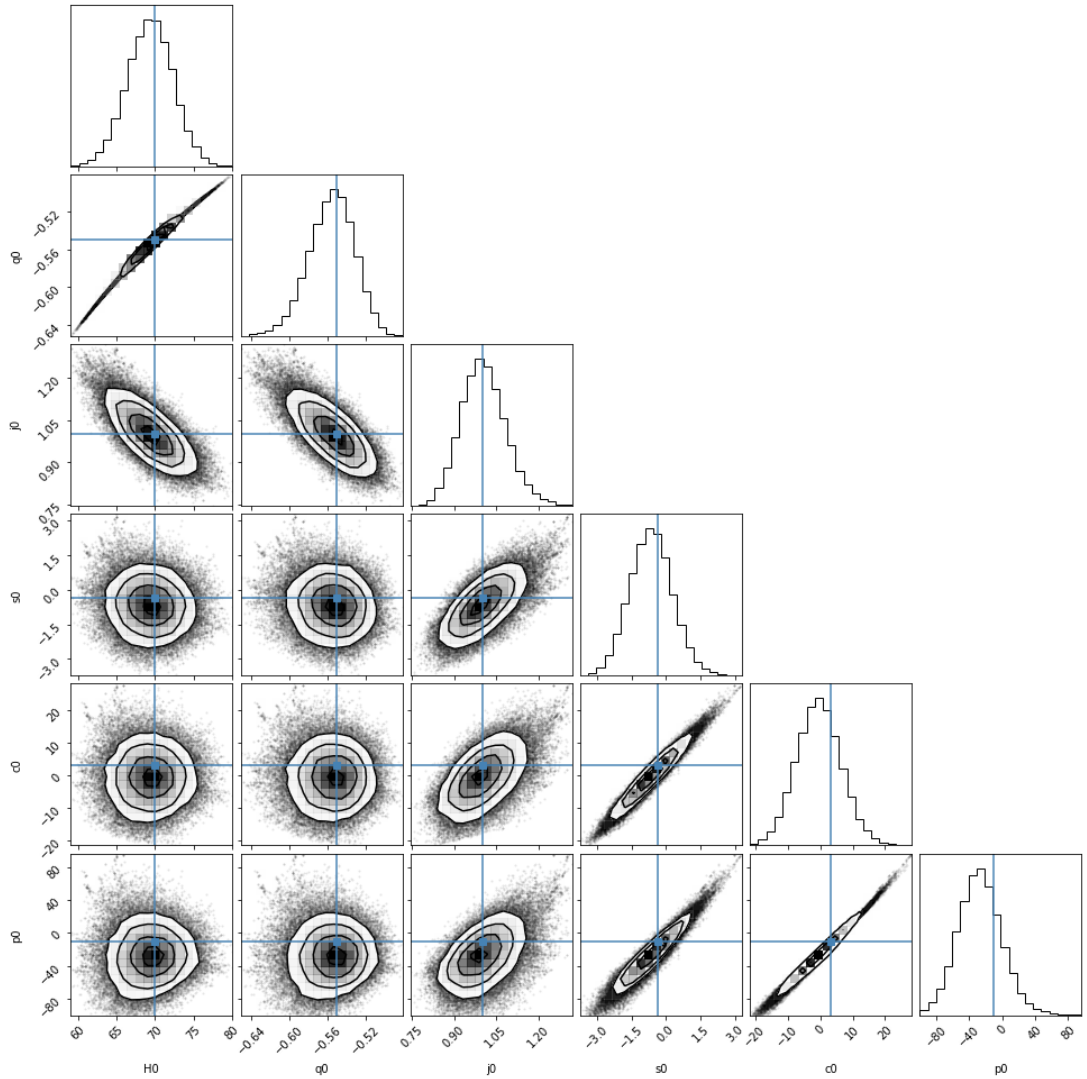

Figure 5.23: Corner plot for the cosmographic parameters obtained from 100 SKA + 100 ELT observations when using only the x redshift parameterization and N prior. The data followed a flat ΛCDM model with $\Omega_{m0} = 0.3$. In blue we have the true values for each parameter.

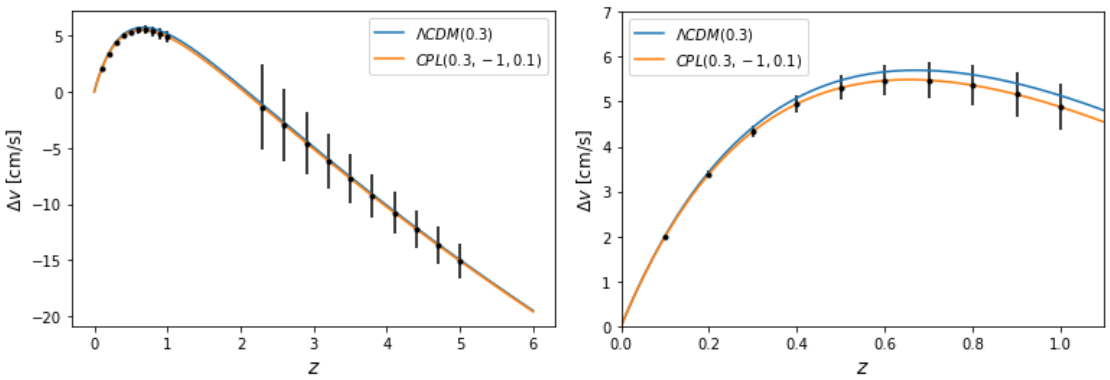

Figure 5.24: Comparison between a flat ΛCDM model with $\Omega_{m0} = 0.3$ and flat CPL model with parameters (0.3,-1,0.1). As it can be seen, the difference between them is lower than the expected observations uncertainties.

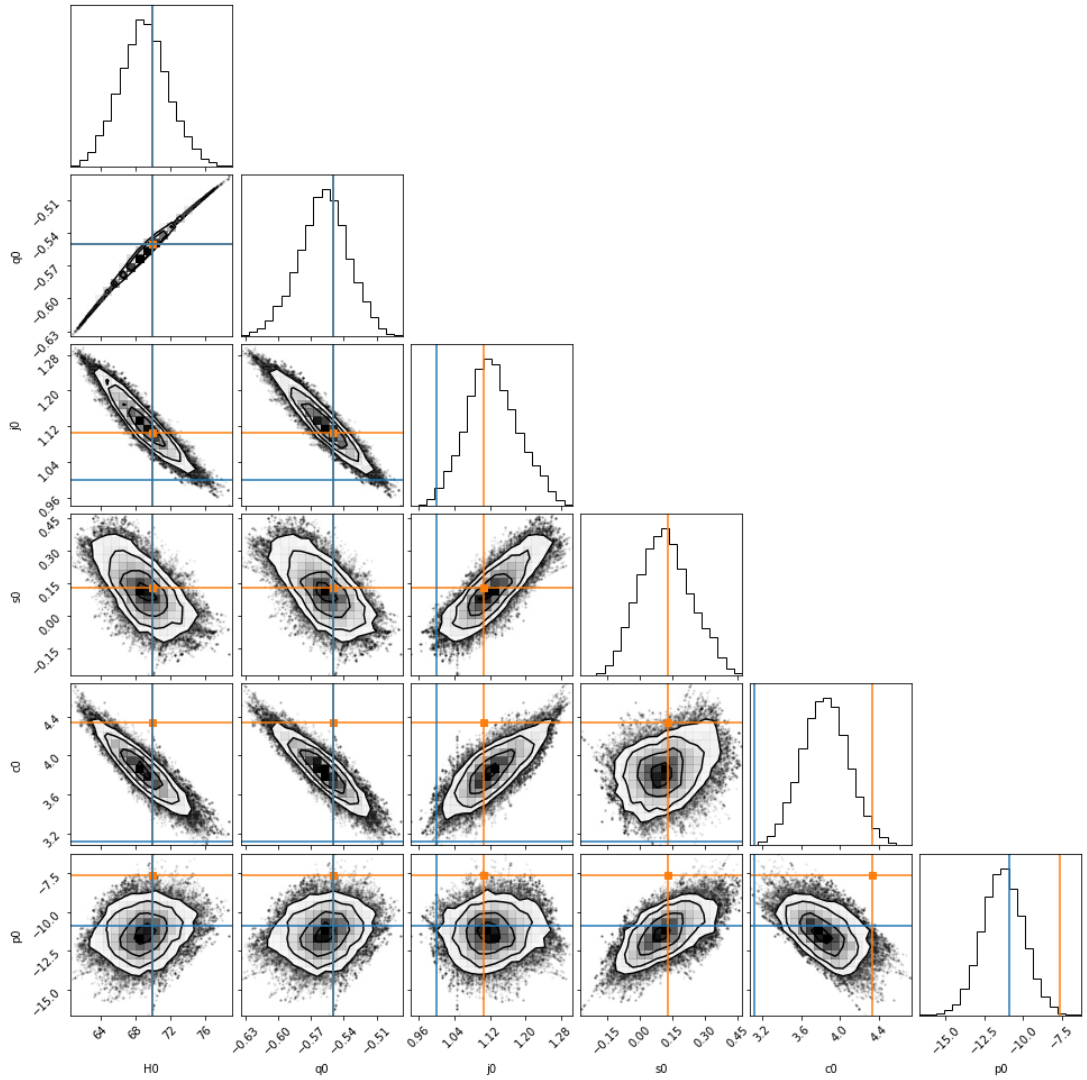

Figure 5.25: Corner plot for the cosmographic parameters obtained from SKA + ELT data when using only the z redshift parameterization and N prior. The data followed a flat CPL model with parameters (0.3,-1,0.1). In orange we have the true values for the cosmographic parameters for the CPL model and in blue we have the parameter values for the case of the flat ΛCDM model with $\Omega_{m0} = 0.3$.

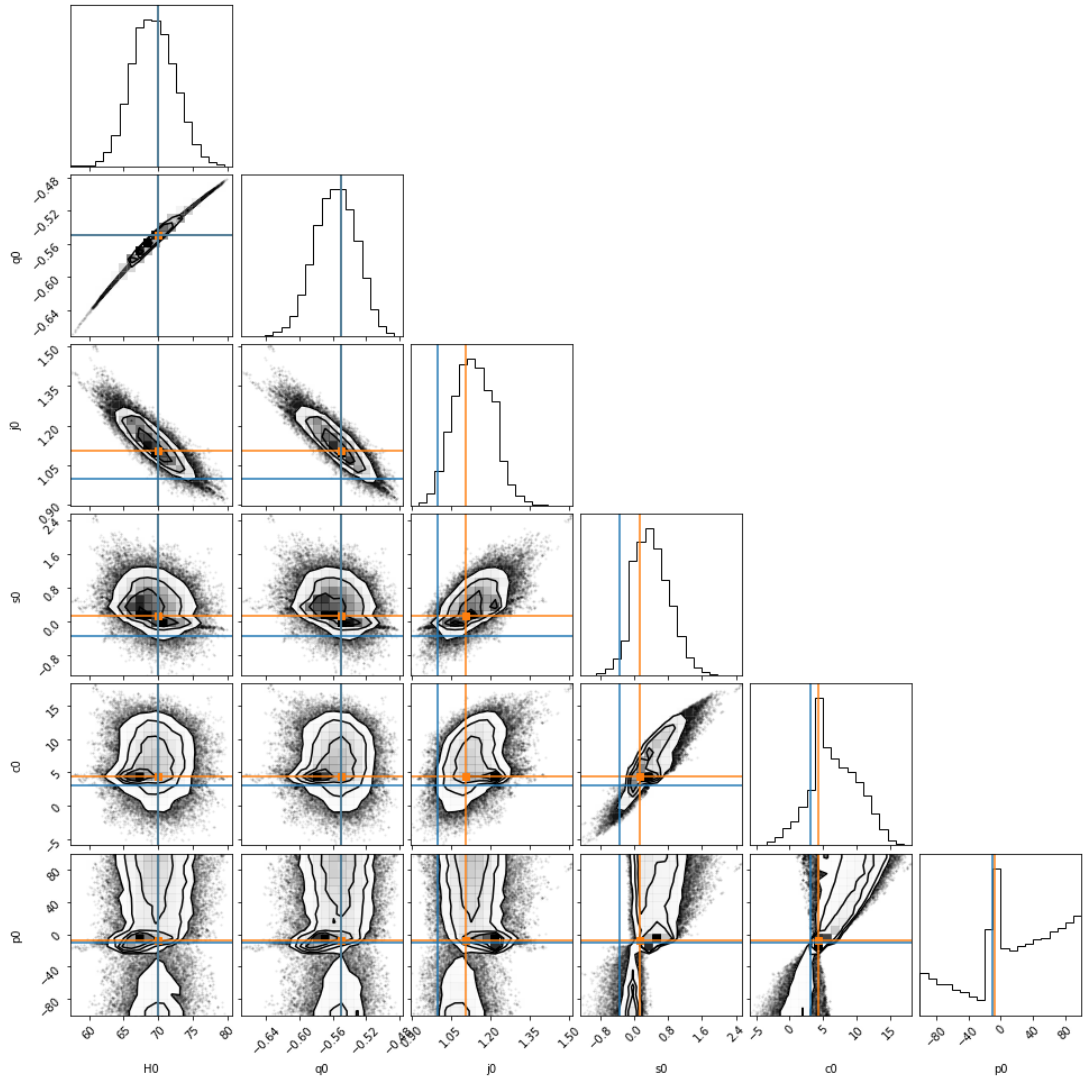

Figure 5.26: Corner plot for the cosmographic parameters obtained from SKA + ELT data when using the z redshift parameterization with Padé approximant [3/2] and N prior. The data followed a flat CPL model with parameters (0.3,-1,0.1). In orange we have the true values for the cosmographic parameters for the CPL model and in blue we have the parameter values for the case of the flat ΛCDM model with $\Omega_{m0} = 0.3$.

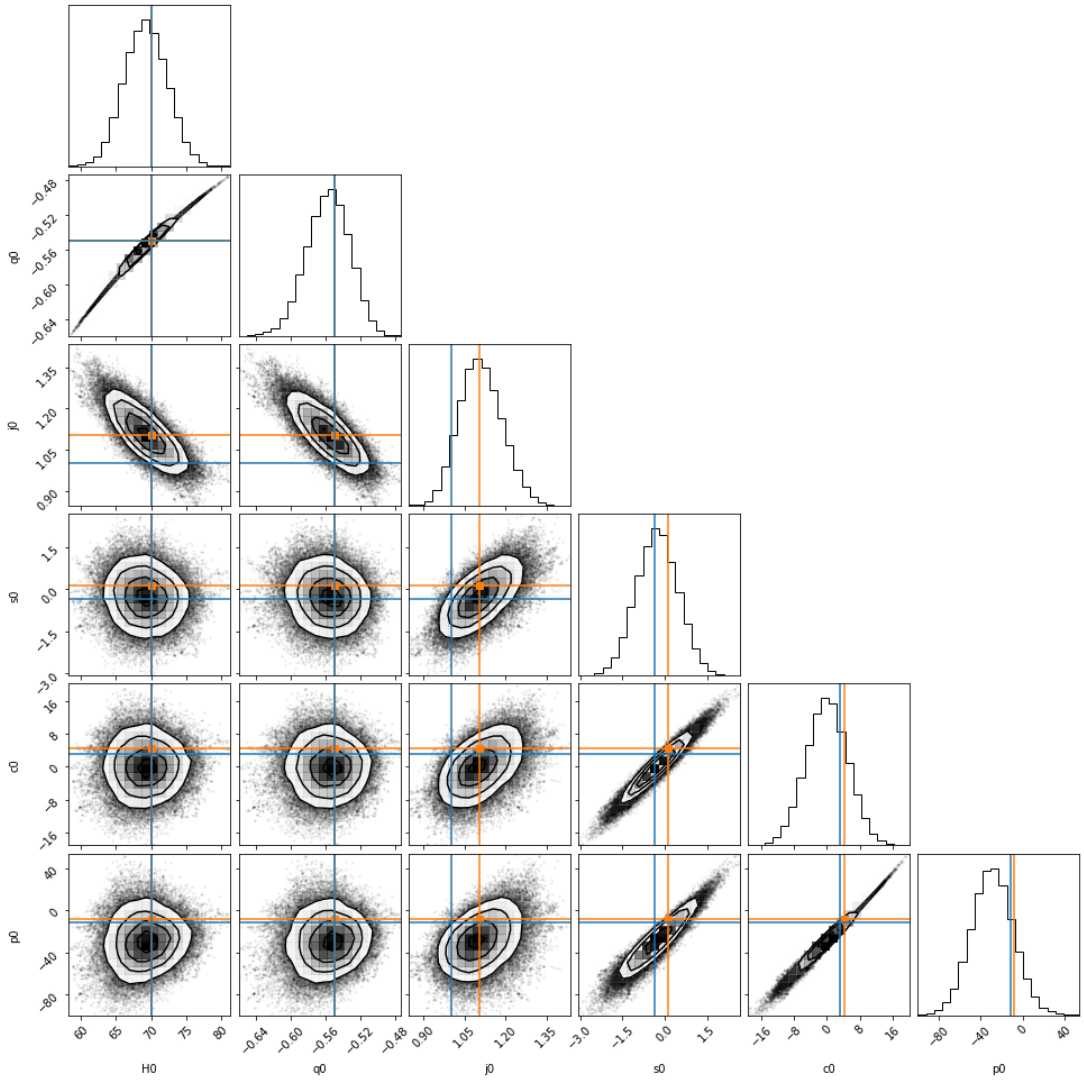

Figure 5.27: Corner plot for the cosmographic parameters obtained from SKA + ELT data when using only the x redshift parameterization and N prior. The data followed a flat CPL model with parameters (0.3,-1,0.1). In orange we have the true values for the cosmographic parameters for the CPL model and in blue we have the parameter values for the case of the flat ΛCDM model with $\Omega_{m0} = 0.3$.

Chapter 6

Final Remarks and Conclusions

The main goal of this work was to assess the model discriminating power that future data on redshift drift when using together with a cosmographic approach. With the cosmographic parameters, we conducted an analysis of the fitness for each approximation. It was shown that the z parameterization has the highest mean relative errors, making it less reliable in recovering the true values. It was also shown that, in the neighbourhood of ΛCDM values, the mean relative error for the y parameterization is independent of every CPL parameter. The x parameterization has the lowest mean relative error of the cosmographic series that don't use Padé approximants. The use of Padé approximants has lowered the mean relative errors. Finally, we studied the predictive power of redshift drift cosmography for future redshift drift data provided by the SKA and ELT.

For the low redshift data that will be obtained from the Square Kilometer Array it was concluded that the z and x parameterizations can accurately determine low order cosmographic parameters. The z-Padé[3/2] cosmographic function has difficulty in recovering the true values. For the high redshift regime from the data that will be obtained by the European Extremely Large Telescope, the z-Padé[3/2] cosmographic function was once again shown to be non predictive. It was also shown that for the z parameterization the values of s_0, c_0 and p_0 were predicted correctly with trade off being inaccurate values for q_0 and j_0. When combining the two types of data it was observed that now, the z-Padé[3/2] cosmographic function could predict well the true values, with exception of the p_0 parameter. The opposite happened for the z parameterization where the junction of the two types caused a worse determination of the true values. The x parameterization appears to also predict correctly true values. It was also shown that a good cosmographic theory can be

used to distinguish degenerated models that have different sources of dark energy. Overall, it can be said that all the studied expansions work well for the low redshift regime. Meanwhile, for high redshifts the chosen expansion will be important for the recovery of true values. Not only that, each expansion will benefit from different types data. For example, the z parameterization performed worse with data simultaneously from low and high redshifts while the z-Padé[3/2] suffers the opposite problem, it needs data from both regions.

There is still a clear need to study more high redshift cosmography to fully utilize the information obtained from future high redshift data. In a future work one could possibly experiment this same analysis with other rational approximations like Chebyshev rationals [43] [44]. Other method that is recently being explored to tackle cosmography's shortcomings is the use of orthogonalized logarithmic polynomials, although it is still being debated if said polynomials applications would be useful [45] [46]. Since there is also a truncation when defining the Taylor series expansion in time for the scale factor (equation 3.1), maybe it would be useful to implement immediately rational approximations so that equation 3.4 would be something like

$$\frac{1}{1+z} \approx \frac{p(t_H)}{q(t_H)} \tag{6.1}$$

These new functions for the numerator and denominator would have a less clear meaning but they could potentially be determined by relations between cosmographic parameters.

Bibliography

[1] J. R. Primack, “Precision cosmology,” *New Astronomy Reviews*, vol. 49, no. 2-6, p. 25–34, May 2005. [Online]. Available: http://dx.doi.org/10.1016/j.newar.2005.01.039 [Cited on page 1.]

[2] A. Del Popolo and M. Le Delliou, “Small scale problems of the λcdm model: A short review,” *Galaxies*, vol. 5, no. 1, p. 17, Feb 2017. [Online]. Available: http://dx.doi.org/10.3390/galaxies5010017 [Cited on page 1.]

[3] L. Amendola, S. Appleby, A. Avgoustidis, D. Bacon, T. Baker, M. Baldi, N. Bartolo, A. Blanchard, C. Bonvin, and et al., “Cosmology and fundamental physics with the euclid satellite,” *Living Reviews in Relativity*, vol. 21, no. 1, Apr 2018. [Online]. Available: http://dx.doi.org/10.1007/s41114-017-0010-3 [Cited on page 2.]

[4] J. Liske, A. Grazian, E. Vanzella, M. Dessauges, M. Viel, L. Pasquini, M. Haehnelt, S. Cristiani, F. Pepe, G. Avila, and et al., “Cosmic dynamics in the era of extremely large telescopes,” *Monthly Notices of the Royal Astronomical Society*, vol. 386, no. 3, p. 1192–1218, May 2008. [Online]. Available: http://dx.doi.org/10.1111/j.1365-2966.2008.13090.x [Cited on pages 2, 5, 6, and 36.]

[5] Y. Liu, J.-F. Zhang, and X. Zhang, “Real-time cosmology with ska,” *The European Physical Journal C*, vol. 80, no. 4, Apr 2020. [Online]. Available: http://dx.doi.org/10.1140/epjc/s10052-020-7863-4 [Cited on page 2.]

[6] H. R. Klöckner, D. Obreschkow, C. Martins, A. Raccanelli, D. Champion, A. Roy, A. Lobanov, J. Wagner, and R. Keller, “Real time cosmology - a direct measure of the expansion rate of the universe,” 2015. [Cited on pages 2, 7, and 28.]

[7] C. Martins, M. Martinelli, E. Calabrese, and M. Ramos, “Real-time cosmography with redshift derivatives,” *Phys. Rev. D*, vol. 94, no. 4, p. 043001, 2016. [Cited on pages 2, 28, and 42.]

[8] C. Quercellini, L. Amendola, A. Balbi, P. Cabella, and M. Quartin, "Real-time cosmology," *Physics Reports*, vol. 521, no. 3, p. 95–134, Dec 2012. [Online]. Available: http://dx.doi.org/10.1016/j.physrep.2012.09.002 [Cited on pages 2 and 7.]

[9] A. Sandage, "The Change of Redshift and Apparent Luminosity of Galaxies due to the Deceleration of Selected Expanding Universes." *Astrophysical Journal*, vol. 136, p. 319, Sep. 1962. [Cited on page 3.]

[10] G. C. McVittie, "Appendix to The Change of Redshift and Apparent Luminosity of Galaxies due to the Deceleration of Selected Expanding Universes." *Astrophysical Journal*, vol. 136, p. 334, Sep. 1962. [Cited on page 3.]

[11] S. Koksbang, "Another look at redshift drift and the backreaction conjecture," *Journal of Cosmology and Astroparticle Physics*, vol. 2019, no. 10, p. 036–036, Oct 2019. [Online]. Available: http://dx.doi.org/10.1088/1475-7516/2019/10/036 [Cited on page 3.]

[12] K. Bolejko, C. Wang, and G. F. Lewis, "Direct detection of the cosmic expansion: the redshift drift and the flux drift," 2019. [Cited on pages 3 and 4.]

[13] M. Rauch, "The lyman alpha forest in the spectra of quasistellar objects," *Annual Review of Astronomy and Astrophysics*, vol. 36, no. 1, p. 267–316, Sep 1998. [Online]. Available: http://dx.doi.org/10.1146/annurev.astro.36.1.267 [Cited on page 6.]

[14] A. Loeb, "Direct measurement of cosmological parameters from the cosmic deceleration of extragalactic objects," *The Astrophysical Journal*, vol. 499, no. 2, p. L111–L114, Jun 1998. [Online]. Available: http://dx.doi.org/10.1086/311375 [Cited on page 6.]

[15] R. Lazkoz, I. Leanizbarrutia, and V. Salzano, "Forecast and analysis of the cosmological redshift drift," *The European Physical Journal C*, vol. 78, no. 1, Jan 2018. [Online]. Available: http://dx.doi.org/10.1140/epjc/s10052-017-5479-0 [Cited on page 6.]

[16] B. Keel, "Quasars as lighthouses: the lyman-alpha forest at low and high redshift." [Online]. Available: http://pages.astronomy.ua.edu/keel/agn/forest.html [Cited on pages xi, 6, and 7.]

[17] B. W. Carroll and D. A. Ostlie, *An introduction to modern astrophysics*, 2nd ed. San Francisco, CA: Addison-Wesley, 2007. [Cited on pages xi, 7, and 8.]

[18] J. Darling, "Toward a direct measurement of the cosmic acceleration," *The Astrophysical Journal*, vol. 761, no. 2, p. L26, Dec 2012. [Online]. Available: http://dx.doi.org/10.1088/2041-8205/761/2/L26 [Cited on page 7.]

[19] P. K. S. Dunsby and O. Luongo, "On the theory and applications of modern cosmography," *Int. J. Geom. Meth. Mod. Phys.*, vol. 13, no. 03, p. 1630002, 2016. [Cited on pages 10, 13, 15, 23, and 27.]

[20] V. Vitagliano, J.-Q. Xia, S. Liberati, and M. Viel, "High-Redshift Cosmography," *JCAP*, vol. 03, p. 005, 2010. [Cited on page 10.]

[21] A. R. Neben and M. S. Turner, "Beyond H_0 and q_0: Cosmology is no longer just two numbers," *Astrophys. J.*, vol. 769, p. 133, 2013. [Cited on page 10.]

[22] G. B. Arfken and H. J. Weber, *Mathematical methods for physicists*, 6th ed. San Diego, CA: Academic Press, 2005. [Cited on page 10.]

[23] F. S. Lobo, J. P. Mimoso, and M. Visser, "Cosmographic analysis of redshift drift," *Journal of Cosmology and Astroparticle Physics*, vol. 2020, no. 04, p. 043–043, Apr 2020. [Online]. Available: http://dx.doi.org/10.1088/1475-7516/2020/04/043 [Cited on pages 12 and 14.]

[24] C. Cattoen and M. Visser, "The Hubble series: Convergence properties and redshift variables," *Class. Quant. Grav.*, vol. 24, pp. 5985–5998, 2007. [Cited on pages 13 and 14.]

[25] ——, "Cosmographic Hubble fits to the supernova data," *Phys. Rev. D*, vol. 78, p. 063501, 2008. [Cited on page 13.]

[26] J.-Q. Xia, V. Vitagliano, S. Liberati, and M. Viel, "Cosmography beyond standard candles and rulers," *Phys. Rev. D*, vol. 85, p. 043520, 2012. [Cited on pages 14 and 24.]

[27] S. Capozziello, R. D'Agostino, and O. Luongo, "High-redshift cosmography: auxiliary variables versus padé polynomials," *Monthly Notices of the Royal Astronomical Society*, vol. 494, no. 2, p. 2576–2590, Apr 2020. [Online]. Available: http://dx.doi.org/10.1093/mnras/staa871 [Cited on page 15.]

[28] W. H. Press, S. A. Teukolsky, W. T. Vetterling, and B. P. Flannery, *Numerical Recipes 3rd Edition: The Art of Scientific Computing*, 3rd ed. USA: Cambridge University Press, 2007. [Cited on page 16.]

[29] W. F. Guthrie, "Nist/sematech e-handbook of statistical methods (nist handbook 151)," 2020. [Online]. Available: https://www.itl.nist.gov/div898/handbook/ [Cited on pages 16 and 17.]

[30] P. Tsiapi, S. Basilakos, M. Plionis, R. Terlevich, E. Terlevich, A. L. G. Moran, R. Chavez, F. Bresolin, D. F. Arenas, and E. Telles, "Cosmological Constraints using the newest VLT-KMOS HII Galaxies and the full Planck CMB spectrum," 7 2021. [Cited on page 20.]

[31] M. Chevallier and D. Polarski, "Accelerating universes with scaling dark matter," *International Journal of Modern Physics D*, vol. 10, no. 02, p. 213–223, Apr 2001. [Online]. Available: http://dx.doi.org/10.1142/S0218271801000822 [Cited on page 23.]

[32] E. V. Linder, "Exploring the expansion history of the universe," *Physical Review Letters*, vol. 90, no. 9, Mar 2003. [Online]. Available: http://dx.doi.org/10.1103/PhysRevLett.90.091301 [Cited on page 23.]

[33] D. Foreman-Mackey, D. W. Hogg, D. Lang, and J. Goodman, "emcee: The mcmc hammer," *Publications of the Astronomical Society of the Pacific*, vol. 125, no. 925, p. 306–312, Mar 2013. [Online]. Available: http://dx.doi.org/10.1086/670067 [Cited on page 27.]

[34] D. Foreman-Mackey, "corner.py: Scatterplot matrices in python," *The Journal of Open Source Software*, vol. 1, no. 2, p. 24, jun 2016. [Online]. Available: https://doi.org/10.21105/joss.00024 [Cited on page 27.]

[35] M.-J. Zhang, H. Li, and J.-Q. Xia, "What do we know about cosmography," *The European Physical Journal C*, vol. 77, no. 7, Jun 2017. [Online]. Available: http://dx.doi.org/10.1140/epjc/s10052-017-5005-4 [Cited on page 27.]

[36] S. Kumar, "Observational constraints on hubble constant and deceleration parameter in power-law cosmology," *Monthly Notices of the Royal Astronomical Society*, vol. 422, no. 3, p. 2532–2538, Mar 2012. [Online]. Available: http://dx.doi.org/10.1111/j.1365-2966.2012.20810.x [Cited on page 27.]

[37] S. K. Array, *Advancing astrophysics with the square kilometre array*. SKA Ogranisation, 2015. [Cited on page 28.]

[38] ESO, "The extremely large telescope the world's biggest eye on the sky." [Online]. Available: https://elt.eso.org/ [Cited on page 36.]

[39] S. S. Eikenberry *et al.*, "Astro2020 Project White Paper: The Cosmic Accelerometer," 7 2019. [Cited on page 36.]

[40] R. Cooke, "The ACCELERATION programme: I. Cosmology with the redshift drift," *Mon. Not. Roy. Astron. Soc.*, vol. 492, no. 2, pp. 2044–2057, 2020. [Cited on page 36.]

[41] M. Killedar and G. F. Lewis, "Lyα absorbers in motion: consequences of gravitational lensing for the cosmological redshift drift experiment," *Monthly Notices of the Royal Astronomical Society*, vol. 402, no. 1, p. 650–656, Dec 2009. [Online]. Available: http://dx.doi.org/10.1111/j.1365-2966.2009.15913.x [Cited on page 36.]

[42] C. Alves, A. O. Leite, C. A. Martins, J. B. Matos, and T. Silva, "Forecasts of redshift drift constraints on cosmological parameters," *Mon. Not. Roy. Astron. Soc.*, vol. 488, no. 3, pp. 3607–3624, 2019. [Cited on page 41.]

[43] C. Z. Munõz and C. Escamilla-Rivera, "Inverse cosmography: testing the effectiveness of cosmographic polynomials using machine learning," *Journal of Cosmology and Astroparticle Physics*, vol. 2020, no. 12, p. 007–007, Dec 2020. [Online]. Available: http://dx.doi.org/10.1088/1475-7516/2020/12/007 [Cited on page 58.]

[44] S. Capozziello, R. D'Agostino, and O. Luongo, "Cosmographic analysis with chebyshev polynomials," *Monthly Notices of the Royal Astronomical Society*, vol. 476, no. 3, p. 3924–3938, Feb 2018. [Online]. Available: http://dx.doi.org/10.1093/mnras/sty422 [Cited on page 58.]

[45] A. Banerjee, E. O. Colgáin, M. Sasaki, M. M. Sheikh-Jabbari, and T. Yang, "On cosmography in the cosmic dark ages: are we still in the dark?" 9 2020. [Cited on page 58.]

[46] G. Bargiacchi, G. Risaliti, M. Benetti, S. Capozziello, E. Lusso, A. Saccardi, and M. Signorini, "Cosmography by orthogonalized logarithmic polynomials," 1 2021. [Cited on page 58.]

Appendix A

Padé Approximants

For any given power series A(x), the Padé approximant can be calculated by doing

$$A(x) - \frac{p(x)}{q(x)} = 0 \tag{A.1}$$

With $p(x) = p_0 + p_1 x + p_2 x^2 + ... + p_m x^m$ and $q(x) = 1 + q_1 x + q_2 x^2 + ... + q_n x^n$. Expanding equation A.1 one can determine all the coefficients for $p(x)$ and $q(x)$.

$$\begin{gathered} a_0 = p_0 \\ a_1 + a_0 q_1 = p_1 \\ a_2 + a_1 q_1 + a_0 q_2 = p_2 \\ ... \\ a_m + a_{m-1} q_1 + ... + a_0 q_m = p_m \\ a_{m+1} + a_m q_1 + ... + a_{m-n+1} q_n = 0 \\ ... \\ a_{m+n} + a_{m+n-1} q_1 + ... + a_m q_n = 0 \end{gathered} \tag{A.2}$$

The sections A.1, A.2 and A.3 contain the numerator ($p(x)$) and denominator ($q(x)$) for the Hubble parameter of the cosmographic functions z-Padé[3/2], y-Padé[1/4] and x-Padé[4/1] respectively.

A.1 z-Padé[3/2]

$$
\begin{aligned}
p(z) = H_0 \Bigg[& 1 + z[(q_0+1) + (-13c_0j_0q_0 - 30c_0j_0 + 18c_0q_0^3 + 30c_0q_0^2 + 5c_0s_0 + 130j_0^3q_0 \\
& + 120j_0^3 - 280j_0^2q_0^3 - 230j_0^2q_0^2 + 25j_0^2s_0 - 3j_0p_0 + 270j_0q_0^5 + 240j_0q_0^4 + 40j_0q_0^2s_0 + 110j_0q_0s_0 \\
& + 3p_0q_0^2 - 90q_0^7 - 90q_0^6 - 30q_0^3s_0 + 35q_0s_0^2 + 40s_0^2)/(5(-3c_0j_0 + 3c_0q_0^2 + 12j_0^3 - 23j_0^2q_0^2 \\
& + 24j_0q_0^4 + 11j_0q_0s_0 - 9q_0^6 - 3q_0^3s_0 + 4s_0^2))] + z^2[(j_0 - q_0^2)/2 + (q_0+1)(-13c_0j_0q_0 \\
& - 30c_0j_0 + 18c_0q_0^3 + 30c_0q_0^2 + 5c_0s_0 + 130j_0^3q_0 + 120j_0^3 - 280j_0^2q_0^3 - 230j_0^2q_0^2 + 25j_0^2s_0 - 3j_0p_0 \\
& + 270j_0q_0^5 + 240j_0q_0^4 + 40j_0q_0^2s_0 + 110j_0q_0s_0 + 3p_0q_0^2 - 90q_0^7 - 90q_0^6 - 30q_0^3s_0 + 35q_0s_0^2 \\
& + 40s_0^2)/(5(-3c_0j_0 + 3c_0q_0^2 + 12j_0^3 - 23j_0^2q_0^2 + 24j_0q_0^4 + 11j_0q_0s_0 - 9q_0^6 - 3q_0^3s_0 + 4s_0^2)) \\
& + (5c_0^2 - 40c_0j_0^2 + 74c_0j_0q_0^2 - 52c_0j_0q_0 - 60c_0j_0 - 18c_0q_0^4 + 72c_0q_0^3 + 60c_0q_0^2 + 26c_0q_0s_0 \\
& + 20c_0s_0 + 80j_0^4 + 120j_0^3q_0^2 + 520j_0^3q_0 + 240j_0^3 - 475j_0^2q_0^4 - 1120j_0^2q_0^3 - 460j_0^2q_0^2 + 240j_0^2q_0s_0 \\
& + 100j_0^2s_0 - 16j_0p_0q_0 - 12j_0p_0 + 450j_0q_0^6 + 1080j_0q_0^5 + 480j_0q_0^4 - 230j_0q_0^3s_0 + 160j_0q_0^2s_0 \\
& + 220j_0q_0s_0 + 60j_0s_0^2 + 12p_0q_0^3 + 12p_0q_0^2 - 4p_0s_0 - 135q_0^8 - 360q_0^7 - 180q_0^6 + 90q_0^5s_0 \\
& - 60q_0^3s_0 + 5q_0^2s_0^2 + 140q_0s_0^2 + 80s_0^2)/(20(-3c_0j_0 + 3c_0q_0^2 + 12j_0^3 - 23j_0^2q_0^2 + 24j_0q_0^4 \\
& + 11j_0q_0s_0 - 9q_0^6 - 3q_0^3s_0 + 4s_0^2))] + z^3[(j_0 - q_0^2)(-13c_0j_0q_0 - 30c_0j_0 + 18c_0q_0^3 + 30c_0q_0^2 \\
& + 5c_0s_0 + 130j_0^3q_0 + 120j_0^3 - 280j_0^2q_0^3 - 230j_0^2q_0^2 + 25j_0^2s_0 - 3j_0p_0 + 270j_0q_0^5 + 240j_0q_0^4 \\
& + 40j_0q_0^2s_0 + 110j_0q_0s_0 + 3p_0q_0^2 - 90q_0^7 - 90q_0^6 - 30q_0^3s_0 + 35q_0s_0^2 + 40s_0^2)/(10(-3c_0j_0 \\
& + 3c_0q_0^2 + 12j_0^3 - 23j_0^2q_0^2 + 24j_0q_0^4 + 11j_0q_0s_0 - 9q_0^6 - 3q_0^3s_0 + 4s_0^2)) \\
& + (q_0+1)(5c_0^2 - 40c_0j_0^2 + 74c_0j_0q_0^2 - 52c_0j_0q_0 - 60c_0j_0 - 18c_0q_0^4 \\
& + 72c_0q_0^3 + 60c_0q_0^2 + 26c_0q_0s_0 + 20c_0s_0 + 80j_0^4 + 120j_0^3q_0^2 + 520j_0^3q_0 + 240j_0^3 - 475j_0^2q_0^4 \\
& - 1120j_0^2q_0^3 - 460j_0^2q_0^2 + 240j_0^2q_0s_0 + 100j_0^2s_0 - 16j_0p_0q_0 - 12j_0p_0 + 450j_0q_0^6 + 1080j_0q_0^5 \\
& + 480j_0q_0^4 - 230j_0q_0^3s_0 + 160j_0q_0^2s_0 + 220j_0q_0s_0 + 60j_0s_0^2 + 12p_0q_0^3 + 12p_0q_0^2 - 4p_0s_0 \\
& - 135q_0^8 - 360q_0^7 - 180q_0^6 + 90q_0^5s_0 - 60q_0^3s_0 + 5q_0^2s_0^2 + 140q_0s_0^2 + 80s_0^2)/(20(-3c_0j_0 + 3c_0q_0^2 \\
& + 12j_0^3 - 23j_0^2q_0^2 + 24j_0q_0^4 + 11j_0q_0s_0 - 9q_0^6 - 3q_0^3s_0 + 4s_0^2)) \\
& - (4j_0q_0 + 3j_0 - 3q_0^3 - 3q_0^2 + s_0)/6] \Bigg]
\end{aligned}
\tag{A.3}
$$

$$q(z) = 1 + z[(-13c_0j_0q_0 - 30c_0j_0 + 18c_0q_0^3 + 30c_0q_0^2 + 5c_0s_0 + 130j_0^3q_0 + 120j_0^3 - 280j_0^2q_0^3 - 230j_0^2q_0^2 + 25j_0^2s_0 - 3j_0p_0 + 270j_0q_0^5 + 240j_0q_0^4 + 40j_0q_0^2s_0 + 110j_0q_0s_0 + 3p_0q_0^2 - 90q_0^7 - 90q_0^6 - 30q_0^3s_0 + 35q_0s_0^2 + 40s_0^2)/(5(-3c_0j_0 + 3c_0q_0^2 + 12j_0^3 - 23j_0^2q_0^2 + 24j_0q_0^4 + 11j_0q_0s_0 - 9q_0^6 - 3q_0^3s_0 + 4s_0^2))] + z^2[(5c_0^2 - 40c_0j_0^2 + 74c_0j_0q_0^2 - 52c_0j_0q_0 - 60c_0j_0 - 18c_0q_0^4 + 72c_0q_0^3 + 60c_0q_0^2 + 26c_0q_0s_0 + 20c_0s_0 + 80j_0^4 + 120j_0^3q_0^2 + 520j_0^3q_0 + 240j_0^3 - 475j_0^2q_0^4 - 1120j_0^2q_0^3 - 460j_0^2q_0^2 + 240j_0^2q_0s_0 + 100j_0^2s_0 - 16j_0p_0q_0 - 12j_0p_0 + 450j_0q_0^6 + 1080j_0q_0^5 + 480j_0q_0^4 - 230j_0q_0^3s_0 + 160j_0q_0^2s_0 + 220j_0q_0s_0 + 60j_0s_0^2 + 12p_0q_0^3 + 12p_0q_0^2 - 4p_0s_0 - 135q_0^8 - 360q_0^7 - 180q_0^6 + 90q_0^5s_0 - 60q_0^3s_0 + 5q_0^2s_0^2 + 140q_0s_0^2 + 80s_0^2)/(20(-3c_0j_0 + 3c_0q_0^2 + 12j_0^3 - 23j_0^2q_0^2 + 24j_0q_0^4 + 11j_0q_0s_0 - 9q_0^6 - 3q_0^3s_0 + 4s_0^2))]$$

(A.4)

A.2 y-Padé[1/4]

$$p(y) = H_0\left[1 + y[q_0 + 1 + (16c_0q_0 - 230j_0^2q_0 + 735j_0q_0^3 - 200j_0q_0^2 - 200j_0q_0 - 35j_0s_0 + p_0 - 420q_0^5 + 300q_0^4 + 300q_0^3 + 135q_0^2s_0 - 20q_0s_0 - 20s_0)/(5(c_0 - 10j_0^2 + 105j_0q_0^2 + 40j_0q_0 - 105q_0^4 - 60q_0^3 + 15q_0s_0 + 4s_0))]\right]$$

(A.5)

$$
\begin{aligned}
q(y) = 1 + y[&(16c_0q_0 - 230j_0^2q_0 + 735j_0q_0^3 - 200j_0q_0^2 - 200j_0q_0 - 35j_0s_0 + p_0 - 420q_0^5 \\
&+ 300q_0^4 + 300q_0^3 + 135q_0^2s_0 - 20q_0s_0 - 20s_0)/(5(c_0 - 10j_0^2 + 105j_0q_0^2 + 40j_0q_0 - 105q_0^4 \\
&- 60q_0^3 + 15q_0s_0 + 4s_0))] + y^2[(-5c_0j_0 - 27c_0q_0^2 - 42c_0q_0 - 10c_0 + 50j_0^3 - 115j_0^2q_0^2 \\
&+ 360j_0^2q_0 + 100j_0^2 - 420j_0q_0^4 - 1620j_0q_0^3 - 650j_0q_0^2 - 5j_0q_0s_0 + 50j_0s_0 - 2p_0q_0 - 2p_0 \\
&+ 315q_0^6 + 990q_0^5 + 450q_0^4 - 195q_0^3s_0 - 360q_0^2s_0 - 110q_0s_0)/(10(c_0 - 10j_0^2 + 105j_0q_0^2 \\
&+ 40j_0q_0 - 105q_0^4 - 60q_0^3 + 15q_0s_0 + 4s_0))] + y^3[(-13c_0j_0q_0 + 114c_0q_0^3 + 126c_0q_0^2 + 30c_0q_0 \\
&+ 5c_0s_0 + 340j_0^3q_0 - 300j_0^2q_0^3 + 320j_0^2q_0^2 + 300j_0^2q_0 + 55j_0^2s_0 - 3j_0p_0 + 1050j_0q_0^5 + 1560j_0q_0^4 \\
&+ 450j_0q_0^3 + 330j_0q_0^2s_0 + 190j_0q_0s_0 + 60j_0s_0 + 9p_0q_0^2 + 6p_0q_0 - 630q_0^7 - 1170q_0^6 - 450q_0^5 \\
&+ 240q_0^4s_0 + 660q_0^3s_0 + 270q_0^2s_0 + 75q_0s_0^2 + 20s_0^2)/(30(c_0 - 10j_0^2 + 105j_0q_0^2 + 40j_0q_0 \\
&- 105q_0^4 - 60q_0^3 + 15q_0s_0 + 4s_0))] + y^4[(-5c_0^2 + 100c_0j_0^2 - 210c_0j_0q_0^2 + 52c_0j_0q_0 + 60c_0j_0 \\
&- 210c_0q_0^4 - 456c_0q_0^3 - 180c_0q_0^2 - 66c_0q_0s_0 - 20c_0s_0 - 500j_0^4 - 700j_0^3q_0^2 - 1360j_0^3q_0 - 600j_0^3 \\
&+ 1575j_0^2q_0^4 + 1200j_0^2q_0^3 + 100j_0^2q_0^2 - 1020j_0^2q_0s_0 - 220j_0^2s_0 + 40j_0p_0q_0 + 12j_0p_0 - 3150j_0q_0^6 \\
&- 4200j_0q_0^5 - 1200j_0q_0^4 - 210j_0q_0^3s_0 - 1320j_0q_0^2s_0 - 700j_0q_0s_0 - 140j_0s_0^2 - 60p_0q_0^3 - 36p_0q_0^2 \\
&+ 4p_0s_0 + 1575q_0^8 + 2520q_0^7 + 900q_0^6 - 630q_0^5s_0 - 960q_0^4s_0 - 300q_0^3s_0 - 285q_0^2s_0^2 - 300q_0s_0^2 \\
&- 80s_0^2)/(120(c_0 - 10j_0^2 + 105j_0q_0^2 + 40j_0q_0 - 105q_0^4 - 60q_0^3 + 15q_0s_0 + 4s_0))]
\end{aligned}
\tag{A.6}
$$

A.3 x-Padé[4/1]

$$p(x) = H_0\Big[1 + x[q_0 + 1 + (11c_0q_0 + 5c_0 - 70j_0^2q_0 - 20j_0^2 + 210j_0q_0^3 + 125j_0q_0^2 + 20j_0q_0 - 15j_0s_0 + p_0 - 105q_0^5 - 75q_0^4 - 15q_0^3 + 60q_0^2s_0 + 35q_0s_0 - q_0 + 5s_0 - 1)/(5c_0 - 20j_0^2 + 125j_0q_0^2 + 40j_0q_0 + 5j_0 - 75q_0^4 - 30q_0^3 - 5q_0^2 + 35q_0s_0 + 5q_0 + 10s_0 + 5)] + x^2[j_0/2 - q_0^2/2 + q_0/2 + (q_0 + 1)(11c_0q_0 + 5c_0 - 70j_0^2q_0 - 20j_0^2 + 210j_0q_0^3 + 125j_0q_0^2 + 20j_0q_0 - 15j_0s_0 + p_0 - 105q_0^5 - 75q_0^4 - 15q_0^3 + 60q_0^2s_0 + 35q_0s_0 - q_0 + 5s_0 - 1)/(5c_0 - 20j_0^2 + 125j_0q_0^2 + 40j_0q_0 + 5j_0 - 75q_0^4 - 30q_0^3 - 5q_0^2 + 35q_0s_0 + 5q_0 + 10s_0 + 5) + 1/2] + x^3[-2j_0q_0/3 + q_0^3/2 + q_0/6 - s_0/6 + (j_0/2 - q_0^2/2 + q_0/2 + 1/2)(11c_0q_0 + 5c_0 - 70j_0^2q_0 - 20j_0^2 + 210j_0q_0^3 + 125j_0q_0^2 + 20j_0q_0 - 15j_0s_0 + p_0 - 105q_0^5 - 75q_0^4 - 15q_0^3 + 60q_0^2s_0 + 35q_0s_0 - q_0 + 5s_0 - 1)/(5c_0 - 20j_0^2 + 125j_0q_0^2 + 40j_0q_0 + 5j_0 - 75q_0^4 - 30q_0^3 - 5q_0^2 + 35q_0s_0 + 5q_0 + 10s_0 + 5) + 1/6] + x^4[c_0/24 - j_0^2/6 + 25j_0q_0^2/24 + j_0q_0/3 + j_0/24 - 5q_0^4/8 - q_0^3/4 - q_0^2/24 + 7q_0s_0/24 + q_0/24 + s_0/12 + (-2j_0q_0/3 + q_0^3/2 + q_0/6 - s_0/6 + 1/6)(11c_0q_0 + 5c_0 - 70j_0^2q_0 - 20j_0^2 + 210j_0q_0^3 + 125j_0q_0^2 + 20j_0q_0 - 15j_0s_0 + p_0 - 105q_0^5 - 75q_0^4 - 15q_0^3 + 60q_0^2s_0 + 35q_0s_0 - q_0 + 5s_0 - 1)/(5c_0 - 20j_0^2 + 125j_0q_0^2 + 40j_0q_0 + 5j_0 - 75q_0^4 - 30q_0^3 - 5q_0^2 + 35q_0s_0 + 5q_0 + 10s_0 + 5) + 1/24]]\Big] \tag{A.7}$$

$$q(x) = 1 + x[(11c_0q_0 + 5c_0 - 70j_0^2q_0 - 20j_0^2 + 210j_0q_0^3 + 125j_0q_0^2 + 20j_0q_0 - 15j_0s_0 + p_0 - 105q_0^5 - 75q_0^4 - 15q_0^3 + 60q_0^2s_0 + 35q_0s_0 - q_0 + 5s_0 - 1)/(5c_0 - 20j_0^2 + 125j_0q_0^2 + 40j_0q_0 + 5j_0 - 75q_0^4 - 30q_0^3 - 5q_0^2 + 35q_0s_0 + 5q_0 + 10s_0 + 5)] \tag{A.8}$$

Appendix B

Data with Dispersion

In this appendix it will be conducted the same analysis as in section 5 but for this case the measurements of the mock data set will have dispersion. The new data is presented in figure B.1. The results are shown in figures B.2-B.4 and in table B.1. As it can be seen, there are no significant deviations from what was obtained before except an even more accentuated difficulty in recovering true values of high order cosmographic parameters for the z and x parameterizations.

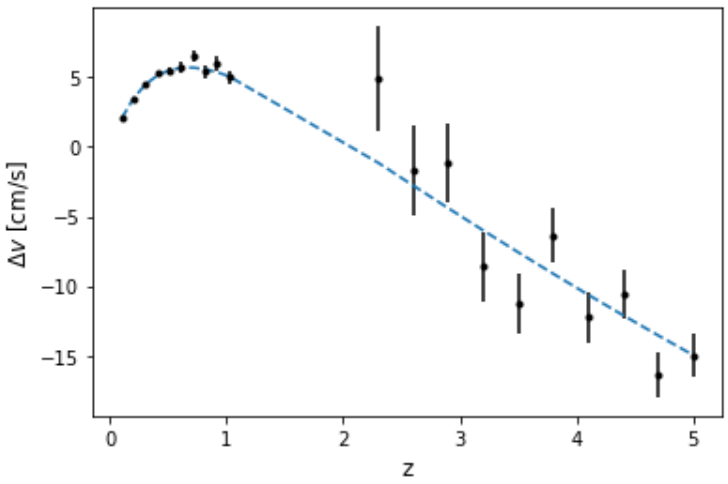

Figure B.1: Spectroscopic velocity drift mock data for SKA observations from a flat ΛCDM model with $\Omega_{m0} = 0.3$. The blue dashed line represents the true curve for this fiducial model.

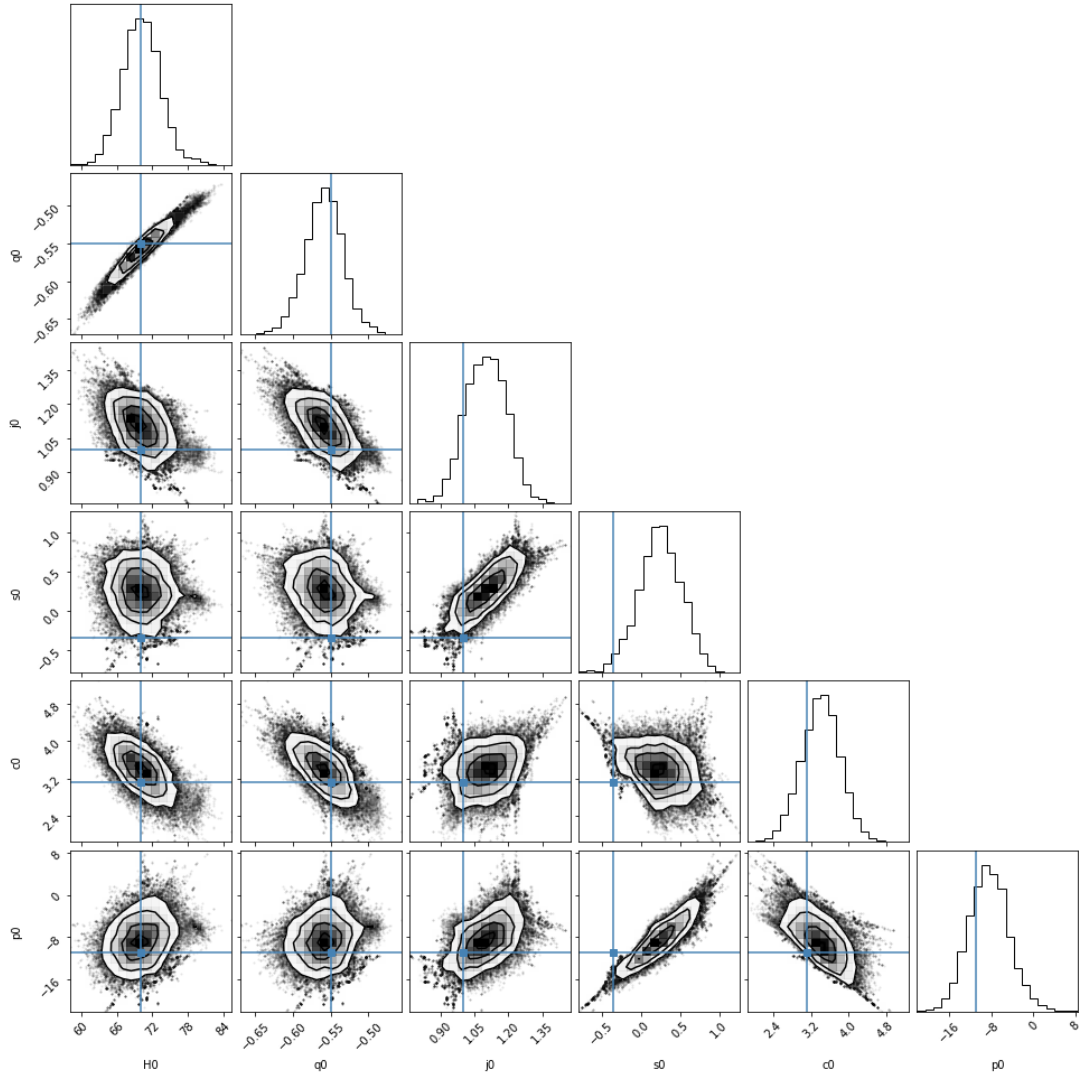

Figure B.2: Corner plot for the cosmographic parameters for the z redshift parameterization and N prior (case with dispersion). In blue we have the true values for each parameter.

Dispersed SKA + ELT results for the N prior				
Parameters	Expected	z	z-P[3/2]	x
H_0	70	$70.10^{+3.07}_{-3.08}$	$69.76^{+2.92}_{-3.04}$	$69.65^{+3.01}_{-3.03}$
q_0	-0.55	$-0.56^{+0.02}_{-0.03}$	$-0.56^{+0.02}_{-0.03}$	$-0.57^{+0.03}_{-0.03}$
j_0	1	$1.10^{+0.09}_{-0.09}$	$1.09^{+0.19}_{-0.18}$	$1.33^{+0.24}_{-0.32}$
s_0	-0.35	$0.25^{+0.28}_{-0.27}$	$0.38^{+1.51}_{-1.26}$	$2.03^{+2.12}_{-3.08}$
c_0	3.115	$3.41^{+0.39}_{-0.42}$	$7.08^{+7.33}_{-8.60}$	$9.31^{+12.33}_{-17.25}$
p_0	-10.88675	$-8.61^{+3.73}_{-3.71}$	$30.64^{+50.32}_{-95.05}$	$9.60^{+61.85}_{-68.11}$

Table B.1: MCMC results for the case with dispersion. The prior used was the N prior.

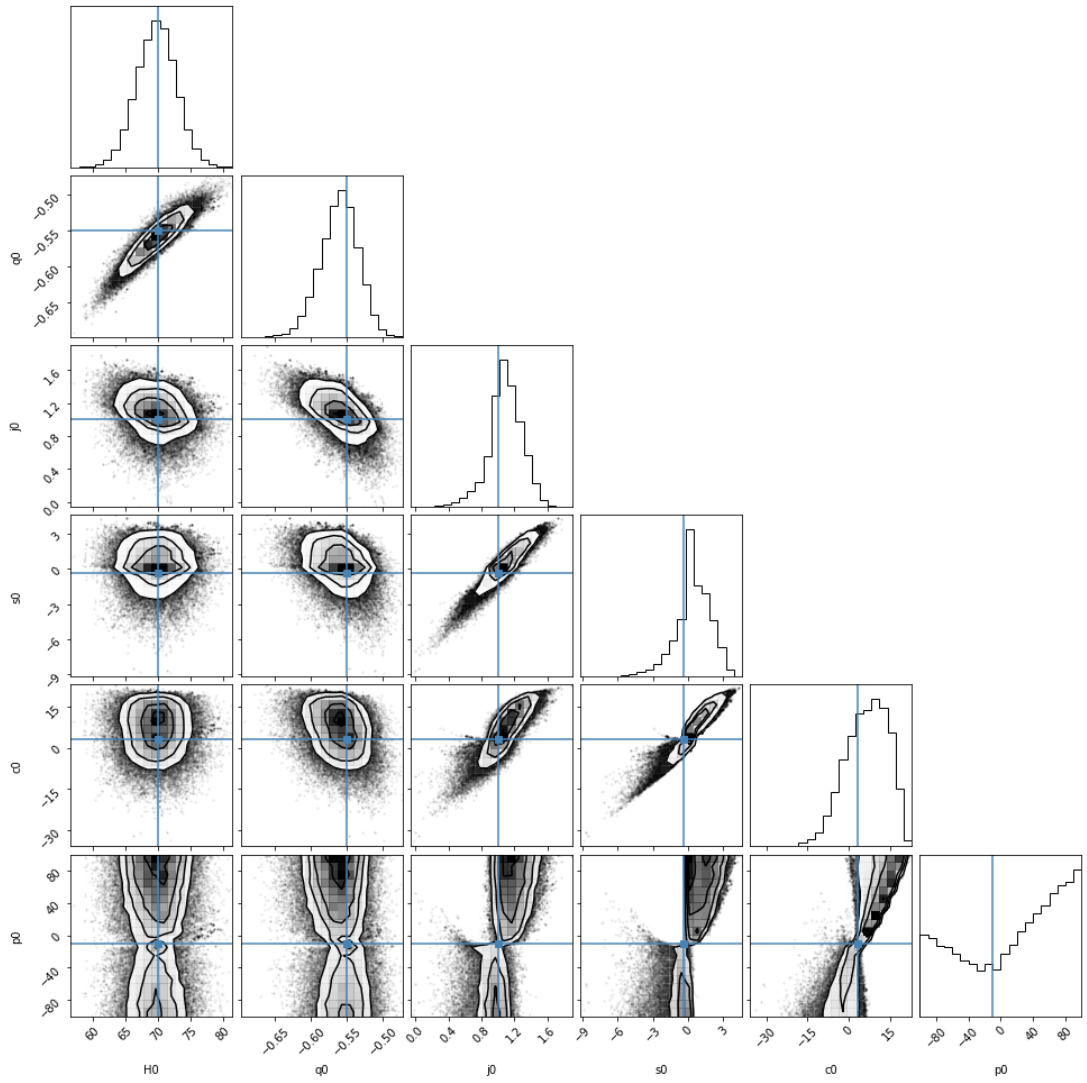

Figure B.3: Corner plot for the cosmographic parameters for the z redshift parameterization with Padé approximant [3/2] and N prior (case with dispersion). In blue we have the true values for each parameter.

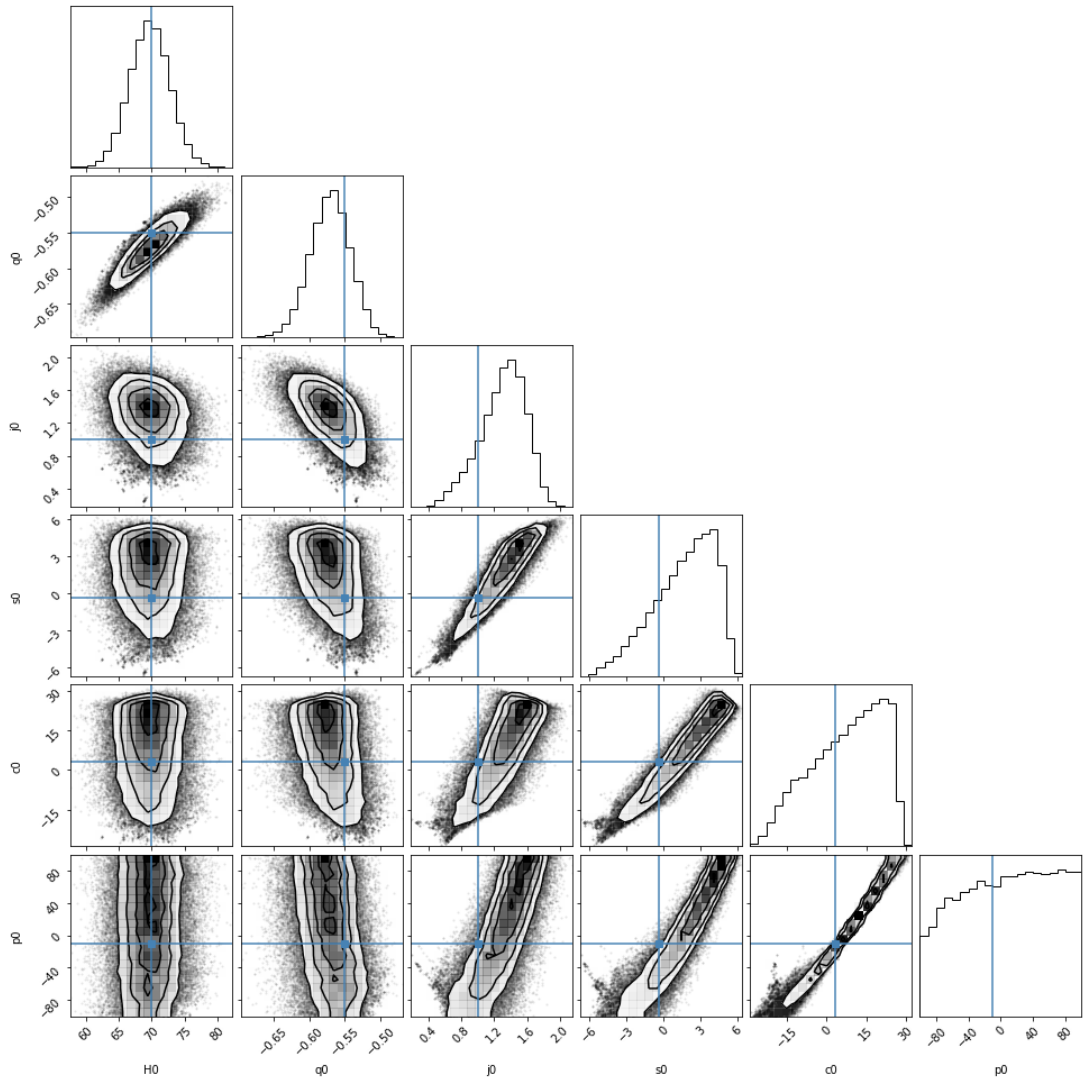

Figure B.4: Corner plot for the cosmographic parameters obtained for the x redshift parameterization and N prior (case with dispersion). In blue we have the true values for each parameter.